MERCURY PARTITIONING IN SUPER-PERMAFROST GROUNDWATER, TRUELOVE LOWLAND, DEVON ISLAND, NUNAVUT

A Thesis Submitted to the College of Graduate Studies and Research

in Partial Fulfillment of the Requirements for the degree of

Master of Science

in the

Department of Soil Science

University of Saskatchewan

Saskatoon

By

Alanna Louise Dickson

Keywords: mercury, partitioning, super-permafrost, groundwater, Arctic

PERMISSION TO USE

In presenting this thesis in partial fulfillment of the requirements for a Postgraduate degree from the University of Saskatchewan, I agree that the Libraries of this University may make it freely available for inspection. I further agree that permission for copying of this thesis in any manner, in whole or in part, for scholarly purposes may be granted by the professor or professors who supervised my thesis work or, in their absence, by the Head of the Department or the Dean of the College in which my thesis work was done. It is understood that any copying or publication or use of this thesis or parts thereof for financial gain shall not be allowed without my written permission. It is also understood that due recognition shall be given to me and to the University of Saskatchewan in any scholarly use which may be made of any material in my thesis.

Requests for permission to copy or to make other uses of materials in this thesis in whole or part should be addressed to:

Head of the Department of Soil Science
University of Saskatchewan
Saskatoon, Saskatchewan S7N 5A8
Canada

OR

Dean
College of Graduate Studies and Research
University of Saskatchewan
107 Administration Place
Saskatoon, Saskatchewan S7N 5A2
Canada

DISCLAIMER

Reference in this thesis to any specific commercial products by trade name, trademark, manufacturer, or otherwise, does not constitute or imply its endorsement, recommendation, or favoring by the University of Saskatchewan. The views and opinions of the author expressed herein do not state or reflect those of the University of Saskatchewan, and shall not be used for advertising or product endorsement purposes.

ABSTRACT

The objective of this study was to determine the dominant biogeochemical controls on mercury partitioning in super-permafrost groundwater at Truelove Lowland, Devon Island, Nunavut. Mercury partitioning in snow, ephemeral standing water, and super-permafrost groundwater was investigated.

Results indicate that partitioning differs between matrices, and that particulate mercury is spatially and temporally dynamic in Truelove Lowland groundwater. Particulate mercury in groundwater was 73 % of total mercury, while snow had only 22 % particulate mercury. Particulate mercury in groundwater rose by over 20 % from Julian day 181 to 189, and decreased slightly on Julian day 191. No single geochemical parameter was a good predictor of particulate mercury concentrations.

To expand upon the findings of the field study a laboratory microcosm study was conducted to determine whether certain biogeochemical processes influence mercury partitioning in super-permafrost groundwater. Particulate mercury in the dissimilatory iron reducing bacteria inhibited microcosm was 61 % of total mercury, approximately 18 % lower than in all other treatments. Iron (III) concentrations had a positive correlation with particulate mercury while chloride concentrations had a negative correlation with particulate mercury. Sulfate reducing bacteria were not found to influence mercury partitioning.

ACKNOWLEDGMENTS

It is with the unwavering support and encouragement of family, friends and mentors that I have completed my MSc. Thank-you to my supervisor, Dr. Siciliano, who challenged me and encouraged me to excel. Many thanks to the members of my committee: Dr. Bing Si, Dr. Derek Peak, Dr. Diane Knight; and to the external examiner, Dr. Ian Fleming. To Sarah Armstrong, Shannon Gerrard, Simone Levy, Danielle Renaud, Wai Ma, Pete Burnett, Jennifer Arnold, Dani Xu and Stefanie Drummond – your friendship and the many laughs we shared brightened the journey. And, to my family, thank-you for love and support through graduate school and in all my endeavors.

The extraordinary time at Truelove was made even more memorable by the friendship (and help) of Simone Levy, Alexandra Schautz and Dr. LeeAnn Fishback. To Edenise and Alexandre (from the Amyot laboratory at Université du Montreal) your kind generosity (and Ultrapure HCl) in Resolute was appreciated.

This research could not have been conducted without financial support from the Natural Science and Engineering Research Council (NSERC), Northern Scientific Training Program (NSTP) and Saskatchewan Synchrotron Institute (SSI). Thank-you to the Department of Soil Science for providing a tuition scholarship. A sincere thank-you to Elaine Farkas, Kim Heidinger and Lorna Mead for lending a hand when it was most needed.

TABLE OF CONTENTS

LIST OF TABLES

LIST OF FIGURES

LIST OF ABBREVIATIONS

AC	Aerobic control
ANC	Anaerobic control
ANOVA	Analysis of variance
CE	Capillary electrophoresis
DIRB	Dissimilatory iron reducing bacteria
DIRB-	Dissimilatory iron reducing bacteria inhibited
DIRB+	Dissimilatory iron reducing bacteria stimulated
DMHg	Dimethylmercury – $(CH_3)_2Hg$
DOC	Dissolved organic carbon
DOM	Dissolved organic matter
DHg	Dissolved mercury
EPA	Environmental Protection Agency
EtHg	Ethylmercury – $CH_3CH_2Hg^+$
GLM	General linear model
HDPE	High density polyethylene
HFO	Hydrous ferric oxide – $Fe_5HO_8 \bullet 4H_2O$ (ferrihydrite)
Hg	Mercury
IBP	International biological programme
LFS	Lower foreslope
MDE	Mercury depletion event
MDL	Method detection limit
MMHg	Monomethylmercury – CH_3Hg^+
MDS	Matrix duplicate spike
MS	Matrix spike
NS	Not significant
OD	Oxidative demethylation
PHg	Particulate mercury
POC	Particulate organic carbon
POM	Particulate organic matter
PTFE	Polytetrafluoroethylene

PVC	Polyvinylchloride
PVDF	Polyvinylidene difluoride
R	Percent Recovery
RD	Reductive demethylation
RPD	Relative percent difference
RSD	Relative standard deviation
S	Standard deviation
SCM	Surface complexation model
SRB	Sulfate reducing bacteria
SRB-	Sulfate reducing bacteria inhibited
SRB+	Sulfate reducing bacteria stimulated
t	Students' t value
TC	True concentration
THg	Total mercury
TiNTA	Titanium(III)nitrilotriacetate
TOC	Total organic carbon
UHP	Ultra high purity
USEPA	United States Environmental Protection Agency
UV	Ultraviolet
WSM	Wet sedge meadow

1. INTRODUCTION

Arctic regions, though remote, are linked to lower latitudes by atmospheric and oceanic currents and are thus subject to contamination by pollutants released in temperate and equatorial regions. Gaseous elemental mercury (Hg) has a residence time in the atmosphere of approximately one year and is efficiently transported to the Arctic where it is oxidized at polar sunrise and deposited on land and water (Fitzgerald et al., 1998). Mercury is released naturally to the atmosphere through weathering of rock and entrainment of dust particles in the atmosphere, volcanic eruptions, forest fires and emission of biogenic volatile compounds (Morel et al., 1998). Anthropogenic sources include metal production, the chlor-alkali and pulp industries, waste handling and treatment, and coal, peat and wood combustion (Morel et al., 1998). Based on lake sediment cores it is estimated that Hg flux has increased three to seven-fold in the 150 years since the industrial revolution (Fitzgerald et al., 1998; Morel et al., 1998; Pirrone et al., 1998).

Mercury exists in three oxidation states (0, I, II) (Silberberg, 1996). In the environment it is primarily found as inorganic and organic complex ions (Freeze and Cherry, 1979). Charged complex ions are subject to interaction with charged functional groups on particle surfaces and this interaction is governed by the geochemistry of the environment. Partitioning of Hg between the aqueous and particulate phase in soil and groundwater is important because it has implications for its bioavailability, fate and transport in the environment.

Research indicates that particulate-bound Hg is not bioavailable and can not be methylated (Benoit et al., 2001a). Inorganic Hg complexes do not bioaccumulate and biomagnify in the manner that organomercury complexes do (Casarett and Doull, 2001; Morel et al., 1998). Consequently, partitioning of Hg into the particulate phase can potentially prevent methylation and thereby pose less risk to human and ecosystem health.

Sulfate reducing bacteria are thought to be the primary methylators of Hg in the environment (Morel et al., 1998). Since SRB require anoxic, sulfidic conditions for growth their primary niche is wet, low-lying areas. For Hg to be methylated by SRB it must move through the landscape to the wet, low-lying areas where SRB are active. Facilitated transport is a process

whereby particulate- or colloid-associated ions move through the soil matrix at a velocity greater than the average velocity of the groundwater (Guine et al., 2003). Clearly, partitioning of Hg into the particulate phase is an important determination of both methylation and transport of Hg.

At present, there is significant scholarly interest in the biogeochemistry of Hg in freshwater. However, there is a paucity of research investigating biogeochemistry and partitioning of Hg in High Arctic aquatic environments. Effective risk assessment and management of Hg in the High Arctic depends upon a comprehensive understanding of Hg biogeochemistry in this environment. The principles of Hg biogeochemistry that have been elucidated for temperate freshwaters are an important first step to understanding Hg in High Arctic environments. However, profound differences between temperate and High Arctic ecosystems necessitate research into the controls of Hg biogeochemistry and partitioning in High Arctic superpermafrost groundwater.

The research presented in this thesis is the first report of the temporal variation of Hg partitioning in High Arctic superpermafrost groundwater. In addition, this is the first investigation of the influence of functional groups of bacteria on Hg partitioning. Based on a review of the pertinent scientific literature, and the current understanding of Hg partitioning the following hypotheses were developed:

Partitioning of Hg in snow, standing water and superpermafrost groundwater will differ, and Hg partitioning in superpermafrost groundwater will change through the summer thaw;

Free sulfide, and bacterial surface-associated sulfide is the predominant sorbent of Hg in High Arctic superpermafrost groundwater; and

By altering the biogeochemistry of the superpermafrost groundwater system, functional groups of bacteria will alter the partitioning of Hg in High Arctic superpermafrost groundwater.

The thesis is organized into 6 chapters. This, Chapter 1, is an introduction to the thesis. Chapter 2 presents a review of the relevant scientific literature, highlighting: the unique properties of Hg; the origin of Hg in the environment; biological transformation and toxicity of Hg; the reaction, speciation and transport of Hg in the environment; and unique features of High Arctic hydrology.

Hypothesis 1 was tested with an observational study of Hg partitioning in snow, standing water and superpermafrost groundwater at Truelove Lowland, Devon Island, Nunavut; these results are presented in Chapter 3. Prior to snowmelt total Hg (THg) and dissolved Hg (DHg)

concentrations were determined in snow. From June to June 29, 2004, during the rapid summer thaw, standing water was sampled from the wet sedge meadow of 4 catenas. When a sufficient depth of active layer had developed (approximately 30 cm), slotted polyvinylchloride (PVC) monitoring wells were installed in the wet sedge meadow (WSM) of six catenas. Sampling was conducted every second day from June 29 to July 9, 2004. Prior to sampling the pH, Eh and temperature of the water was recorded, the well was then purged dry, or purged of three well volumes, and allowed to recharge. Samples for determination of THg and DHg, and samples for measurement of ancillary parameters such as anions, sulfide, iron speciation, and organic carbon were collected. Soils from four catenas that had monitoring wells installed were collected for later use in laboratory experiments. Analytical results and results of speciation modeling (conducted by Daughney and Siciliano) were used to test Hypothesis 2. Based on the results, detailed in Chapter 3, Hypothesis 2 was rejected.

Hypothesis 3 was tested via laboratory microcosm experiments; results are presented in Chapter 4. In these experiments functional groups of bacteria, sulfate reducing bacteria (SRB) and dissimilatory iron reducing bacteria (DIRB), were either inhibited or stimulated. In addition aerobic and anaerobic control microcosms were incubated. Microcosms were incubated aerobically and anaerobically at 10C in the dark. An intial microcosm experiment ran for 49 days, and a subsequent microcosm experiment ran for 74 days. Based on results from the microcosm experiment, Hypothesis 3 was accepted.

Chapter 5 is a synthesis and general discussion of the results and conclusions from the field and laboratory research chapters.

2. LITERATURE REVIEW

2.1 Mercury

Mercury (Hg) is a naturally occurring transition metal identified as a pollutant of global concern (Macdonald et al., 2000; Van Oostdam et al., 2003). This pollutant is reactive in the environment (Morel et al., 1998). Its oxidation state and speciation depend upon the redox potential, pH, and availability of potential ligands (Freeze and Cherry, 1979; Haitzer et al., 2003; Morel et al., 1998). Mercury exists in three valence states: elemental (Hg^0), mercurous ion (Hg^{+1}) and mercuric ion (Hg^{+2}). In its elemental form Hg is silver in color and is the only metal that is liquid at room temperature. This unique property arises from two factors: 1) a distorted crystal structure with each Hg atom surrounded by 6 rather than 12 nearest neighbours; and 2) a filled, tightly held *d* subshell leaving only two 6*s* electrons for metallic bonding (Silberberg, 1996). The condensed electron configuration of Hg^{+2} (the most common oxidation state) is [Xe] $4f^{14}$ $5d^{10}$ (Silberberg, 1996). The weak interaction among Hg atoms results in a low melting point (-38.9C) and volatility which afford it environmental mobility. This mobility allows Hg to spread globally from point sources (Schroeder and Munthe, 1998).

2.2 Origin of Mercury in the Environment

Mercury is widely distributed in the terrestrial environment with an average crustal abundance of 80 μg kg^{-1} (Taylor, 1964). This weighted average is based on a variety of rock types whose Hg contents vary widely, from 270 μg kg^{-1} in shales to <50 μg kg^{-1} in limestones (Faust and Aly, 1981). Mercury is a chalcophile element, readily forming sulfide compounds such as cinnabar (HgS) and hence, Hg often exists as an impurity in sphalerite, pyrite and other sulfide ores (Garrett, 1995a; Garrett, 1995c). Sequestration of Hg in liquid hydrocarbon reservoirs, coal beds, and organic rich sediments is prevalent due to its affinity for organic and thio-organic rich compounds (Garrett, 1995a).

The release of Hg from natural reservoirs to the atmosphere occurs through forest fires, volcanic eruption, seismic activity, geothermal activity, entrainment of dust particles in the air, soil degassing and weathering of Hg containing minerals (Morel et al., 1998). These sources of

Hg are not subject to influence by humans and in the present day, are responsible for approximately one-third of annual atmospheric Hg emissions (Lindberg et al., 2002). Mercury emissions have roughly tripled in the last 100 years (Fitzgerald et al., 1998; Lin et al., 2001) due to the exploitation of previously untapped Hg containing reservoirs.

Ore smelting, metal production, the pulp and chlor-alkali industries, and peat, coal and fossil fuel combustion are major anthropogenic sources of gaseous Hg (Morel et al., 1998). In North America and Europe, improvements in flue gas desulfurization equipment (which removes not only sulfur oxides, but also gaseous Hg) has resulted in a decrease in Hg emissions (Pacyna et al., 2003). Despite decreasing emissions in North America and Europe, Hg emissions in Asia have been steadily increasing and in 1995 were more than 50% (1704.3 tonnes) of total anthropogenic emissions (1912.8 tonnes) (Pacyna et al., 2003). Asian emissions are primarily from fossil fuel and coal combustion (Jaffe et al., 2005; Pacyna et al., 2003) and are expected to continue rising to satisfy energy demands of rapidly expanding Asian economies (Pacyna et al., 2003).

2.2.1 Naturally occurring mercury in the High Arctic

As rocks are physically and chemically weathered their constituents are released to the environment. In Arctic environments weathering processes that leach inorganic Hg into the environment are retarded by low temperatures and the presence of permafrost in the soil profile (Tedrow, 1977). Only a small amount of chemical weathering takes place in the Arctic (Tedrow, 1977). Washburn (1969, as cited by Tedrow, 1977) identified oxidation, desert varnish formation, surface cementation, carbonate coating, salt wedging, granular disintegration (caused by differential expansion), exfoliation, frost cracking, and frost wedging to be the primary modes of weathering in northeastern Greenland. Microbial transformation of mineral soil and parent material results in the solubilization of trace metals contained in these constituents (Quantin et al., 2002). The internal contribution of metal inputs to soil via weathering is recognized, but its magnitude is largely unknown (Starr et al., 2003).

The magnitude of natural Hg inputs from underlying bedrock is governed by the composition of the geological unit. Truelove Lowland, Devon Island is underlain by two geological units: the Canadian Shield and the Arctic Platform (Krupicka, 1977). Over half of the bedrock underlying Truelove lowland is composed of metamorphic granulites and gneisses; much of the remaining bedrock is dolomitic sandstone (Krupicka, 1977). Mercury content of

typical geologic material of the Arctic Platform and Canadian Shield are: sandstone, 0.04 mg kg^{-1}; limestone, 0.05 mg kg^{-1}; granitic igneous, 0.06 mg kg^{-1}; and basaltic igneous, 0.05 mg kg^{-1} (Sparks, 2003). The soil of Truelove Lowland will contain background Hg concentrations representative of the parent materials, from which they were derived.

2.2.2 Anthropogenic sources of mercury in the High Arctic

Indian and Northern Affairs Canada (INAC) summarized direct anthropogenic inputs of Hg to the Canadian Arctic in 2003 (Gregor et al., 2003). The primary sources of contaminants in the Canadian Arctic are abandoned mines, military installations and industrial sites. Terra #1 (Northrim Mine), Discovery Mine, Aishihik airstrip and the Border pump station/Rainy Hollow were identified as current or former point sources of Hg to the Arctic environment. There are few point sources anthropogenic sources of Hg in the Arctic and anthropogenic inputs are thought to be primarily derived from Hg emitted in temperate regions (Gregor et al., 2003) which undergoes long-range atmospheric transport to the Arctic region.

2.2.2.1 Long-range atmospheric transport

The residence time of volatile Hg^0 in the atmosphere ranges from 0.4 to 3 years (Lamborg et al., 2003; Schroeder and Munthe, 1998; Schroeder et al., 1998; WHO, 1990). This long residence time allows Hg to be transported globally. Atmospheric scientists back calculating the trajectory of air masses reaching the Arctic have determined that long-range transport of Hg only occurs during winter (Lin et al., 2001). During summer the model Lin et al. (2001) indicates that most air masses (<55%) originate over the Arctic Ocean and do not come in contact with continents. This model also identifies fall and winter Arctic air masses as originating in populated regions of Russia, Europe and North America. The authors conclude that these fall and winter air masses, in contact with continental sources of Hg, are responsible for the long-range atmospheric transport of Hg.

2.2.2.2 Mercury depletion events (MDE)

Mercury moves into the Arctic during the winter and then during Hg depletion events (MDE) deposits on the Arctic landscape (Ariya et al., 2002; Fitzgerald et al., 1998; Lindberg et al., 2002; Skov et al., 2004; St. Louis et al., 2005). During MDEs, Hg^0 that undergoes long-range transport from temperate latitudes is oxidized to Hg^{+2} and deposited on the Arctic landscape. Lindberg et al. (2002) observed MDE with a co-incident decrease in boundary layer ozone.

These authors hypothesize that halogen-oxide radicals produced during the ozone destruction (reaction 2.1) serve of as the primary oxidants of Hg^0 (reactions 2.2 and 2.3).

$$Br/Cl + O_3 \rightarrow ClO/BrO + O_2 \quad [2.1]$$

followed by:

$$BrO/ClO + Hg^0 \rightarrow HgO + Br/Cl \quad [2.2]$$

$$Hg^0 + 2Br/Cl \rightarrow HgBr_2/HgCl_2 \quad [2.3]$$

Ariya et al. (2002) conclude that reactions of Hg^0 with molecular halogens (Br_2 and Cl_2) are too slow to be important in the atmospheric transformation of Hg. Reactions with atomic halogens (Br and Cl) are considerably faster, however due to inferred and observed atomic Cl and Br concentrations Br is the only likely candidate to act as an oxidant during MDEs (Ariya et al., 2002). Observed decreases in atmospheric BrO, Br and Cl during MDEs supports the Hg oxidation reactions proposed above by Skov et al. (2004) and Lindberg et al. (2002). Lindberg et al. (2002) also reports that incident solar UV-B, which increases as ozone decreases, is capable of producing BrO from photolyzable Br.

Lindberg et al. (2002) documented MDEs in the Arctic atmosphere beginning within a few days of polar sunrise and persisting until snowmelt. Inorganic mercury deposited on/in the snowpack during MDEs rapidly disappears (Lindberg et al., 2002; St. Louis et al., 2005) Researchers hypothesize that it is reduced to Hg^0 and volatilized back into the atmosphere (Lindberg et al., 2002; St. Louis et al., 2005). A decrease in Hg^{+2} in surface snow accompanied by an increase in Hg^0 in interstitial air following MDEs supports this hypothesis (St. Louis et al., 2005). Despite the volatilization of Hg from the snowpack following MDEs, the results of Lindberg et al. (2002) indicate that the remaining Hg^{+2} is transported to the tundra in snow meltwater.

Methylmercury (MMHg) is present at low concentrations in air and precipitation (Schroeder and Munthe, 1998) and it has been identified in the snowpack on an Ellesmere Island glacier (St. Louis et al., 2005). St. Louis et al. (2005) did not observe a relationship between concentrations of MMHg and total Hg (THg) prompting them to hypothesize that MMHg in the snowpack is evaded from open ocean and polynya as dimethyl mercury (DMHg). They suggest that airborne DMHg is rapidly photolyzed to MMHg according to the following reaction:

$$Cl + CH_3HgCH_3 \rightarrow CH_3HgCl + CH_3 \quad [2.4]$$

St. Louis et al. (2005) also hypothesize that MDEs will not alter the MMHg concentrations in the snowpack because Hg^0 is not oxidized directly to MMHg.

2.3 Biological transformation and toxicity of mercury

Only the bioavailable fraction of Hg can be biotransformed. However, this fraction is difficult to quantify with traditional chemistry techniques (Harkins et al., 2004; Morel et al., 1998). Lamborg et al. (2003) consider the fraction of Hg reduced upon the addition of Sn(II) or BH_4^- to a sample in which organic matter has not been destroyed to be the bioavailable fraction. This is thought to correspond to the fraction that is inorganically bound (Morel et al., 1998).

Sulfate reducing bacteria (SRB) are thought to methylate Hg co-incidentally during metabolism of organic substrates (Benoit et al., 2001c; Morel et al., 1998). Researchers have demonstrated the ability of pure laboratory SRB cultures (Benoit et al., 2001c; Ekstrom et al., 2003) and environmental isolates (Ekstrom et al., 2003) to methylate Hg under controlled conditions. The role of SRB in MMHg production has also been demonstrated by the decrease in MMHg production when molybdate (a SRB inhibitor) is added to methylating cultures (Ekstrom et al., 2003).

Choi et al. (1994) concluded that a corrinoid-containing protein in the acetyl-coenzyme A (CoA) pathway is involved in Hg methylation in *Desulfovibrio desulfuricans*. Acetyl-CoA breaks down acetate into CO and a methyl group after which both are oxidized to CO_2 (Ekstrom et al., 2003). Although the mechanism of Hg methylation has been investigated (Choi et al., 1994; Ekstrom et al., 2003; Siciliano and Lean, 2002), it has yet to be conclusively resolved for all species of SRB.

In 2006, Fleming et al. demonstrated that the iron-reducing bacterium (IRB), *Geobacter* sp., methylated mercury at environmentally significant rates (Fleming et al., 2006). Kerin et al. (2006) observed the ability to methylate Hg in *Desulfuromonas palmitatis* SDBY-1, *Geobacter metallireducens*, *G. sulfurreducens*, and *G. hydrogenophilus*. Although the pathway of Hg methylation by these IRB has not been elucidated, results indicate that the ability to methylate Hg is not ubiquitous, but may be common among the *Geobacteraceae* (Kerin et al., 2006).

Lindberg et al. (2002), in the first study of Hg bioavailability in the Arctic, reported the bioavailable fraction of Hg in snow samples using the *mer-lux* bioreporter *Vibrio anguillarum*. The bioavailable fraction of Hg in snow prior to polar sunrise was undetectable rising to 0.22ng L^{-1} (~1% of total Hg) on March to 8.8ng L^{-1} (~13% of total Hg) in May (Lindberg et al., 2002).

MMHg has been identified in the High Arctic snowpack, meltwater, lakes, ponds and groundwater (Loseto et al., 2004; St. Louis et al., 2005). Both St. Louis et al. (2005) and Loseto et al. (2004) observed an initial pulse of MMHg in snowmelt (0.24 ng L^{-1} and 0.14 ng L^{-1}, respectively) indictating that snowmelt is a source of MMHg to High Arctic ecosystems.

2.3.1 Organo-mercury complexes

In natural waters, Hg exists as dissolved gaseous Hg (Hg^0) and inorganic and organic complexes. The three major organic forms are: monomethylmercury (MMHg, CH_3Hg^+), dimethylmercury (DMHg, $(CH_3)_2Hg$) and ethylmercury (EtHg, $CH_3CH_2Hg^+$) (Morel et al., 1998). Methylation of inorganic Hg occurs primarily in the anoxic layer of the water column and in sediments (Morel et al., 1998). Each oxidation state and organic species of Hg has different melting points, vapor pressure, solubility and air-water and octanol-water partitioning (Table 2.1). Organo-mercury complexes form when an alkyl group(s), such as CH_3^-, bonds to a Hg^{+2} ion. This reaction does not occur spontaneously in aqueous systems because the alkyl group is a strong base, which is highly unstable in water (Morel et al., 1998). Consequently, these reactions are photochemically or biologically catalyzed. Methylmercury is usually present as chloro- and hydroxo- complexes in oxic waters (Morel et al., 1998).

Methylation of Hg has received attention because of the health hazard it poses. However, the methylmercury concentration in aquatic systems depend upon the balance of methylation and demethylation reactions (Compeau and Bartha, 1984; Hintelmann et al., 2000; Marvin-Dipasquale et al., 2000; Marvin-Dipasquale and Oremland, 1998; Siciliano et al., 2005). Demethylation can occur via biotic (Compeau and Bartha, 1984; Hintelmann et al., 2000; Marvin-Dipasquale et al., 2000; Marvin-Dipasquale and Oremland, 1998; Schaeffer et al., 2002) and abiotic (Sellers et al., 1996; Siciliano et al., 2005) processes. Reductive demethylation (RD) and oxidative demethylation (OD) are two known biotic pathways of methylmercury degradation (Compeau and Bartha, 1984; Marvin-Dipasquale et al., 2000; Marvin-Dipasquale and Oremland, 1998; Schaeffer et al., 2002). Reductive methylation occurs when methylmercury is cleaved to produce Hg^{+2} and CH_4. This reaction is catalyzed by organomercurial-lyase (Marvin-Dipasquale et al., 2000). Marvin-Dipasquale and Oremland (1998) propose that RD is a result of co-metabolism of MMHg by methanogens and SRB. Isotope ratios in reaction products from this study suggest that under low MMHg concentrations methanogens are the primary demethylators whereas under higher MMHg concentrations SRB are more involved.

Table 2.1 Physical and chemical properties of mercury and some of its compounds. Values stated with temperature conditions in parentheses.

Property	Hg^0	$HgCl_2$	HgO	HgS	CH_3HgCl	$(CH_3)_2Hg$
Melting point (ºC)	-39	277	500[1]	584[2]	167[2]	-
Boiling point (ºC at 101.3 KPa)	357	303	-	-	-	96
Vapor pressure (Pa)	0.180 (20ºC)	8.99×10^{-3} (20ºC)	9.20×10^{-12} (25ºC)	n.d[3]	1.76 (25ºC)	8.30×10^{3} (25ºC)
Water solubility (g L^{-1})	49.4×10^{-6} (20ºC)	66 (20ºC)	5.3×10^{-2} (25ºC)	$\sim 2 \times 10^{-24}$ (25ºC)	~5-6 (25ºC)	92.95 (24ºC)
Henry's law coefficient (Pa $m^3 mol^{-1}$)	729 (20ºC)	3.69×10^{-5} (20ºC)	3.76×10^{-11} (25ºC)	n.d	1.6×10^{-5} (25ºC, pH 5.2)	646 (25ºC)
Octanol-water partition coefficient (unitless)	4.2	0.5	-	n.d.	2.5	180

Adapted from Schroeder and Munthe (1998) and references cited therein

[1]Decomposes

[2]Sublimates

[3]not defined

Photodegradation of MMHg has been observed in field studies (Sellers et al., 1996; Siciliano et al., 2005). Bloom et al. (2001) propose that photodegradation of MMHg occurs by indirect photolysis via a hydroxyl radical [2.5] and [2.6].

$$CH_3Hg^+ + \cdot OH \rightarrow CH_3OH + Hg^+ \quad [2.5]$$

$$Hg^+ + \cdot OH \rightarrow Hg^{+2} + OH^- \quad [2.6]$$

Abiotic MMHg degradation may also occur by disproportionation to DMHg (Compeau and Bartha, 1984; Wood, 1985). This reaction is mediated by H_2S (Wood, 1985) (reaction 2.7).

$$2CH_3Hg^+ + H_2S \rightarrow (CH_3)_2Hg + HgS + 2H^+ \quad [2.7]$$

2.3.2 Bioconcentration and biomagnification

The combination of physical, chemical and biological processes that Hg undergoes in air and water allow it to bioconcentrate in tissues and biomagnify in aquatic food webs (Casarett and Doull, 2001; Steffen et al., 2003; WHO, 1990). After MMHg is produced it enters aquatic food chains via plankton (Casarett and Doull, 2001; WHO, 1990). Unlike inorganic Hg, MMHg is lipophilic and concentrates in a water-soluble form in muscle tissue (Casarett and Doull, 2001). Mercury is bioconcentrated in individuals, which are consumed and the MMHg in their tissues is bioconcentrated yet further in the next trophic level (Morel et al., 1998). Finally, in fish-consuming sea mammals at the top of the aquatic food chain, Hg levels rise up to a millionfold higher than in the surrounding water (Casarett and Doull, 2001). Figure 2.1 diagramatically presents the Hg cycle, methylation, and a model food web.

2.3.3 Exposure

In the absence of occupational exposure to Hg, diet is considered the primary route of exposure (WHO, 1990). Traditional or country foods are an integral part of the social, cultural, spiritual, nutritional and economic well-being of Aboriginal peoples in the Canadian Arctic (Van Oostdam et al., 2003). In a survey conducted by Indian and Northern Affairs (Van Oostdam et al., 2003) aboriginal peoples identified over 250 species of wildlife, plants and animals in their diet. The most frequently mentioned traditional/country foods include salmon, whitefish, grayling, Arctic char, beluga muktuk, ringed seal and narwhal muktuk (Van Oostdam et al., 2003) all of which may have high concentrations of MMHg. Unlike inorganic Hg, whose gastrointestinal absorption is low (~15%), MMHg is efficiently absorbed (90-95%)

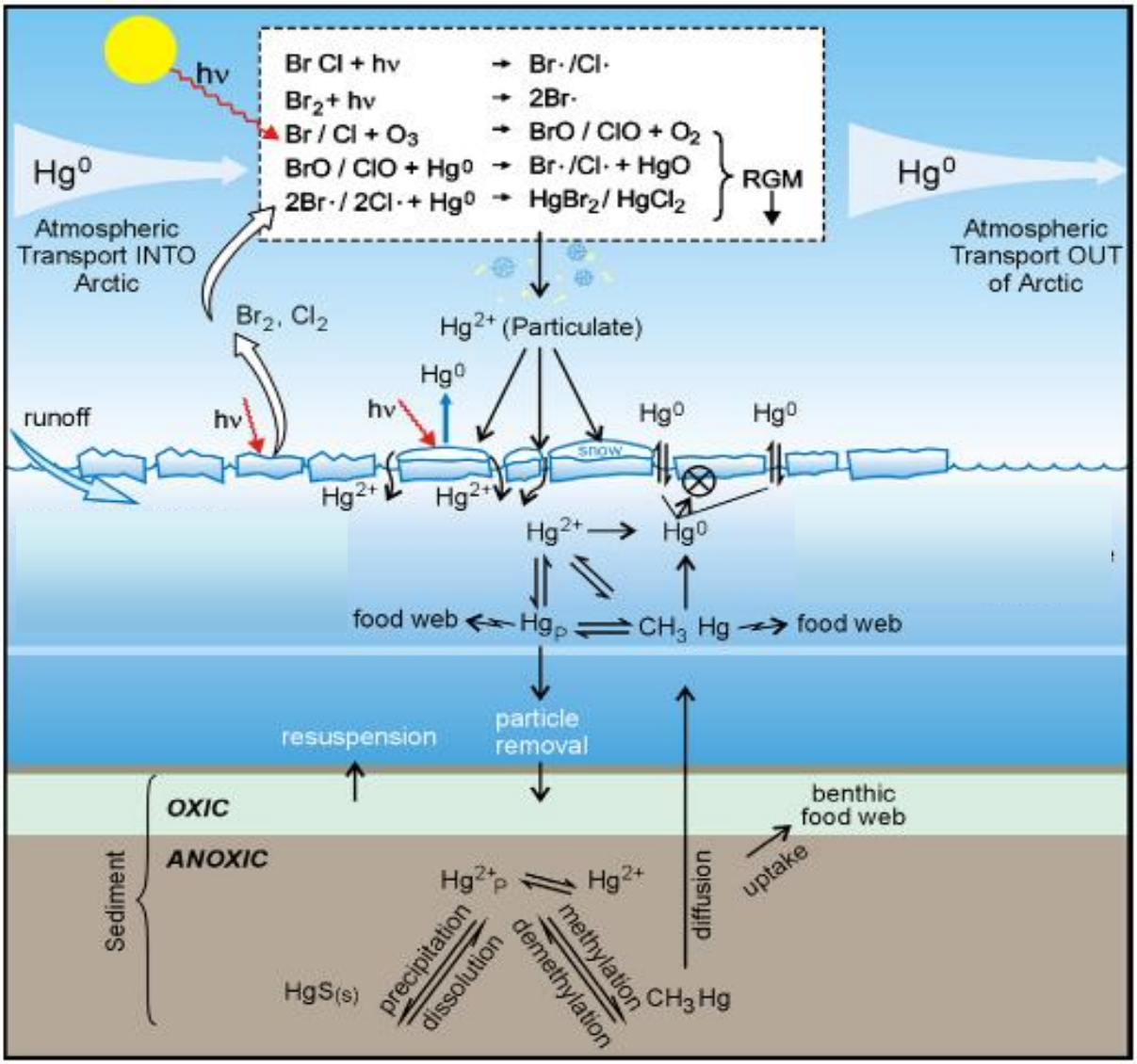

Figure 2.1 A schematic diagram illustrating the mercury cycle in the Arctic. The chemical processes initiated by light radiation after polar sunrise are listed in the inset box (Macdonald et al., 2005). (RGM = reactive gaseous mercury; hν = ultraviolet radiation).

(Casarett and Doull, 2001). Methylmercury is stored in edible, high protein tissues rather than fat and cooking does not decrease Hg content (Casarett and Doull, 2001). There is a wide variation in the Hg body burden amongst Arctic residents (Table 2.2) and this is postulated to be due to differences in diets by region (Gregor et al., 2003).

2.3.4 Mechanism of toxicity

Monomethylmercury, due to its toxicity and ability to bioaccumulate in the food chain, poses a great human health risk (Casarett and Doull, 2001; Morel et al., 1998; WHO, 1990). Organic Hg compounds, which can cross the blood brain barrier and placenta, have a high affinity for the brain, particularly the posterior cortex (Casarett and Doull, 2001). Mercury vapor also has an affinity for the central nervous system whereas inorganic Hg tends to accumulate in the kidneys (Casarett and Doull, 2001; WHO, 1990). Within body tissues, elemental and MMHg are biotransformed to Hg^{+2}. Oxidized Hg^{+2} may bind to a variety of enzyme systems within cells causing cell injury or death (Casarett and Doull, 2001; WHO, 1990). Mercury has a particular affinity for ligands (enzymes, genetic material) containing sulfhydryl groups (Casarett and Doull, 2001). The earliest biochemical effects following MMHg exposure in animals is inhibition of protein synthesis (Casarett and Doull, 2001).

In adults neurotoxic effects are the major human health effect resulting from exposure to MMHg (Casarett and Doull, 2001). Neurotoxic effects in adults are: 1) parasthesia, numbness and tingling around the mouth, lips and extremities; 2) ataxia, a clumsy, stumbling gait, difficulty in swallowing and articulating words; 3) neurasthenia, a generalized sensation of weakness, fatigue and inability to concentrate; 4) vision and hearing loss; 5) spasticity and tremor; and in serious cases 6) coma and death (Casarett and Doull, 2001). Toxicity to the fetuses of mothers exposed to MMHg during pregnancy is also a concern. Exposure of a fetus *in utero* to high levels of Hg results in abnormal neuronal migration and poor organization of neuron clusters (Casarett and Doull, 2001; WHO, 1990).

2.4 Reaction and Speciation of Mercury

Dissolved Hg in aqueous systems exists as a complex ion with inorganic and organic ligands rather than as a free ion (Morel et al., 1998). The speciation of Hg is dependent on the pH, redox potential, the strength of dissolved organic matter (DOM) interactions, the amount of DOM, the concentration of preferred inorganic ligands and the distribution of Hg between the dissolved and solid phases (Haitzer et al., 2003; Morel et al., 1998). Mercury is a "soft metal"

Table 2.2 Concentration and range of mercury in maternal blood, by ethnicity and region, values are geometric means followed by range of values in parentheses, (μg L^{-1} whole blood)

				Inuit				
	Caucasian (n = 134)	Dene and Métis (n = 92)	Other (n = 13)	Baffin (n = 31)	Inuvik (n = 31)	Kitikmeot (n = 63)	Kivalliq (n = 17)	Nunavik (n = 162)
Mercury (total)	0.9 (nd[1] - 4.2)	1.4 (nd - 6.0)	1.3 (0.20 - 3.4)	6.7 (nd - 34)	2.1 (0.60 - 0.24)	3.4 (nd - 13)	3.7 (0.60 - 12)	10.4 (2.6 - 44)
Mercury (organic)	0.69 (0.0 - 3.6)	0.80 (0.0 - 4.0)	1.2 (0.0 - 3.0)	6.0 (0.0 - 29)	1.8 (0.0 - 21)	2.9 (0.0 - 11)	2.7 (0.4 - 9.7)	not available

Adapted from van Oostdam (2003)

[1] non detectable

and prefers ligands of sulfur, less electronegative halides and nitrogen (Stumm and Morgan, 1995). Consequently, sulfide and chloride are important in the speciation of Hg. Table 2.3 presents thermodynamic stability constants (reported as log K) for some important inorganic Hg complexes. The generic formula for calculating these stability constants is:

$$Hg^{+2} + L^{n-} \rightarrow HgL^{(2-n)+} \quad [2.7]$$

$$k = (HgL^{(2-n)+}) / (Hg^{+2})(L^{n-}) \quad [2.8]$$

where round brackets indicate chemical activity of a species.

Reactions of inorganic Hg occur relatively quickly and Hg species, including those associated with the particulate phase, are considered to be in equilibrium (Morel et al., 1998). However, Lamborg et al. (2003) concluded that complexation of reducible Hg (Hg_r) with organic ligands is not instantaneous and occurs with a pseudo-first-order rate constant, [2.9], where k = 0.01 min^{-1}, and w is the rate constant for adsorption to the bottle walls.

$$[Hg_r]_t = [Hg_r]_0 e^{-(k+w)t} \quad [2.9]$$

Recent experimental evidence suggests that dissolved organic matter (DOM) is responsible for complexing a large proportion of Hg in aquatic systems (Haitzer et al., 2003; Lamborg et al., 2003; Ravichandran, 2004; Ravichandran et al., 1998). The interactions between Hg and DOM are discussed in section 2.4.3.

2.4.1 Sulfide-mercury interactions

Sulfur is present in natural aqueous systems and undergoes microbially mediated reduction and oxidation (Kirk, 2004). Sulfur exists as sulfate (SO_4^{-2}), sulfide ($S^{-2}/HS^-/H_2S$) and elemental sulfur (S^0). Under reducing conditions dissimilatory sulfate-reducing bacteria transform sulfate to sulfide to obtain energy (Morel et al., 1998). Sulfide is very reactive and forms strong complexes with metals such as Hg (Morel et al., 1998). In sulfidic waters Hg speciation is dominated by sulfide and bisulfide complexes such as HgS_2H_2, HgS_2H^-, and HgS_2^{-2} (Jay et al., 2000; Morel et al., 1998). The solubility of HgS increases with pH as does the concentration of dissolved mercuric sulfide species (Jay et al., 2000; Morel et al., 1998)

Polysulfides form readily in sulfidic waters by reaction of sulfide with elemental sulfur or as intermediates in the biological oxidation or reduction of sulfur (Jay et al., 2000). The chemical formula of polysulfide complexes is S_x^{-2} (where x = 3-6) (Jay et al., 2000). Jay et al. (2000) observed a marked increase in the solubility of cinnabar in the presence of polysulfides. In the presence of polysulfides, dissolved Hg species were 3-fold higher at pH 4 and 200-fold higher at

Table 2.3 Thermodynamic stability constants for some Hg_2^{+2}, Hg^{+2} complexes

Ionic complexes

Hg(I)	Complex[1]	Hg_2Cl_2							
	logK	12.4							
Hg(II)	Complex[2]	$HgCl^+$	$HgCl_2$	$HgCl_3^-$	$HgCl_4^-$	$HgOH^+$	$Hg(OH)_2$	$Hg(OH)_3^-$	HgClOH
	logK	7.2	14	15.1	15.4	10.6	21.8	20.9	18.1
	Complex[3]	HgS	HgS_xHS^-	HgS_x^0	HgS_xS^{2-}	HgS_xOH^-	$Hg(S_x)_2^{2-}$		
	logK	39.1	3.8	5.9	11.7	15.4	11.7		
	Complex[1]	$HgCO_3$	$Hg(CO_3)_2^{-2}$	$HgHCO_3^+$	$HgOHCO_3^-$				
	logK	4.5	17.7	0.35	11.4				

[1] Smith and Martell, 1989
[2] Smith, Martell, and Moitekaitis, 2003
[3] Paquette, Helz and Jay data as cited by Jay, Morel and Hemond, 2000
[4] Martell et al., 1998
[5] Drexel et al., 2002
[6] Tiffreau et al., 1995

Table 2.3 Continued

Organic Complexes

Complex[4]	Cysteine	EDTA	Glycine	Thioglycolic acid
logK	14.4	21.5	10.3	34.5

Complex[5]	Peat $_{strong}$	Peat $_{weak}$	DOM $_{strong}$	DOM $_{weak}$
logK	22	11.8	23.2	7.3

Hydrous Ferric Oxide Complexes

Complex[6]	S-OHg^{+}	S-OHgOH	S-OHgCl
logK	6.9	-0.9	9.8

[1] Smith and Martell, 1989
[2] Smith, Martell, and Moitekaitis, 2003
[3] Paquette, Helx and Jay data as cited by Jay, Morel and Hemond, 2000
[4] Martell et al., 1998
[5] Drexel et al., 2002
[6] Tiffreau et al. 1995

pH 11. When Hg is in equilibrium with cinnabar the presence of polysulfides may increase bioavailability of Hg by increasing the concentration of dissolved species (Jay et al., 2000). Figure 2.2 shows the unique structure of a polysulfide ($HgS_4(SH)^{-1}$).

2.4.2 Effect of pH on mercury chemistry

Changes in pH can alter Hg speciation, adsorption/desorption and precipitation/dissolution reactions thereby influencing aqueous Hg concentrations (Freeze and Cherry, 1979). The pH of an aqueous system determines whether functional groups on surfaces are protonated or deprotonated. At high pH functional groups are deprotonated; at low pH functional groups tend to be protonated. Deprotonated sites are negatively charged and therefore present possible binding sites for Hg. The availability of surface binding sites for Hg changes with pH.

Speciation of Hg is affected by pH. At high pH (~9-11) under oxidizing conditions Hg primarily exists as hydroxyl species ($Hg(OH)^{+}$, $Hg(OH)_2$) while at low pH (~0-4) chloride complexes prevail ($Hg(Cl)^{+}$, $Hg(Cl)_2$, $Hg(Cl)_3^{-}$, $Hg(Cl)_4^{-2}$) (Freeze and Cherry, 1979; Ravichandran, 2004). In the normal pH range of groundwater, under oxidizing conditions and high chloride concentrations (10^{-1} molal Cl) the dominant aqueous species is $HgCl_2$ (Freeze and Cherry, 1979). Under low chloride concentrations (10^{-3} molal Cl) in normal groundwater pH range under oxidizing conditions the equilibrium solid phase is $HgO_{(s)}$ and the dominant aqueous species is $Hg(OH)_2$ (Freeze and Cherry, 1979). Figure 2.3 shows stability diagrams for aqueous and solid species of Hg for a range of pH and Eh conditions.

2.4.3 Effect of redox potential on mercury chemistry

Redox potential is a measure of the tendency of a system to oxidize or reduce compounds. High redox potential indicates oxidizing conditions, while under reducing conditions redox potential is low. Mercury, like other trace metals, is influenced by redox conditions through changes in oxidation state and/or changes in the oxidation state of its primary ligands (Freeze and Cherry, 1979). Much like pH, redox potential can also indirectly influence Hg concentrations through reduction and dissolution of Hg bearing compounds/minerals such as hydrous ferric oxides (HFO) (Davranche and Bollinger, 2000).

Mercury is oxidized and reduced in natural waters, and empirical evidence suggests that many redox reactions are photochemically induced

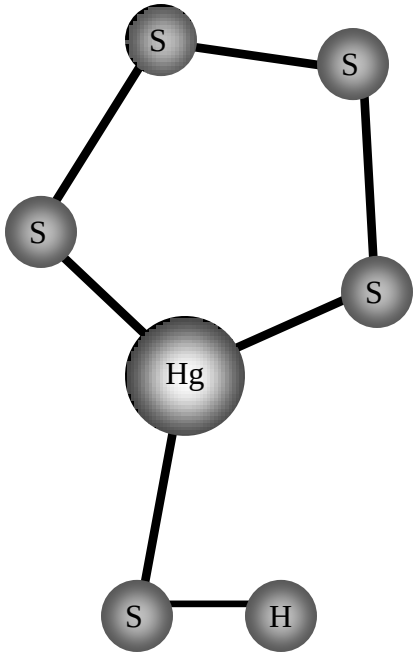

Figure 2.1 Calculated structure for $HgS_4(SH)^{-1}$, a model for the bisulfide, polysulfide species. Adapted from Tossell (1999).

(a)

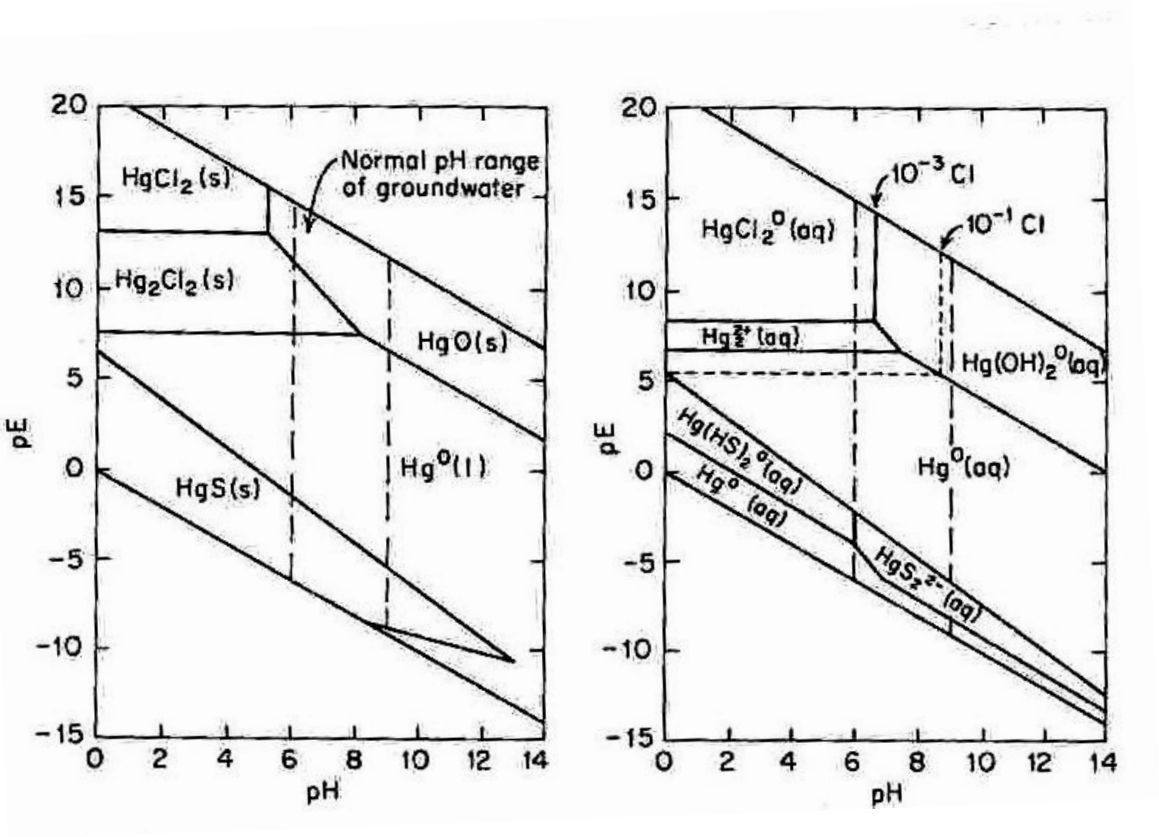

Figure 2.3 Stability diagrams for (a) solid and (b) aqueous mercury species by pH and pE. Stability diagram for solid species are calculated for conditions of 10^{-3} Cl^- and SO_4^{-2}. Stability diagram for aqueous species is calculated for conditions of 10^{-3} SO_4^{-2} and 10^{-1} Cl^- (Freeze and Cherry, 1979).

(Amyot et al., 1997; Amyot et al., 1994; Costa and Liss, 1999; Lalonde et al., 2001). Ababneh et al. (2006) found that Hg in natural waters is reduced according to reactions 2.10 and 2.11 (Ababneh et al., 2006),

$$Hg^{+2} + CO_2^{\bullet} \rightarrow Hg^{+} + CO_2 \quad [2.10]$$

$$2Hg^{+} \leftrightarrow Hg^{0} + Hg^{+2} \quad [2.11]$$

whereas, empirically derived evidence suggests that oxidation/reduction reactions are photochemically induced.

2.4.4 Mercury-dissolved organic matter (DOM) interactions

Dissolved organic matter is a heterogeneous class of compounds with variable chemical structure (Ravichandran, 2004). Approximately 20% of DOM is carbohydrate, carboxylic acids, amino acids, hydrocarbons and other structurally resolved compounds (Ravichandran, 2004). The remaining fraction consists of poorly resolved humic substances from the decomposition of plants and animals (Ravichandran, 2004). Dissolved organic matter affects the speciation, solubility, mobility and toxicity of Hg in natural waters (Benoit et al., 2001c; Lamborg et al., 2003; Ravichandran, 2004). Spectroscopic and indirect evidence (stability constants), suggest that Hg-DOM interactions are likely through covalent bonding at a thiol-type structure (Drexel et al., 2002; Haitzer et al., 2003; Ravichandran, 2004). Although sulfur is a small fraction (0.5% - 2% by weight) of DOM, the strong affinity of Hg for sulfur ligands makes reduced sulfur sites in DOM important in Hg binding (Ravichandran, 2004). A recent study by Drexel et al. (2003) indicate that thermodynamic stability constants derived for Hg^{+2} – thiolate complexes are high enough ($10^{26} – 10^{27}$) to compete with sulfide as a Hg ligand. These stability constants explain the results of Ravichandran et al. (1998) which report enhanced dissolution of cinnabar, a very insoluble solid ($K_{sp} = 10^{39.1}$, (Smith et al., 2004)), by DOM isolated from the Florida Everglades.

2.5 Transport of mercury in the environment

2.5.1 Solute transport in soil

Solute transport through porous media, such as soil and aquifers, occurs by advection and dispersion (Domenico and Schwartz, 1990). Advective transport is a result of the bulk movement of groundwater in which the solute is dissolved (Domenico and Schwartz, 1990). Dispersion, also known as mechanical dispersion, results from mixing between fluids of different compositions (Domenico and Schwartz, 1990).

Mechanical dispersion, on a microscopic scale, occurs by three mechanisms resulting from the heterogeneity of the porous media. First, drag exerted by the surface roughness of pores creates different fluid velocities at different points across the pore. The second dispersive process occurs due to different pore sizes along the flow path. A difference in surface area and roughness relative to the volume of water transported causes different pore channels to have different bulk fluid velocities. The third process is related to the branching, interfingering of pores and tortuosity of the pore channels which results in areas of different velocities. The processes described above create longitudinal (parallel to the flowpath) dispersion of solutes (Freeze and Cherry, 1979). Diffusivity of Hg in water at 23.6ºC is 2.9 x 10^{-5} cm^2 s^{-1} and the diffusivity of Hg in air at 25ºC is 0.131 cm^2 s^{-1} (Thibodeaux, 1996).

2.5.1.2 Diffusion

Diffusion of ions or molecules, a result of their kinetic energy, occurs in the absence of bulk hydraulic movement and causes molecules to move from areas of high concentration to areas of low concentration (Freeze and Cherry, 1979). When a concentration gradient is non-existent, molecules continue to move due to their kinetic energy, but net diffusion ceases. Temperature has a large effect on diffusion whereas the effect of ionic strength is very small (Freeze and Cherry, 1979).

The mass of a solute passing through a given cross section per unit time is proportional to the concentration gradient (Freeze and Cherry, 1979). Mass flux due to diffusion can be described using Fick's first law.

$$F = -D\,(dC/dx) \qquad [2.12]$$

where F, mass flux, is the mass of solute per unit area per unit time (M/L^2T); D is the diffusion coefficient (L^2/T); C is the solute concentration (M/L^3) and dC/dx is the concentration gradient (negative in the direction of diffusion) (Freeze and Cherry, 1979). The diffusion coefficient in equation 2.11 is the value obtained for pure water. The rate of diffusion in porous media is less than in pure water because of the presence of particles in the matrix (Freeze and Cherry, 1979). An apparent diffusion coefficient (D^*) taking into account the effect of the porous medium is represented in by the mathematical relationship:

$$D^* = \omega D \qquad [2.13]$$

where ω is an empirical coefficient (less than 1) related to the tortuosity. In laboratory studies values of ω between 0.5 and 0.01 are commonly observed. Fick's (Freeze and Cherry,

1979) second law, relates the concentration of a diffusing solute in one dimension to space and time. The expression of Fick's second law is:

$$\partial C/\partial t = D^{*}(\partial^2 C/\partial x^2) \quad [2.14]$$

Mercury is a reactive substance and therefore mechanical dispersion and diffusion alone cannot adequately describe its movement in the subsurface. In porous media Hg is subject adsorption/desorption, precipitation/dissolution, cation exchange, biotransformation and volatilization (Figure 2.4). Considering the law of the conservation of matter a generic statement for the transport of Hg in the subsurface is:

ΔC = [flux of Hg out of the element] – [flux of Hg into the element] ± [loss or gain of Hg due to reactions adsorption/desorption, precipitation/dissolution, volatilization] (adapted from Freeze and Cherry, 1979). [2.15]

2.5.2 Facilitated/colloidal transport in soil

Facilitated transport has three stages: 1) adsorption of solute to the colloid/particle; 2) colloid/particle mobilization; and 3) transport of the colloid/particle. Physical and chemical perturbation mobilize colloids, resulting in brief, rapid release of colloids into groundwater (Lowry et al., 2004; Slowey et al., 2005). Conditions of low ionic strength and high pH are conducive to colloid release (Slowey et al., 2005). Facilitated transport results in solute velocities greater than bulk fluid velocities. A host of colloidal/particulate materials are known to facilitate transport of solutes, such as Hg. Aluminum, iron and silicon oxides, amorphous hydrous ferric oxides (HFO), clay minerals, and bacteria act as vectors for Hg transport (Davranche and Bollinger, 2000; Freeze and Cherry, 1979; Guine et al., 2003; Lowry et al., 2004; Rancourt et al., 2005; Slowey et al., 2005; Tiffreau et al., 1995).

2.5.2.1 Bacteria

Bacteria are ubiquitous in the soil and groundwater environment (Freeze and Cherry, 1979; Sparks, 2003). Sorption and desorption rates affect bacterial transport through porous media (Murphy and Ginn, 2000). The physicochemical characteristics of the bacterial surface (Becker et al., 2004; Murphy and Ginn, 2000) and the physical properties of the porous medium (Hall et al., 2005; Jordan et al., 2004; Murphy and Ginn, 2000) affect sorption/desorption and thus, transport. In a review of microbial processes in porous media Murphy and Ginn (2000) report that ionic strength, pH and mineralogy are important factors in bacterial sorption. Oates et

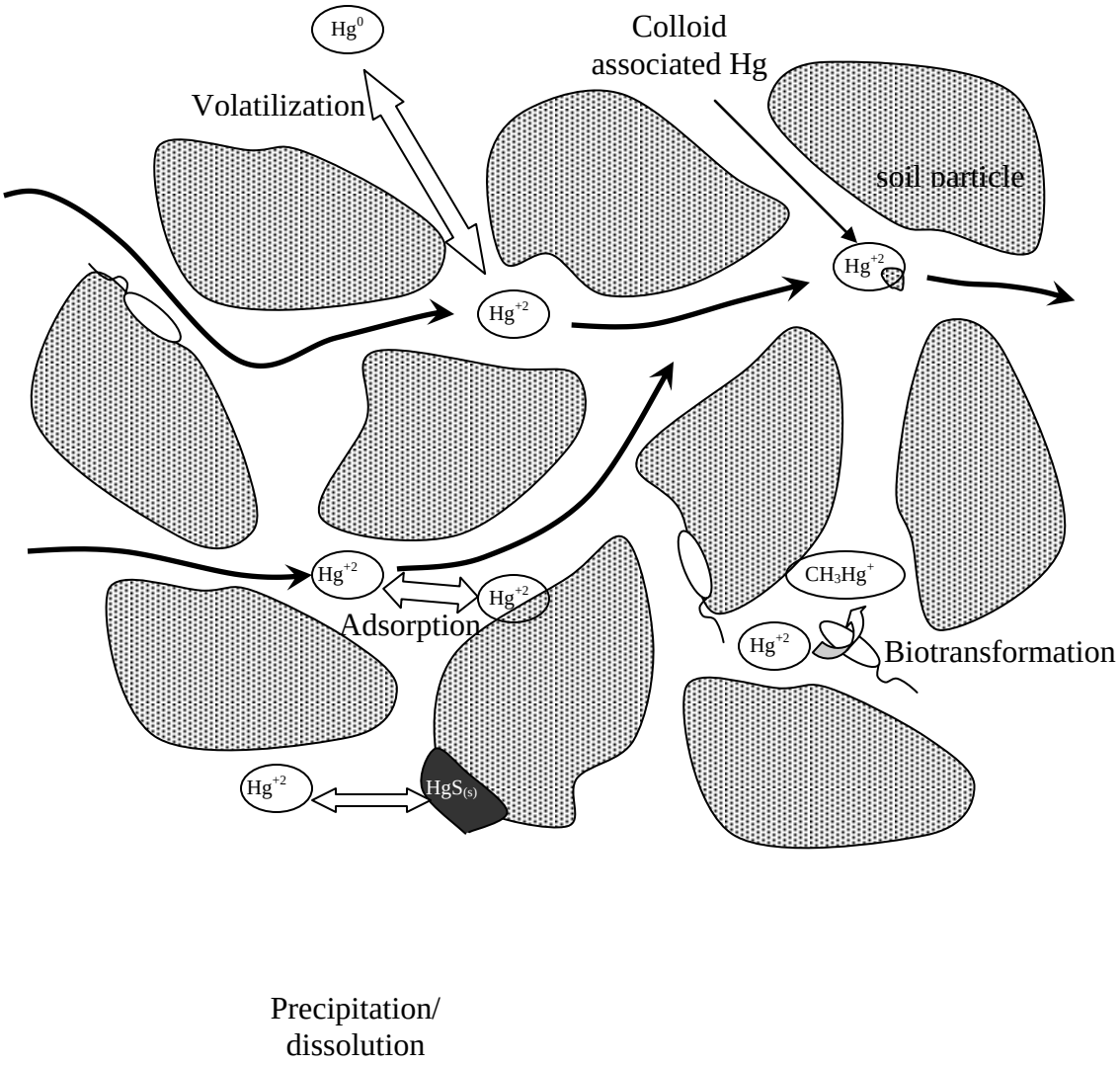

Figure 2.4 Potential mass transfers of mercury during transport through porous media.

al (2005) cite metabolic activity, supply of nutrients/electron acceptors, and population growth as biotic factors affecting transport.

Microbes experience physical transport phenomenon that accelerate and retard their movement, and that of adsorbed ions, in the subsurface. Straining, retardation of particles that exceed pore throat diameters, (Murphy and Ginn, 2000; Oates et al., 2005) is known to retard bacterial transport. Whereas, microbes and other large colloids, because of their size preferentially experience higher velocities near pore centerlines yielding a higher average velocity than bulk groundwater (Murphy and Ginn, 2000). This phenomenon is known as size exclusion (Murphy and Ginn, 2000).

Guiné et al. (2003) investigated the transport of Hg through Fontainbleu sand. In a sterile column experiment Hg had a retardation factor of 1.4. In the presence of *Ralstonia metallidurans CH34* and *Echerichia coli pGreen* (DSHα) no retardation was observed. Furthermore, transport of bio-sorbed metal was 4 to 6 times faster than the transport of dissolved metal by advection alone. The ability of microbes to adsorb metals to their cell wall is well documented in the literature (Boyanov et al., 2003; Daughney et al., 2001; Daughney et al., 2002; Ferris, 1989; Hard et al., 1999). Recently, adsorption of specific metals such as aluminum (Hard et al., 1999), cadmium (Boyanov et al., 2003; Daughney et al., 1998; Daughney et al., 2001), europium (Markai et al., 2003), and Hg (Daughney et al., 2002) has been investigated. Metals associated with the cell wall of bacteria may undergo facilitated transport when bacteria enter the bulk solution.

The ability of microbes to adsorb metals is based on deprotonation of functional groups on the cell surface (Doyle, 1989; Ferris, 1989; Geesey and Jang, 1989). The gram-negative cell wall has an outer lipid bi-layer in which the hydrophilic heads of amphipathic lipids are exposed to the external environment (Ferris, 1989). These molecules, with their carboxyl and phosphoryl functional groups, determine the surface reactivity of the cell (Ferris, 1989). The cell wall of gram-positive bacteria contain large amounts of peptidoglycan and an anionic polymer such as teichoic or teichuronic acid (Doyle, 1989). Carboxyl functional groups, from the peptidoglycan, and phosphoryl functional groups, from the teichoic acid on the gram positive cell wall act as sites for metal sorption (Doyle, 1989).

2.5.2.2 Colloidal/particulate organic carbon

Organic matter can exist in the dissolved and particulate phase. Particulate organic carbon (POC) is operationally defined as the fraction that does not pass through a 0.45μm filter. Bacteria make up approximately 80% of the surface area of POC in freshwater lakes (Daughney et al., 2002). The large proportion of bacterial surface area and their reactive surfaces (discussed in the previous section) make POC a good vector for Hg transport in the subsurface. The remaining 20% of POC, largely detritus from plant and animal decay, has functional groups capable of binding Hg. Daughney et al. (2002) were able to accurately predict the association of Hg with the particulate phase using a surface complexation model (SCM). The SCM including chloride concentration, POC, and DOC as input parameters provided the best fit of Hg distribution in surface waters of Kejimkujik Park, NS (Daughney et al., 2002).

2.4.2.3 Hydrous ferric oxides

Hydrous ferric oxides (HFO) exist in most oxic aquatic environments and have the capacity to adsorb metals (Davranche and Bollinger, 2000; Rancourt et al., 2005; Tiffreau et al., 1995). Ferrihydrite, $Fe_5HO_8 \cdot 4H_2O$, a HFO, is semicrystalline and is commonly found in soils (Schwertman and Cornell, 1991 as cited by Sparks, 2003). Tiffreau et al. (1995) determined that sorption of Hg to amorphous HFO can be described using the surface complexation approach. Tiffreau et al. (1995) modeled the adsorption of Hg to HFO and found that sorption takes place at hydroxyl surface sites. In the study, the surface phase varied from a combination of adsorbed ion and pure precipitate to a pure precipitate. Interaction of Hg with HFO includes processes such as: adsorption, surface precipitation and coprecipitation or substitution (Davranche and Bollinger, 2000; Tiffreau et al., 1995). Equilibrium constants for the binding of Hg species with HFO are included in Table 2.3. Hydrous ferric oxides persist in oxic waters, but undergo reduction and dissolution in low Eh conditions. Davranche and Bollinger (2000) found that under reductive conditions solubilization of adsorbed or coprecipitated metals in HFO was increased. The rate of solubilization was dependent upon the crystalline state of the solid and whether the metal was coprecipitated within the HFO or adsorbed to the HFO surface (Davranche and Bollinger, 2000).

2.6 High Arctic Hydrology

2.6.1 Physics and chemistry of snowmelt

The energy balance near the upper boundary of the snowpack controls melt rate (Pomeroy and Brun, 2001). In cold climates the change in internal energy (*dU/dt*) is an important term in the energy balance during snowmelt (Pomeroy and Brun, 2001). Energy deficits at night must be compensated for the following day before the pack can become isothermal at 0ºC and begin to release water (Pomeroy and Brun, 2001). Meltwater is released from the snowpack in a diurnal cycle corresponding to the cycling of energy inputs (Pomeroy and Brun, 2001). The energy balance for melting snow is:

$$Q_m = K^* + L^* + Q_H + Q_E + Q_G + Q_R - \left(\frac{dU}{dt} \right) \qquad [2.16]$$

where Q_m is the energy available for melting a certain volume of snow, K^* is the net shortwave radiation flux, L is the net long-wave radiation flux, Q_H is sensible heat flux, Q_E is latent heat flux, Q_G is ground heat flux, Q_R is the energy flux from precipitation and dU/dt is the change in internal energy of the snow pack (Pomeroy and Brun, 2001). Incoming radiation is the dominant energy flux at the beginning of melt with sensible heat growing in contribution through the melt (Pomeroy and Brun, 2001).

The chemistry of snow crystals varies according to atmospheric conditions at the time of formation (Tranter and Jones, 2001) and post-deposition metamorphism (Cragin et al., 1996; Kuhn, 2001; Tranter and Jones, 2001). Incorporation of solute into the snow crystals occurs by three main processes: 1) imprisonment during initial formation of ice crystals, 2) capture of gases, aerosols and particulates within clouds, and 3) scavenging of these materials below the cloud layer during snowfall (Barrie, 1991, as cited by Tranter and Jones, 2001). The main soluble species present in snow crystals are NH_4^+, SO_4^{-2}, NO_3^-, Ca^{+2}, K^+, Mg^+, Na^+ and Cl^- (Kuhn, 2001; Tranter and Jones, 2001). Some snow, such as rimed snow or soft snow pellets, contain more concentrated solutes because the rapidly cooled water droplet captures solute, unlike snow formed by vapor transport (Tranter and Jones, 2001).

The chemical composition of the snowpack and meltwaters are influenced by two types of processes: 1) those involving the heat and mass fluxes that occur during melt and sublimation, and 2) those involved in chemical transformations (Pomeroy and Brun, 2001). Areas of concentrated solute are present at the snow-grain surface where water exists in a quasi-liquid

state (Cragin et al., 1996). These droplets contain most of the solute and during the melt period, as wet metamorphism occurs, large grains of snow grow at the thermal expense of smaller grains. Anion exclusion during refreezing creates droplets of even more concentrated solute (Cragin et al., 1996; Tranter and Jones, 2001). As meltwater runs through the snowpack it leaches solute from snow grains causing fractionation of solute species between the snow grain and the liquid medium (Tranter and Jones, 2001). During the initial stages of snowmelt the progressing meltwater front becomes more concentrated with solutes; however, by the end of the snowmelt period solute concentrations in the meltwater are much more dilute (Cragin et al., 1996; Kuhn, 2001; Tranter and Jones, 2001). Temporally, this creates an initial pulse of solute in meltwater (Tranter and Jones, 2001). Laboratory investigations indicate that approximately 80% of the solute in the snow pack is eluted in the first 30% of the meltwater (Cragin et al., 1996; Kuhn, 2001).

Volatilization, photochemical reactions, and microbial/algal activity are all known to influence snow and meltwater chemistry (Tranter and Jones, 2001). Although direct evidence supporting photochemical reactions is difficult to obtain, indirect evidence supports the existence of photochemical reactions in the snowpack (St. Louis et al., 2005; Tranter and Jones, 2001). Microbial activity is enhanced by the presence of liquid water and solar radiation during snowmelt (Tranter and Jones, 2001). Microbial and algal growth can markedly decrease nutrient concentrations in snow and meltwaters (Tranter and Jones, 2001).

2.6.2 Superpermafrost groundwater

Continuous and discontinuous permafrost underlies approximately one-half of Canada's land mass (Bliss, 1997). Permafrost is distinguished from seasonally frozen soil by remaining frozen for more than one year (Williams and Smith, 1979). The active layer, which thaws seasonally, often has a shallow profile, poor soil development and unique geomorphology resulting from cryoturbation (freeze-thaw induced churning) (Tedrow, 1977). Cryoturbation results in patterned ground features such as earth hummocks, sorted and non-sorted circles, nets, steps and stripes (Bliss, 1997) which influence lateral subsurface flow (Carey and Woo, 2000; Hodgson and Young, 2001; Quinton and Marsh, 1998; Quinton et al., 2000).

During the Arctic winter organic surface horizons lose water vapor to the snow pack resulting in desiccation, unrestricted infiltration and rapid saturation during snowmelt (Carey and Woo, 2000). Ice-rich permafrost in the profile, often found at the organic – mineral soil interface,

acts as a near-surface barrier to deep percolation resulting in rapid saturation of the organic layer from the base upward during snowmelt (Carey and Woo, 2000; Hinkel et al., 2001). Carey and Woo (2000) report that initial downward flow (percolation through the solum) yields to lateral and overland flow after saturation of the active layer. Likewise, in the Siberian Arctic Pokrovsky and Dupré (2006) observed percolation of meltwater through the solum followed by lateral movement of meltwater along the permafrost table. In rare cases of extremely high porosity (and low water retention capacity), lateral subsurface flow will begin prior to saturation of the active layer (Carey and Woo, 2000). Alternatively, when meltwater flux exceeds the infiltration capacity of the frozen soil and there is a strong negative thermal flux from the snow to the soil a basal ice layer may develop (Pomeroy and Brun, 2001). The basal ice layer may persist through snowmelt (Pomeroy and Brun, 2001) thus decreasing infiltration and increasing overland flow of meltwater (Figure 2.5).

Arctic soils are organized in layers of increasingly decomposed organic material over mineral soil (Hinkel et al., 2001). The lightly decomposed surface layer usually has a low bulk density, high porosity and high K_s (hydraulic conductivity). Bulk density increases while porosity and K_s decrease with depth through the organic layers. The underlying mineral soil typically has yet higher bulk density, and lower porosity and K_s (Carey and Woo, 2000; Hinkel et al., 2001; Quinton and Marsh, 1999). Hinkel et al. (2001) found distinct layers of differing hydraulic conductivities (anisotropy) in the organic layer of Alaskan soils. They attributed the decrease in hydraulic conductivity with depth to increasing humification and a resulting decrease in porosity.

Soils in the Canadian Arctic are spatially variable (heterogeneous) and have unique surface geomorphology resulting from cryoturbation (Tedrow, 1977). The effect of earth hummocks (Quinton and Marsh, 1998; Quinton et al., 2000), sorted nets (Hodgson and Young, 2001), and soil pipes (Carey and Woo, 2000) on water movement through saturated soil underlain by permafrost (i.e. superpermafrost groundwater) has been investigated. Results from these studies indicate that cryoturbation results in sorting of soil particles, and the creation of preferential flow pathways of higher hydraulic conductivity altering subsurface flow rates.

Quinton and Marsh (1998) found that earth hummocks (which are prevalent at Truelove Lowland) influence subsurface drainage in four ways: 1) concentrating flow in the inter-hummock area, 2) increasing the tortuosity of the flowpath, 3) attenuating flow by interacting

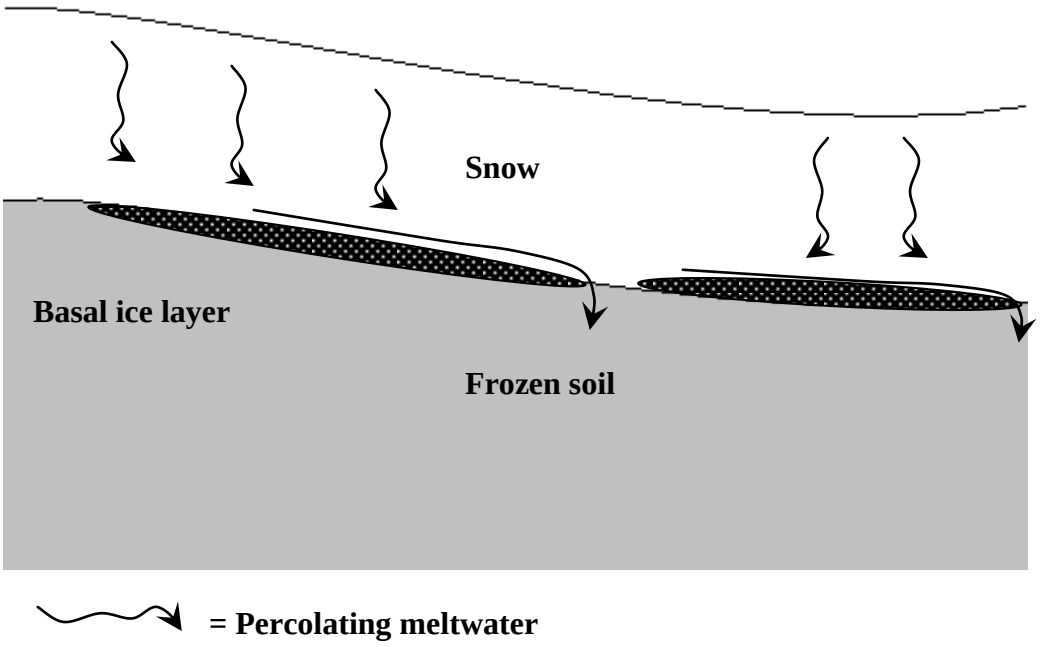

Figure 2.5 Diagram showing basal ice layer, which forms when the flux of meltwater reaching the base of the snowpack exceeds the infiltration rate of underlying frozen soil, and there is a strong negative thermal flux from the snowpack to the soil.

with the saturated layer of the inter-hummock area, and 4) increasing the water table elevation in the inter-hummock area by displacement. Earth hummocks, usually composed of silt and clays, can have a hydraulic conductivity of three to six orders of magnitude lower than the inter-hummock area and as a result flow is channeled preferentially through the inter-hummock area (Quinton and Marsh, 1998).

2.6.3 Biogeochemistry of saturated soils

Superpermafrost groundwater in the High Arctic saturates depressional soils (Fishback, 2002; Quinton and Marsh, 1998). Upon saturation, the microbial community and plant root respiration begin to consume oxygen in the soil and Eh begins to fall (Sparks, 2003). When microbes oxidize organic carbon an electron acceptor must be reduced (Kirk, 2004). Typically, there is a sequential consumption of electron acceptors (O_2, NO_3^-, Mn^{+2}, Fe^{+3}, SO_4^{-2}, CO_2) that corresponds to the metabolic activity of different functional groups of bacteria (Kirk, 2004). As each successive electron receptor is consumed the Eh falls further (Kirk, 2004) until it reaches an equilibrium. Heterogeneity at the aggregate and landscape level results in zones of differing redox potential across the landscape (Kirk, 2004).

2.7 Truelove Lowland, Devon Island, Nunavut

2.7.1 Polar Oases

A large proportion of the Canadian High Arctic is barren polar desert characterized by high winds, minimal precipitation, poorly developed soils and very little plant cover. Within the polar desert there are localized areas where biodiversity and productivity is high; these areas are known as polar oases (Tedrow, 1977). Truelove Lowland (approximately 75°40'N, 85°35'W) is located in the Canadian Arctic Archipelago on the northeastern coast of Devon Island, Nunavut. It is a polar oasis and coastal lowland approximately 42 km^2 (Fishback, 2002).

A scientific research base camp was established on Truelove Lowland in 1960 and in the early 1970's was an International Biological Programme (IBP) research site (Courtin and Labine, 1977; Ryden, 1977). During the IBP extensive research into the soils, vegetation, climate, hydrology, and ecology of Truelove Lowland was conducted. Since that time researchers have continued to investigate Truelove Lowland and extensive soil data has been collected. Truelove Lowland was selected as a field site because there is extensive background geology, pedology, soil microbiology and soil chemistry data available.

2.7.2 Climate

Recent climate information for Truelove Lowland has not been recorded; however, King (1969, cited by Fishback, 2002) reported mean annual air temperature for 1961-1962 as -16°C. In 1977 average daily summer temperatures at several sites across the lowland were 2.8°C to 9.5°C (Courtin and Labine, 1977). In June daytime air temperature exceeds 0°C and snow begins to melt. In early June large radiation inputs hasten snowmelt which usually occurs over a period of two to three weeks (Fishback, 2002), however, in cool years late-lying snowdrifts may persist.

2.7.3 Hydrological regime

The majority of precipitation on Truelove Lowland falls as snow. Rydén (1977) reported average annual precipitation of 185 mm y^{-1} with only 36 mm y^{-1} falling as rain from 1970-1973. Rainfall on Truelove Lowland is rare and when it occurs summer precipitation usually falls in a fine mist. The open landscape and high winds result in considerable snow redistribution (Ryden, 1977) leaving beach crests exposed and dry.

On Truelove Lowland, as in other cold regions, the redistribution of snow by wind and the behavior of meltwater have a profound influence on soil moisture (Pomeroy and Brun, 2001). Summer precipitation events are of low intensity resulting in extremely dry beach crest soils (Ryden, 1977). As the active layer develops saturated soil, superpermafrost groundwater, is perched on the permafrost. This results in saturated depressional soils during and immediately after snowmelt (Ryden, 1977).

2.7.4 Biota

The flora of Truelove lowland has high species richness with 97 species of vascular plants and about 172 species of bryophytes (Muc and Bliss, 1977). The high species richness is characteristic of polar oases and the species occur in 16 distinct plant communities on Truelove lowland (Muc and Bliss, 1977). Six plant communities cover the majority of the lowland and they are: hummocky sedge-moss meadow (21%), frost-boil sedge-moss meadow (18%), dwarf shrub heath-moss (12%), cushion plant-moss (7%), cushion plant-lichen (5%) and wet sedge-moss meadow (2%).

2.7.5 Geomorphology

Truelove lowland is bordered to the south by a Precambrian escarpment largely composed of metamorphosed gneiss and granulite (Krupicka, 1977). To the east the lowland is

bounded by a Cambrian escarpment which is largely composed of dolomite (Lev and King, 2002). During the Holocene the Devon Ice Cap began to retreat, pressure on the Devon Island land mass was relieved and isostatic rebound caused Truelove Lowland to slowly emerge from the sea. The lowland itself was formerly the ocean floor and is a thin veneer of marine deposit (Fishback, 2002; Lev and King, 2002). The lowland has reached a steady state with the rate of rebound equaling the rise in ocean level.

Topographically, Truelove Lowland is a series of raised beaches that increase in age from the west to the east where the beach ridges have been exposed for approximately 10,000 years. The raised beaches act as barriers to drainage creating ponds and lakes on the lowland. In low-lying areas hummocks and ice-wedge polygons are prevalent. There are two major rivers: Truelove River and the Gully River (Fishback, 2002).

2.7.6 Soil

The soils of Truelove lowland are underlain by permafrost (Tedrow, 1977; Walker and Peters, 1977) and belong to the Cryosolic soil order in the Canadian System of Soil Classification (Agriculture and Agri-Food Canada, 1998). The active layer ranges from 0.3 m in low-lying areas to 1.5 m on beach ridges (Fishback, 2002). The soils of Truelove Lowland can be described in a toposequence from beach ridge to wetland; the beach ridge soils are generally Regosolic Static Cryosols, the foreslope and backslopes are Brunisolic Static and Brunisolic Turbic Cryosols, and depressional soils are Gleysolic Turbic and Gleysolic Static Cryosols (Lev and King, 2002). Table 2.4 shows chemical properties of selected soil types and typical horizons.

Table 2.4 Chemical and physical data for selected Cryosols

Horizon	Depth (cm)	pH	Organic Carbon (%)	Total Nitrogen (%)	CaCO3 equiv. (%)	% coarse fragments	Particle Size Distribution sand (%)	Silt (%)	Clay (%)	Bulk Density (g cm^{-3})
Regosolic Static Cryosol in beach material										
Ahk	2-13	8.1	1.2	0.04	11.7	65	88	10	2	1.6
Ck	13-34	8.3	0	0.04	19.7	77	85	16	0	1.6
Ck	34-59	8.3	0	0.01	20.3	75	93	6	1	1.7
Ck	49-82	8.3	0	0.01	18.6	58	95	5	0	1.6
Brunisolic Static Cryosol in beach material										
Ahk	0-8	7.1	8.4	0.81	1.9	45	78	8	14	0.7
Bmk	8-23	7.7	1.4	0.1	11.7	51	86	9	5	1.4
Ck	23-61	7.8	0	0.02	20.2	56	86	12	2	1.7
Brunisolic Turbic Cryosol in beach material										
Ahky1	0-8	7.4	16.5	1.4	3.9	<40				
Ahky2	8-19	7.6	4.3	0.36	17.2	<30	81	9	10	
Bmky1	20-19	7.9			24	<20	84	10	6	
Bmky2	20-24	7.9			26.8	<20	79	15	6	
Cky	0-25	8.2	0.3	0.01	26.2	<20	65	26	9	
Cky	25-56	8.1			30.1	<20	65	27	8	
Gleysolic Turbic Cryosol in undifferentiated material										
Ofy	18-0	7.2	25.9	2.21	1.3	<20				
Ckg	0-40	7.9			23.3	<20	65	27	8	
Ckgy	40-51	8	0.5	0.01	25.3	<10	65	26	9	

Table 2.4 continued

Horizon	Depth (cm)	Exchangeable Cations (me/100g) Ca	Mg	N	K	Total Exchange Capacity (me100g^{-1})	Available Nutrients (μg g^{-1}) NO_3^-	P	K	Na	SO_4^{-2}
Regosolic Static Cryosol in beach material											
Ahk	2-13						2	1	8	2	3.8
Ck	13-34						0	1	6	1	1
Ck	34-59						0	1	5	2	1
Ck	49-82						0	1	5	0	0.5
Brunisolic Static Cryosol in beach material											
Ahk	0-8	59	18.9	0.1	0.1	66.7	9	0	34	7	3.2
Bmk	8-23						1	0	10	1	2.3
Ck	23-61						1	2	7	3	1
Brunisolic Turbic Cryosol in beach material											
Ahky1	0-36	71.2	18.7	0.2	0.3	87.6					
Gleysolic Turbic Cryosol in undifferentiated material											
Ofy	18-0	63.7	21.2	0.3	0.3	86.7					

Adapted from Walker and Peters, 1977

3. MERCURY PARTITIONING IN HIGH ARCTIC SUPER-PERMAFROST GROUNDWATER

3.1 Introduction

Mercury (Hg) deposited on the High Arctic landscape during Hg depletion events (MDEs) remains in the snowpack to be released during snowmelt or is volatilized back to the atmosphere (Lindberg et al., 2002; St. Louis et al., 2005). When radiation inputs are sufficient to initiate snowmelt (Pomeroy and Brun, 2001) Hg remaining in the snowpack flows with meltwater, infiltrating the soil or running overland to surface water bodies. Ultimately, Hg in meltwater remains in the dissolved phase in groundwater and surface water or partitions into the solid/particulate phase.

Recognition that partitioning of Hg influences its fate and transport in the environment has led researchers to examine Hg sorption to particulate matter (Daughney et al., 2002; Guine et al., 2003; Ravichandran, 2004; Tiffreau et al., 1995). Organic matter (Ravichandran, 2004), hydrous ferric oxides (HFO) (Davranche and Bollinger, 2000; Tiffreau et al., 1995), and bacteria (Daughney et al., 2002) are potential sorbents of Hg. Despite research into the nature of Hg-particulate interactions in temperate surface water (Daughney et al., 2002) and groundwater (Lowry et al., 2004; Slowey et al., 2005) there is a dearth of information concerning these associations in the High Arctic.

Snow covers the High Arctic for much of the year. The snow pack acts as a receptor and storage compartment for inorganic and organic compounds and insoluble particulates (Kuhn, 2001). At Truelove Lowland regular contributions of windborne loess from the east (dolomite) escarpment adds particulates to the snow pack (Fishback, 2002). Potential sources of Hg to snow at Truelove Lowland include wet and dry deposition from the atmosphere, and deposition via windborne particulate matter. However, reduction and re-volatilization of Hg deposited on the High Arctic snow pack has been documented (St. Louis et al., 2005) indicating that snow is not simply a sink for Hg. The average crustal abundance of Hg (80μg kg^{-1}) (Garrett, 1995b) is several orders of magnitude greater than Hg concentrations documented in High Arctic snow

(Semkin et al., 2005; St. Louis et al., 2005). It is expected that Hg concentrations will be greater in super-permafrost groundwater and ephemeral standing water due to contact with the Hg-bearing soil matrix.

The objective of this study is to quantify the partitioning of Hg between the aqueous and particulate phase in snow, standing water and groundwater at Truelove Lowland, Devon Island, NU. It is hypothesized that partitioning of Hg will differ between matrices, and that Hg partitioning in super-permafrost groundwater will change through the summer thaw. Snow, standing water and super-permafrost groundwater were collected from spatially independent catenas across Truelove Lowland. Total and dissolved Hg concentrations and the concentration of several constituents known to affect Hg chemistry were determined. In this study we demonstrate that there are differences in Hg partitioning between matrices. In a second study, the temporal dynamics of Hg partitioning in super-permafrost groundwater was investigated. Super-permafrost groundwater was collected from monitoring wells installed in the wet sedge meadow (WSM) of seven spatially independent catenas across Truelove Lowland. Five successive monitoring events occurred at approximately three day intervals spanning the spring thaw. Results of this study indicate that Hg partitioning in groundwater is dynamic, and that a change in the concentration of Hg ligands accompanied the change in partitioning.

Researchers in environmental (Eberhardt and Thomas, 1991) and soil science (Pennock, 2004) acknowledge that traditional statistical methods are not always well suited to observational field studies. Natural systems are inherently "noisy" (Eberhardt and Thomas, 1991), and as a result very high sample numbers, or a very large effect size is required to detect significant differences with the desired power (Pennock, 2004). In order to reduce the required sample number to a manageable size and maintain the desired power in the statistical analysis a lower confidence interval (α=0.2) was used in this study.

3.2 Materials and Methods

3.2.1 Site selection

The field site, Truelove Lowland (75º40'N, 85º35'W), is a coastal lowland and polar oasis located on northeast Devon Island. Nine independent catenas of similar age (ie. time since isostatic rebound from the ocean), aspect, slope and soil type were selected as a sample of the 10,000 year old beach ridges at Truelove Lowland (Figure 3.1). All selected catenas had a soil toposequence with Regosolic Cryosols upslope, Brunisolic Cryosols on the foreslope and

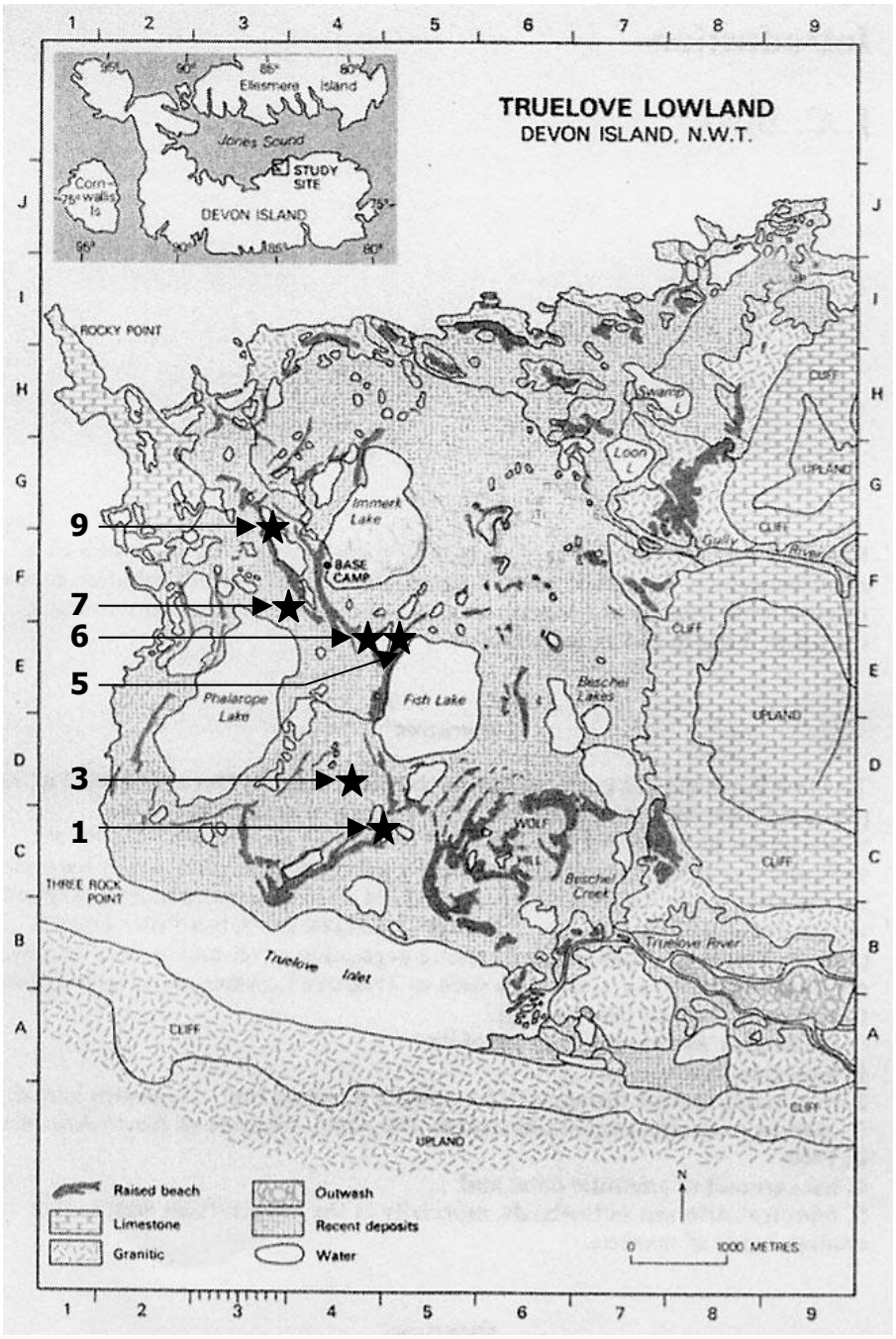

Figure 3.1 Map of Truelove Lowland, Devon Island. Sampling sites (catenas) are identified with stars.

Gleysolic Cryosols on the lower slope area. All Gleysolic Cryosols of selected catenas fall into map units 31, 34, 61 or 71 (Walker and Peters, 1977). These map units were selected because they had detectable levels of sulfate and oxalate-extractable iron (Walker and Peters, 1977). Walker and Peters (1977) and Fishback (2002) were resources of information regarding catena age, aspect, slope and soil type.

3.2.2 Sampling protocol

3.2.2.1 Snow sampling

Between day 164 and 169 (all dates referred to as Julian days) snow sampling was conducted on catenas 5, 6 and 7. A shovel was used to excavate and expose a vertical face in the lower foreslope snowpack. The vertical face was further excavated using a 1L high density polyethylene (HDPE) bottle (Nalgene™) to remove snow that had been in contact with the shovel. Finally, a clean, 1L HDPE bottle was filled with a snow sample representative of the entire depth of the snowpack and the bottle was tightly closed. Upon return to base camp the snow was melted by placing the HDPE bottle in a water bath. Care was taken to ensure that samples were not heated any more than required to melt the snow. The pH, and Eh of the resulting water was determined using the ThermoOrion Pentrode™. The water was sampled with a 50 mL rubber-free Norm-ject™ syringe (Henke-Sass, Wolf GmbH, Tuttlingen, Germany) for the analytes of interest. When filtration was required a syringe mounted 0.45µm pore size polyvinylidene difluoride (PVDF) membrane filter with a polypropylene housing (Whatman Inc, Clifton, NJ) was employed. A ½ inch long, 27 ½ gauge needle (Beckton Dickinson & Co., Franklin Lake NJ) was used for injecting into sample containers with septa.

3.2.2.2 Surface water sampling

Surface water samples were collected between day 167 and day 182 from water pooled in the wet sedge meadow of all catenas (excluding catena 8). Not all catenas were sampled at every sampling time. Water was drawn up into a 50 mL rubber-free Norm-ject™ syringe (Henke-Sass, Wolf GmbH, Tuttlingen, Germany) and injected into the appropriate sample containers. A syringe mounted 0.45µm pore size PVDF membrane filter with a polypropylene housing (Whatman Inc, Clifton, NJ) was used when filtered samples were required. For injection into sample containers with a septum ½ inch long, 27 ½ gauge needle (Beckton Dickinson & Co.,

Franklin Lake NJ) mounted on a 3 mL medical grade plastic syringe (Becton Dickinson & Co., Franklin Lake NJ) was used.

3.2.2.3 Groundwater sampling

Three groundwater monitoring wells were installed in the wet sedge meadow of catenas 1, 2, 3, 5, 6, 7, and 9. Wells were installed, approximately 10m apart, in a transect perpendicular to the shoreline at the base of each catena. Each well was constructed of slotted 5 cm outside diameter polyvinylchloride (PVC) pipe fitted with a PVC slip cap on top and bottom. Using a knife, a hole (approximately 5 cm diameter) was cut in the organic layer. The organic and underlying mineral soil was removed to the full extent of the active layer. Using a dead-blow hammer the slotted PVC pipe, with bottom capped, was seated in the hole. An approximately 5 cm deep bentonite seal (medium bentonite chips, Bemis Company, Vancouver, WA) was installed to prevent surface water from running down the side of the well. At the time of installation the total depth of the well and the depth of the well from the soil surface was recorded. Wells were installed on day 178. Sampling occurred between day 181 and day 191.

Prior to sampling the depth of water in the well was recorded. The pH, Eh and temperature of groundwater in the well was determined with a ThermoOrion Pentrode™ and recorded. Each well was purged dry and allowed to recharge prior to sampling. Sampling was conducted with a rubber-free Normject™ syringe (Henke-Sass, Wolf GmbH, Tuttlingen, Germany) with approximately 60 cm length of Teflon™ tubing serving as an adapter for the syringe.

3.2.3 Reagent water

Nanopure water referred to in this materials and methods section was processed by a NANOpure Diamond Ultrapure water system, Model D11911 (Barnstead International, Dubuque IA). The water generated by this system is pure up to 18.2MΩ cm^{-1} with a final 0.2μm filter.

3.2.4 Mercury

Total and dissolved Hg was analyzed by cold vapor atomic fluorescence spectroscopy using EPA Method 1631 (USEPA, 1999). The analysis was performed in the field on a Tekran 2600 (Tekran Inc., Toronto, ON) using ultra high purity (UHP) argon supplied by Praxair. A 2.4 m x 2.4 m Igloo™ equipment tent (supplied by the Polar Continental Shelf Project) devoted to Hg analysis was set up to house the Tekran 2600 and autosampler at Truelove Lowland base

camp. No outdoor shoes were worn in the tent and outdoor clothing was covered with a clean shirt that was only used in the equipment tent. The generator used to run the Tekran was set up away from the tent in a well-ventilated locale.

Approximately 30 mL of filtered (dissolved Hg) and unfiltered (total Hg) samples were collected in 50 mL polypropylene falcon tubes (Becton Dickinson & Co, Franklin Lakes NJ). Samples were preserved with 250 µL bromine chloride solution (BrCl) (preparation described below) as soon as possible after sampling. Prior to analysis 100µl of hydroxylamine hydrochloride ($NH_2OH{\cdot}HCl$) (preparation described below) was added to consume excess BrCl. Stannous chloride ($SnCl_2$) was used as the reductant according to EPA Method 1631.

The BrCl reagent was prepared as per EPA Method 1631 (USEPA, 1999) by dissolving 27 g of reagent grade potassium bromide (KBr) in 2.5 L of ultrapure hydrochloric acid (HCl) (HX0607-2, EM Science, USA). A clean magnetic stir bar was then placed in the bottle and the KBr solution was stirred for 1 hour. Slowly, 38g of reagent grade potassium bromate ($KBrO_3$) (CAS 7758-01-2, Alfa Aesar, Ward Hill, MA) was added to the solution while stirring. The solution color changed from yellow to red to orange. The orange BrCl solution was loosely capped and stirred for 1 hour.

The $NH_2OH{\cdot}HCl$ solution was prepared according to EPA Method 1631 (USEPA, 1999). Three hundred grams of $NH_2OH{\cdot}HCl$ (CAS 5470-11-1, EM Science, Germany) was dissolved in nanopure water and the volume brought to 1.0 L in a volumetric flask. The $NH_2OH{\cdot}HCl$ solution was prepared in the laboratory and transported to the field in 50 mL polypropylene falcon tubes (Becton Dickinson & Co, Franklin Lakes NJ).

The $SnCl_2$ reductant was prepared by adding 30g reagent grade $SnCl_2{\cdot}2H_2O$ (CAS 10025-69-1, J.T. Baker, Phillipsburg NJ) to 30 mL Omni*Trace* HCl in a 1 L Teflon™ bottle. The $SnCl_2$ and HCl were then swirled to mix and brought up to 1 L volume with water from Immerk Lake. The reductant was purged with UHP argon gas during analysis

3.2.4.1 Quality assurance/quality control

Mercury analysis was conducted by EPA Method 1631 and the quality assurance/quality control requirements detailed therein. Details for method detection limit (MDL), calibration, matrix spikes, blanks, percent recovery, relative percent difference (RPD), and ongoing precision and recovery (OPR) are described below. See Table 3.1 for acceptance criteria for QA/QC

Table 3.1 Quality control acceptance criteria for performance tests in EPA Method 1631

Acceptance Criteria	Limit (%)
Initial precision and recovery	
Precision (RSD)	21
Recovery (X)	79-121
Ongoing precision and recovery	77-123
Matrix spike/matrix spike duplicate	
Recovery	71-125
Relative percent difference (RPD)	24

Adapted from USEPA (1999)

performance tests. All Hg standards and spikes were diluted from a 1000 μg L^{-1} primary standard (6459-04, J.T. Baker, Phillipsburg NJ) using nanopure water.

Method detection limit (MDL) is defined by the EPA as the minimum level of a substance that can be measured with 99% confidence that the concentration is greater than zero. As per EPA Part 126 Appendix B, Revision 1.11 MDL was determined using a concentration in the region where the standard curve is no longer linear (0.5 ng L^{-1}). Seven 60 mL aliquots of groundwater (divided in two, 30 mL spiked (0.5ng L^{-1}) and 30 mL unspiked) were processed through the analytical method outlined above. The Hg peak area in the unspiked aliquot was subtracted from that of the spiked aliquot and

calculations were made to determine Hg concentration in the samples. Variance (s^2) and standard deviation (S) of the Hg concentration were determined by equations [3.1] and [3.2].

$$s^2 = \frac{\left[\sum_{i=1}^{n} x_i^2 - \left(\sum_{i-1}^{n} x_i\right)^2\right] / n}{n-1} \qquad [3.1]$$

$$S = (s^2)^{1/2} \qquad [3.2]$$

where x_i (i = 1 to n) are the analytical results obtained. MDL was then computed as:

$$MDL = t(n-1,1-0.99)(S) \qquad [3.3]$$

where $t(n-1.1-0.99)$ is the Students' t value for a 99% confidence level for n samples and S is the standard deviation of the replicate analyses.

Calibration was performed according to EPA Method 1631 (USEPA, 1999). Five non-zero points and two nanopure water blanks were analysed. For each point the mean peak area of the blank was subtracted from the peak area of the standard. A calibration factor (CF) for each standard was then calculated according to the following equation:

$$CF = \frac{(A_x) - (A_s)}{C_x} \qquad [3.4]$$

where A_X is the area of the standard peak, A_B is the average area of the blank peaks, and C_X is the mass of Hg (ng) in the standard. The mean CF (CF_m), standard deviation (S) of the calibration factors were determined and the relative standard deviation (RSD) of the calibration factor was calculated according to equation 3.5:

$$RSD = 100\left(\frac{S}{CF_m}\right) \qquad [3.5]$$

When the RSD was <15% and recovery of the lowest standard was 75-125% the calibration was considered to be satisfactory (USEPA, 1999).

The performance of EPA Method 1631 for analysis in groundwater was assessed using matrix spikes (MS) and matrix duplicate spikes (MDS). Sixty milliliter aliquots of groundwater were divided in two (spiked and unspiked) and analyzed by EPA Method 1631. Percent recovery (R) was calculated using equation 3.6:

$$R = 100\,\frac{(A-B)}{TC} \qquad [3.6]$$

where A is the measured concentration of the analyte after spiking, B is the measured concentration of the analyte before spiking and TC is the true concentration of the spike.

Relative percent difference (RPD) between the MS and the MDS was determined by the following equation:

$$RPD = \frac{|D1-D2|}{D1+D2/2}\times 100 \qquad [3.7]$$

where D1 is the concentration of Hg in the MS sample and D2 is the concentration of Hg in the MSD. The goal was to achieve a RPD of <20% (USEPA, 1999). Ongoing precision and recovery of the analytical system was addressed by running instrument and reagent blanks and a standard curve prior to each run. Every tenth sample analyzed was a standard.

Quality control of the analytical system and sample processing was ensured through the analysis of instrument blanks, reagent blanks, and field blanks. Instrument blanks were analyzed as Tekran "dry" and "clean" runs to ensure the system (soda lime, gold trap, phase separator) was not contaminated with Hg. Reagent blanks, of nanopure water, was put through the same procedure as a sample and analyzed. This ensured that the reagents (BrCl, $NH_2OH{\cdot}HCl$, and $SnCl_2$) were not contaminated with Hg. Field blanks (nanopure water) were carried in 50 mL Falcon tubes (Becton Dickinson & Co.) in the field to ensure that post-sampling handling was not a source of contamination.

3.2.5 Anions

Capillary electrophoresis was used to determine concentrations of chloride (Cl^-), nitrate/nitrite (NO_3^-/NO_2^-), and sulfate (SO_4^{-2}). A Beckman-Coulter P/ACE MDQ (Beckman Coulter, Inc., USA) was used for the analysis. Samples were field filtered, using a syringe mounted 0.45μm pore size PVDF membrane filter with a polypropylene housing (Whatman Inc,

Clifton, NJ), into 9 mL borosilicate glass Solvent Saver™ vials (Cat # 66022-300, VWR). Prior to analysis 1.5 mL of sample was pipetted into 2 mL, amber, wide-mouth, snap-cap vials (Cat # 5181-3376, Agilent). Samples were then acidified to approximately pH 2.0 with the addition of 45µl of 85% phosphoric acid (H_3PO_4) (EMD Biosciences, Inc., La Jolla CA).

Samples were hydrodynamically injected (5 second injection at 0.5 psi), separated at 30kV (1 minute ramping, reverse polarity), using the pH 8.2 MicroSolv CElixirOA™ buffer system (MicroSolv Technologies Inc., Boston, MA). All samples were separated by a Nanopure water plug (10 second injection at 0.1 psi) on a 0.75µm inside diameter, 65cm long, untreated, fused silica capillary. Anions were detected indirectly at 254nm. Peak areas were integrated by the 32 Karat Software (version 5.0, build 1020, Beckman Coulter, Inc. USA) and concentrations were manually calculated from a standard curve.

The anion method events are: 1) 0.5 minute initiator rinse, 20 psi; 2) 0.5 accelerator rinse, 20 psi; 3) 3.5 minute separation, 30kV, reverse polarity; 4) auto-zero, 1.25 minutes into separation; 5) stop data collection, 3.5 minutes into separation; and 6) 0.5 minute 0.1M NaOH rinse. The capillary was conditioned before and after each run.

One-hundred millimolar stock standards were made from 1 mg mL^{-1} sodium chloride (NaCl) solution (CAS 7647-14-5, VWR, West Chester PA), sodium nitrate ($NaNO_3$) (Fisher Scientific Company, Fair Lawn NJ), and sodium sulfate ($NaSO_4$) (BDH Inc., Toronto ON). Pure and mixed standards (0.01, 0.05, 0.1 and 0.5 mM) were made from these stock solutions.

3.2.6 Sulfide

Dissolved sulfide (S^{-2}, HS^-, H_2S) concentrations were determined using the Cline (Cline, 1969) method. Dissolved sulfide concentration was determined by UV absorbance of the mixed diamine reagent-sulfide complex. The mixed diamine reagent was made by: 1) dissolving 2.0g of *N*,*N*-dimethyl-1,4-phenylenediamine sulfate (CAS 536-47-0, Aldrich Chemical Company, Inc. Milwaukee WI) in 500 mL of cool 50% Omni*Trace* HCl (EMD Biosciences Inc., La Jolla CA); 2) dissolving 3.0g of ferric chloride hexahydrate ($FeCl_3 \cdot 6H_2O$) (CAS 10025-77-1, J.T. Baker, Phillipsburg NJ) in 500 mL of cool 50% Omni*Trace* HCl (EMD Biosciences Inc., La Jolla CA); and 3) mixing the two solutions. The reagent was then stored in the dark.

Prior to sampling, 80 µl of mixed diamine reagent was pipetted into 2.0 mL, wide-mouth, amber vials with PTFE septa and they were closed anaerobically (in a chamber with an atmosphere of 100% N_2). Samples were injected into vials using a 3 mL medical grade plastic

syringe (Becton Dickinson & Co., Franklin Lakes NJ) fitted with a 27 ½ gauge needle. Two-hundred microliters of the complexed sample was pipetted into a 96 well plate (Microtest™ U-bottom polypropylene plate, Beckton Dicksinson & Co., Franklin Lakes, NJ). Absorbance at 680 nm was measured with a multiplate reader (Molecular Devices, Inc).

Sulfide standards were made from a 200 mM stock sodium sulfide nonahydrate ($Na_2S{\cdot}9H_2O$) (BDH Inc., Toronto ON) solution prepared in O_2-free water (autoclaved and cooled under a N_2 atmosphere). The 200 mM stock solution was prepared by dissolving 5.2876 g of $Na_2S{\cdot}9H_2O$ in 100 mL of O_2-free water. Each standard curve was prepared in an anaerobic chamber from fresh stock solutions to minimize oxidation and degradation. Standards were injected anaerobically into wide-mouth, amber, 2.0 mL CE vials containing 80 µl mixed diamine reagent.

3.2.7 Iron speciation

Simultaneous determination of Fe(II) and Fe(III) was achieved using a modification of the method outlined by Takagai and Igarashi (2003) and modified by Levy (2006). In the modified method concentrations are determined by UV absorbance (with a spectrophotometer) rather than by capillary electrophoresis with indirect UV detection (Levy, 2006).

The selective complexation reagent contained 0.4 mL of 5.0 x 10^{-4} mol L^{-1} desferoxmine Mesylate (DFB) (CAS 138-14-7, Calbiochem, EMD Biosciences, Inc. La Jolla CA), 0.4 mL 1.0 x 10^{-3} mol L^{-1} bathophenantholinedisulfonic acid disodium salt (Bap), and 0.5 mL 0.1 mol L^{-1} potassium dihydrogen phosphate (KH_2PO_4) (CAS 7778-77-0, Alfa Aesar, Ward Hill, MA). One milliliter of the complexing reagent was pipetted into a wide mouth borosilicate glass vial (Agilent Technologies, Palo Alto, CA). Each vial was fitted with a polypropylene screw cap with a Teflon™ resin septa (Agilent Technologies, Palo Alto, CA) inside an anaerobic chamber with a N_2 atmosphere. The N_2 headspace ensured minimum contact between the sample and O_2 prior to the complexation reaction. Samples were filtered with a 0.45 µm Whatman syringe-mounted filter and drawn into a 5 mL syringe. The syringe was fitted with a 27 ½ gauge sterile needle (Becton Dickson & Co., Franklin Lakes, NJ) and the sample was injected through the septa into the vial containing the complexing reagent.

After Levy (2006) Fe(III) standards were prepared from ferric chloride 6-hydrate (Mallinckrodt Baker, Inc., Phillipsburg, NJ) and Fe(II) standards were prepared with ferrous sulfate heptahydrate (Merck, KgaA, Darmstadt, Germany). Standards were prepared directly in

the complexing solution to avoid oxidation of Fe(II) during preparation. A standard curve was prepared with serial dilutions of the individual standards. The serial dilutions were prepared with Milli-Q™ ultra-pure water.

This method of Fe speciation assumes that the absorbance of the Fe(III)-DFB complex will be the same at 405 nm and 450 nm and that the difference in absorbance between 405 nm and 450 nm can be attributed to the concentration of Fe(II)-Bap complex.

To determine Fe(II) and Fe(III) concentrations 200 µL of complexed sample was pipetted into a 96 well plate (Microtest™ U-bottom polystyrene plate, Beckton Dicksinson & Co., Franklin Lakes, NJ). Absorbance at 405nm and 450nm was measured with a multiplate reader (Molecular Devices, Inc). The concentrations of iron species in samples was calculated using the following procedure (Levy, 2006):

1. Prepare serial dilutions and construct separate standard curves for Fe(III)-DFB and Fe(II)-Bap. Use formula y = mx + b to express standard curve for each wavelength.
2. Analyze mixed standards of Fe(III)-DFB/Fe(II)-Bap and correct absorbance using equations 3.8 and 3.9 (Levy, 2006).

$$A_{Fe(III)} = A_{450nm} - \left[\left(\frac{1}{1 - \frac{Fe(II)m_{A405nm}}{Fe(II)m_{A450nm}}} \right) (A_{450nm} - A_{405nm}) \right] \qquad [3.8]$$

$$A_{Fe(II)} = \frac{A_{450nm} - A_{405nm}}{1 - \left(\frac{Fe(II)m_{A405nm}}{Fe(II)m_{A450nm}} \right)} \qquad [3.9]$$

where $A_{Fe(III)}$ is the corrected absorbance of Fe(III); $A_{Fe(II)}$ is the corrected absorbance of Fe(II); A_{450nm} is the absorbance of a mixed Fe(III) and Fe(II) solution at 450 nm; A_{405} is the absorbance of a mixed Fe(III) and Fe(II) solution at 405 nm; m_{A450} is the slope of a mixed standard curve at 450 nm; and m_{A405} is the slope of a mixed standard curve at 450 nm.

3. Use corrected absorbance ($A_{Fe(III)}$ and $A_{Fe(II)}$) and create graphs for Fe(III) absorbance vs. Fe(III) actual concentration and Fe(II) absorbance vs. Fe(II) actual concentration. Plot graphs with corrected absorbance on the y-axis and actual concentration on x-axis. Add a linear trend line and obtain the equation (y = mx + b).

4. Rearrange the linear equation in step 3 and solve for x to obtain actual concentration of Fe(III) and Fe(II) in samples.

3.2.8 Organic carbon

Total organic carbon (TOC) and dissolved organic carbon (DOC) was determined using the method outlined in the Shimadzu TOC-5050A manual (Shimadzu).

Total carbon – inorganic carbon = organic carbon [3.10]

Analysis was done on a Shimadzu TOC-5050A. Filtered (DOC) and unfiltered (TOC) samples were collected in 9 mL borosilicate glass Solvent Saver™ vials (Cat # 66022-300, VWR). Samples were stored at ambient temperature (<10ºC) in the field and at 4ºC in the lab until analysis.

Organic and inorganic carbon standards were prepared according to the manual (Shimadzu). The organic carbon stock standard was prepared by dissolving 1.0625 g of reagent grade potassium hydrogen phthalate (Nacalai Tesque, Inc., Kyoto, Japan) in a 500 mL of fresh Nanopure water using a volumetric flask. The inorganic carbon stock standard was prepared by dissolving 1.750 g of reagent grade sodium hydrogen carbonate ($NaHCO_3$) (BDN, Toronto, ON) and 2.21 g of reagent grade anhydrous sodium carbonate (Na_2CO_3) (J.T. Baker, Phillipsburg NJ) (heated at 285 ºC for one hour and cooled in a dessicator) in 500 mL of fresh Nanopure water.

Total carbon samples and inorganic carbon samples were run with a 50 µl injection volume, 3 injections (maximum 5 injections), maximum standard deviation of 200, maximum coefficient of variation of 2, and 4 washes. Analyses were run in range 5 setting.

3.2.9 Statistical analysis

Data was checked for normality using the Anderson-Darling test (P <0.05). Non-normally distributed data was transformed, when possible, so that it conformed to a normal distribution (Johnson and Bhattacharyya, 1992). Bartlett's test is heavily influenced by non-normal data, therefore Levene's test (P <0.05) was used to determine whether variances in the data significantly were significantly different (Sokal and Rohlf, 1995).

When data was normally distributed and variances were homogeneous it was analyzed by analysis of variance (ANOVA) using a general linear model (GLM). Attempts were made to normalize all non-normal data by transforming it. If data could not be normalized and variances were homogenous, ANOVA GLM was also used for statistical analysis. When comparing means between matrices (a random factor) a one-way Model II ANOVA was used (Sokal and Rohlf,

1995). For comparisons of means in groundwater by catena and date (which are random factors) a two-way Model II ANOVA with replication will be used (individual wells as replicates) (Sokal and Rohlf, 1995).

Non-normally distributed data with heterogeneous variances were analyzed for significant differences using a non-parametric test (Sokal and Rohlf, 1995). When analyzing significant differences between matrices and in groundwater results by date the Kruskal Wallis test was used (Sokal and Rohlf, 1995). Table 3.2 summarizes the statistical methods used to analyzing data in this chapter.

Table 3.2 Summary of statistical analysis methods for super-permafrost groundwater parameters

Variable	Inter-matrix study		Ground water study	
	ANOVA (GLM)[1]	Kruskal Wallis	ANOVA (GLM)	Kruskal Wallis
THg[2]	X		X	
DHg[3]		X	X	
PHg[4]	X		X	
Chloride		X	X	
Nitrogen		X		X
Sulfate		X		X
Sulfide		X		X
pH	X		X	
Eh	X		X	
Temperature	X		X	

[1] analysis of variance by general linear model

[2] Total mercury

[3] Dissolved mercury

[4] Particulate mercury

3.3 Results

3.3.1 Mercury partitioning in snow, standing water and groundwater

3.3.1.1 Mercury

Particulate Hg, as percent of THg, was highest in groundwater (73 ± 2.4%) (normally distributed data shown as mean ± standard error; non-normally distributed data shown as median (Q1, Q3)) and lowest in snow (26 ± 10.6%) (p<0.001) (Figure 3.2). Matrices also differed in THg concentrations (p<0.001). Total Hg concentrations were approximately four times greater in groundwater (22 ± 2.30 pmol L^{-1}) than in snow (5.9 ± 1.75 pmol L^{-1} at Truelove Lowland. Unlike PHg and THg, which were highest in groundwater, DHg concentrations were highest in snow (7.1 (0.25, 7.52) pmol L^{-1}) (p=0.148). DHg concentrations were similar in standing water (4.7 (2.88, 13.58) pmol L^{-1}) and groundwater (4.1 (2.74, 5.28) pmol L^{-1}).

3.3.1.2 Anions

Chloride, nitrogen, sulfate and sulfide differed significantly between matrices (p=0.192, chloride; p=0.176, nitrogen; p=0.000, sulfate; p=0.000, sulfide). Chloride, nitrogen and sulfate were undetectable in 7 of 8 snow samples. Chloride and nitrogen concentrations were highest in groundwater (chloride: 1.7 (0.00, 8.57) μmol L^{-1}; nitrogen: 0.0 (0.00, 11.24) μmol L^{-1}). Chloride concentration was 0.2 (0.00, 8.08) μmol L^{-1} and nitrogen was undetectable in standing water. Unlike chloride and nitrogen, sulfate and sulfide concentrations were highest in standing water (sulfate: 27 (15.6, 59.8) μmol L^{-1}; sulfide: 27 (15.3, 59.5) μmol L^{-1}). Sulfate concentration was 9.6 (0.79, 13.2) μmol L^{-1} in groundwater. Sulfide concentration in groundwater (4.8 (3.14, 8.09) μmol L^{-1}) was approximately one-sixth its concentration in surface water.

3.3.1.3 Temperature, Eh and pH

Temperature, Eh and pH differed between snow, ephemeral standing water and super-permafrost groundwater (p=0.000, temperature; p=0.000, Eh; p=0.000, pH). Predictably, the temperature of ephemeral standing water was higher than both melted snow samples and groundwater. The temperature of ephemeral standing water was 9.9 ± 0.65 °C. Eh and pH values followed a similar trend in matrices and were highest in snow and lowest in super-permafrost groundwater. The mean Eh of snow samples was 500 ± 24.6 mV, whereas in groundwater the mean Eh was 380 ± 7.9 mV (Figure 3.3). As illustrated in Figure 3.4, the pH of melted snow samples (9.9 ± 0.22) was more than two pH units greater than the pH of super-permafrost

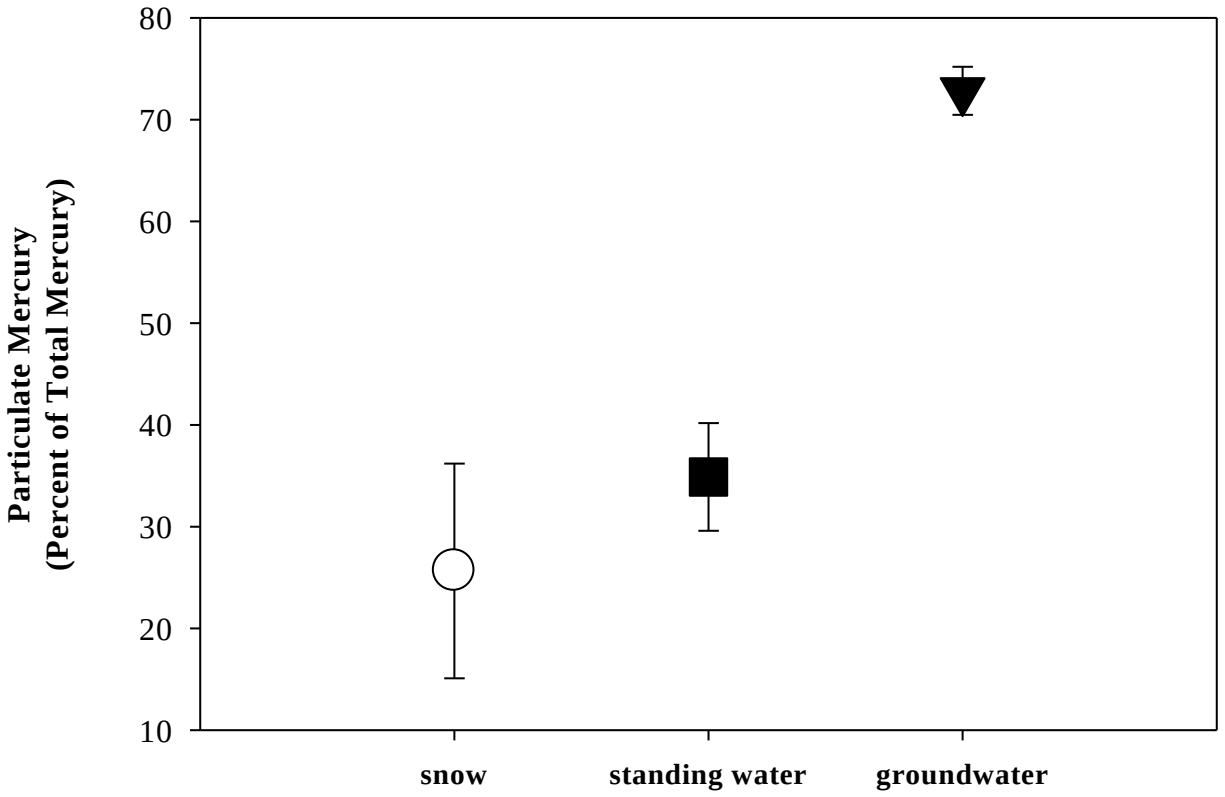

Figure 3.2 Particulate mercury in snow, surface water and super-permafrost groundwater at Truelove Lowland, Devon Island. Error bars represent standard error (snow (●) n = 8, standingwater (■) n = 22, groundwater (▼) n = 54).

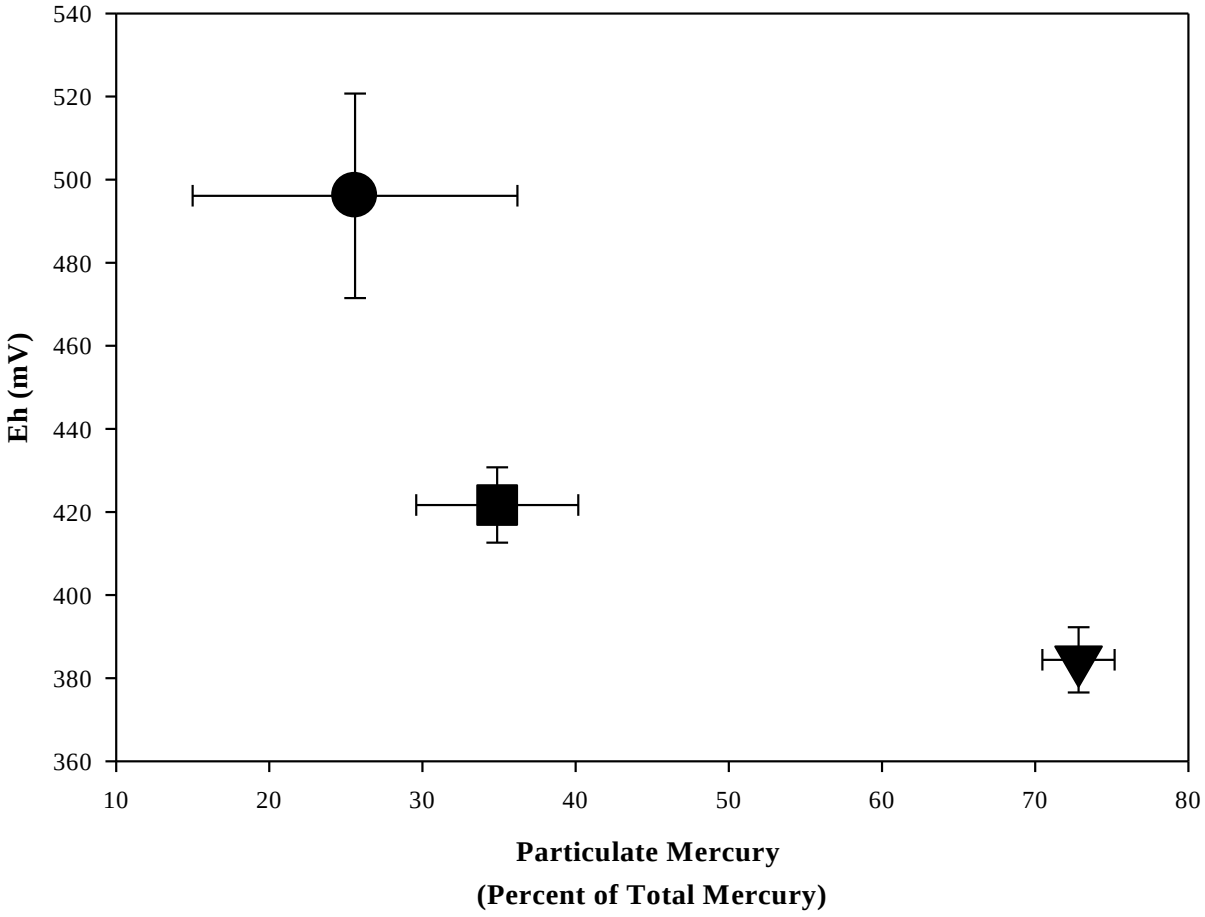

Figure 3.3 Particulate mercury and Eh in snow, surface water and super-permafrost groundwater at Truelove Lowland, Devon Island. Error bars represent standard error (snow (●) n = 8, surface water (■) n = 19, groundwater (▼) n = 50).

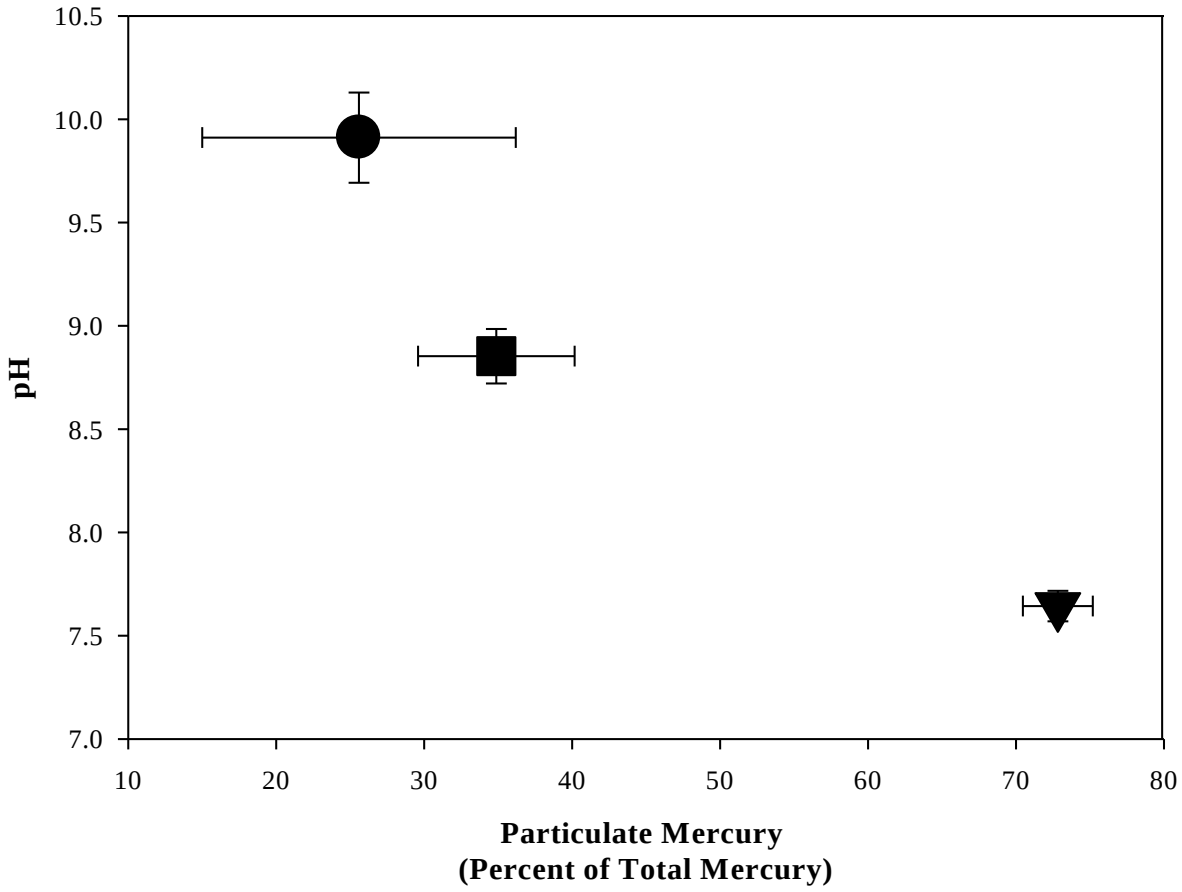

Figure 3.4 Particulate mercury and pH in snow, surface water and super-permafrost groundwater at Truelove Lowland, Devon Island. Error bars represent standard error (snow (●) n = 8, surface water (■) n = 19, groundwater (▼) n = 50).

groundwater (7.6 ± 0.07). A negative correlation (r=0.57) between PHg and pH was observed (Figure 3.5)

3.3.2 Temporal variation in mercury partitioning in groundwater

3.3.2.1 Mercury

Particulate Hg in groundwater in all seven catenas increased (p <0.005) by approximately 20% over the first four sampling days and then decreased on the last sampling day (Figure 3.6). While individual catenas had differing levels of particulate Hg, the temporal trend remained consistent between catenas (p=0.732, date x catena). For example, over the summer thaw, catena 1 had the lowest levels of PHg with only 67 ± 6.9 % and catena 3 had the greatest concentrations of PHg with 77 ± 5.8 %. Yet both catenas responded similarly to the summer thaw with PHg increasing by 21% in catena 1 and by 31% in catena 3. In contrast, THg did not vary spatially (p=0.922) or temporally (p=0.432) with an average concentration of 17 ± 2.30 pmol L^{-1}. Total and dissolved Hg concentrations are reported in Table 3.3 and 3.4, respectively.

3.3.2.2 Anions

Chloride, nitrogen and sulfate concentrations differed spatially and temporally, in Truelove Lowland groundwater. Chloride concentrations in groundwater were significantly different between catenas (p=0.003) but not by sampling dates. Whereas, nitrogen ($N\text{-}NO_2^- + NO_3^-$) in super-permafrost groundwater differed by both date (p=0.002) and catena (p=0.002). Sulfate concentrations differed only by sampling date (p<0.001). Dissolved sulfide (S^{2-}, HS^-, H_2S), unlike the other anions, was not significantly different between sampling dates or catenas. In addition anions did not show a correlation with PHg (chloride, r=0.03, p=0.810) (nitrogen, r=0.14, p=0.246) (sulfate, r=0.19, p=0.095) (sulfide, r=0.24, p=0.050).

Although anion concentrations, with the exception of sulfide, changed spatially and temporally, they did not exhibit similar trends in concentration. Over the sampling period catena 1 had the highest chloride concentration (17 ± 3.5 μmol L^{-1}) while catena 5 had the lowest with none detected. Nitrogen was only detectable in groundwater from catenas 1, 2, 5, and 9. Catena 5 had the highest nitrogen concentration with 10 ± 8.3 μmol L^{-1}. Nitrogen also differed between sampling days. It was undetectable over the early part of the summer thaw (days 181, 183, and 186) and was highest on day 189 (28 (0.0, 59.2) μmol L^{-1}). The nitrogen concentration on the final sampling day (191) was 9.5 (0.00, 15.1) μmol L^{-1}. Sulfate concentration, which was non-

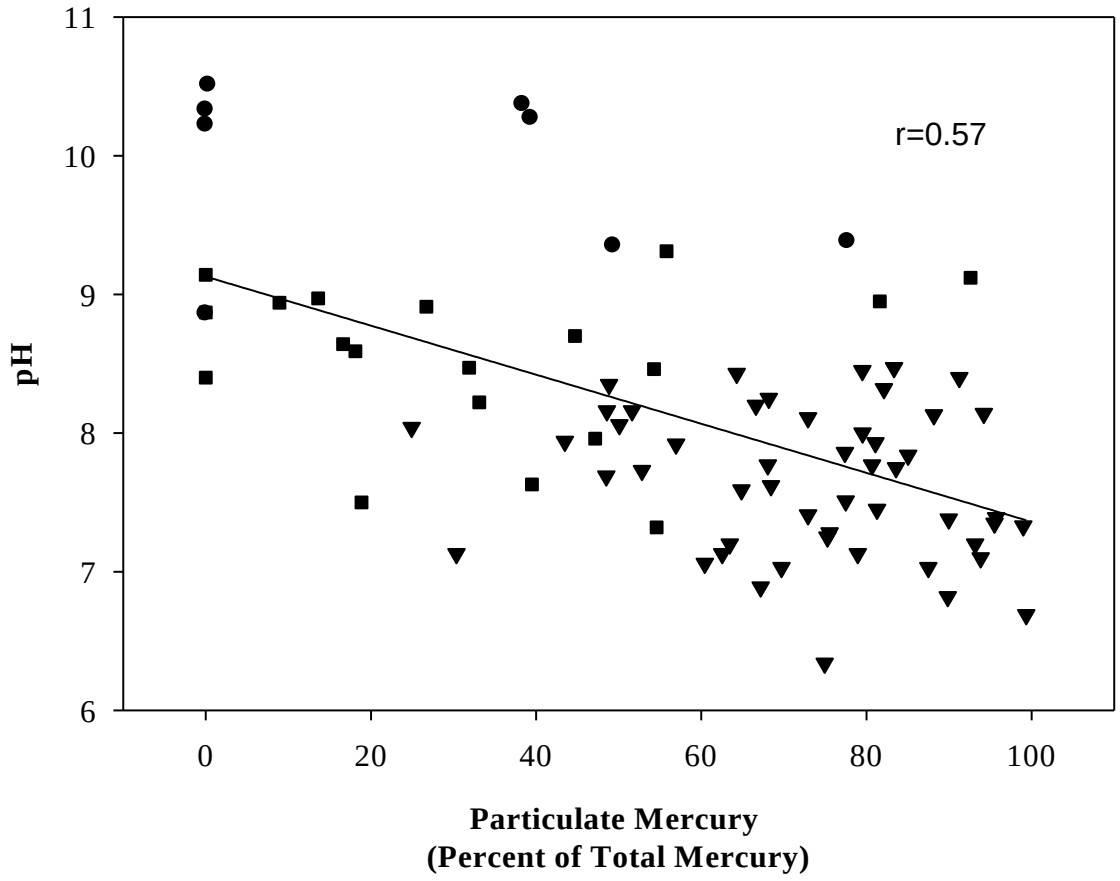

Figure 3.5 Relationship between PHg and pH in Truelove Lowland snow (circle symbol), ephemeral standing water (square symbol) and super-permafrost groundwater (inverted triangle symbol) over the summer thaw. n=77.

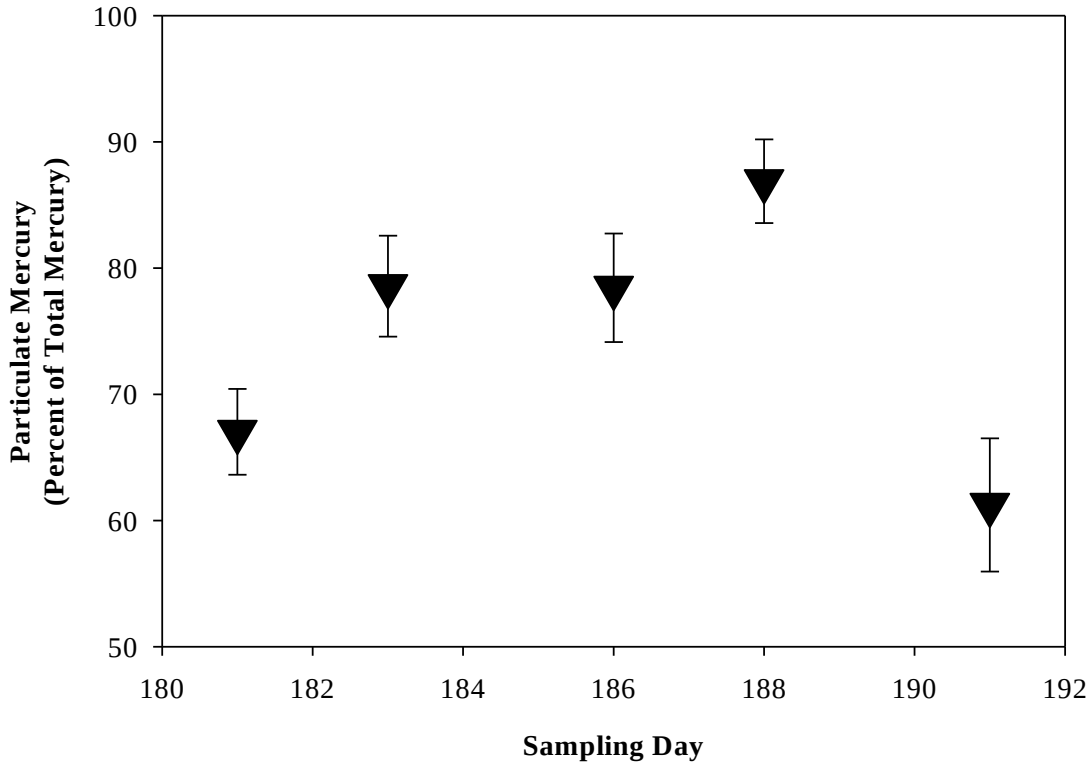

Figure 3.6 Particulate mercury super-permafrost groundwater at Truelove Lowland, Devon Island. Error bars represent standard error (minimum n = 9, maximum n = 12).

Table 3.3 Mean THg concentration (pmol L^{-1}) in Truelove Lowland super-permafrost groundwater by date and catena

Day of Year	Mean (by Date)	Catena						
		1	2	3	5	6	7	9
181	21.95	23.35	-	17.25	-	25.44	19.87	21.57
183	24.96	23.88	-		-	26.20	32.28	17.31
186	29.17	-	16.93	-	31.69	-	28.24	31.77
188	19.49	12.58	-	10.57	9.62	19.84	12.21	20.64
191	14.39	17.27	-	10.18	23.51	-	9.83	31.01
Mean (by Catena)		15.96	16.90	12.60	16.41	21.11	16.44	18.84

Variable	Statistical Analysis		
	Ground water	Ground water	Ground water
	Date[1]	Catena[1]	Date x Catena[1]
Significance or Probability (α=0.2)	NS[2]	NS	NS

[1]analyzed by ANOVA (GLM)
[2]not significant

Table 3.4 Mean DHg concentration (pmol L^{-1}) in Truelove Lowland super-permafrost groundwater by date and catena

		Catena						
Day of Year	Mean (by date)	1	2	3	5	6	7	9
181	6.28	7.44	-	5.40	-	6.65	5.76	6.19
183	3.97	8.74	-	2.79	-	4.41	3.21	3.34
186	4.14	-	4.14	-	4.38	-	3.51	4.52
188	1.69	5.74	-	2.65	3.79	4.35	4.63	4.01
191	4.36	1.94	-	0.07	1.51	-	2.03	1.84
Mean (by Catena)		5.17	4.14	3.26	3.30	5.35	3.83	3.89

	Statistical Analysis		
	Ground water	Ground water	Ground water
Variable	Date[1]	Catena[1]	Date x Catena[1]
Significance or Probability (α=0.2)	<0.001	0.0351	NS[2]

[1] analysis of variance by general linear model

[2] not significant

normally distributed in groundwater, was undetectable on day 181 and was greatest on day 191 (14 (10.4, 22.1) μmol L^{-1}) however, it did not follow a predictable trend through the summer thaw. Moreover, sulfide, unlike the other measured anions in Truelove Lowland groundwater, did not differ in space or time. The median sulfide concentration over the summer thaw was 4.8 (3.14, 8.09) μmol L^{-1}. Anion concentrations are presented in Table 3.5.

3.3.3.4 Iron speciation

The concentration of both iron species (Fe(II) and Fe(III)) changed over the summer thaw (p=0.001, Fe(II); p<0.001, Fe(III)). Iron(II) concentrations did not exhibit a clear temporal trend and reached a maximum on the final sampling day (77 ± 0.04 μmol L^{-1}). Meanwhile, Fe(III) concentrations increased over the first three sampling days from a minimum (13 ± 0.1 μmol L^{-1}) on day 181 to 17 ± 0.9 μmol L^{-1} on day 186. This was followed by a decrease in Fe(III) on day 189 (15 ± 0.1 μmol L^{-1}). The maximum Fe(III) concentration occurring on day 191, the final sampling day (50 ± 0.1 μmol L^{-1}).

Iron species concentrations also differed significantly between catenas (p=0.183, Fe(II); p=0.168, Fe(III)). Iron(II) concentrations were nearly two times greater in catena 3 (100 ± 12.7 μmol L^{-1}) than catena 9 which had the next highest Fe(II) concentrations (56 ± 9.4 μmol L^{-1}). While catena 3 had the highest Fe(II) concentrations it also had the lowest Fe(III) concentrations with 20 ± 5.5 μmol L^{-1}. Catena 7 had the lowest Fe(II) concentrations with 31 ± 10.1 μmol L^{-1}. Concentrations of Fe(II) and Fe(III) varied significantly between catenas and all catenas responded similarly to the summer thaw.

3.3.3.5 Organic carbon

Particulate organic carbon in Truelove Lowland groundwater ranged from 0.0 ± 3.2 mg L^{-1} (day 183) to 15 ± 19.4 mg L^{-1} (day 186) (p=0.095) over the summer thaw. Like POC, TOC differed between sampling days (p=0.154) and was lowest on day 183 (12 ± 3.7 mg L^{-1}) and highest on day 186 (42 ± 19.1 mg L^{-1}). TOC also differed between catenas (p=0.023). Differences in DOC were also observed over the summer thaw (p=0.046). Dissolved organic carbon in groundwater was highest on day 189 (16 ± 5.7 mg L^{-1}) and lowest on day 186 when it was less than the detection limit.. Particulate organic carbon in super-permafrost groundwater followed a similar temporal trend in all catenas (p=0.578, date x catena). Conversely, DOC (p=0.192, date x catena) and TOC (p=0.069, date x catena) did not.

Table 3.5 Mean and median anion concentrations (μmol L^{-1}) in Truelove Lowland superpermafrost groundwater by date and catena.

	Day of Year		Catena						
Chloride		Mean (by Date)	1	2	3	5	6	7	9
	181	2.94	0.00	---	0.00	---	2.23	0.07	14.20
	183	5.45	11.20	---	1.10	---	6.73	1.91	6.35
	186	3.41	--	0.00	---	1.54	---	0.97	8.86
	188	7.48	11.21	---	0.00	0.00	---	1.90	8.94
	191	3.31	9.16	---	0.00	1.92	0.00	0.75	6.01
	Mean (by Catena)		7.89	0	0.22	1.21	3.36	1.12	11.59
Nitrogen		Median (by Date)							
	181	0.00	0.00	---	0.00	---	0.00	0.00	13.50
	183	0.00	10.12	---	0.00	---	0.00	0.00	0.00
	186	0.00	---	7.63	---	0.00	---	0.00	8.33
	188	27.99	4.70	---	0.00	43.60	---	63.98	23.60
	191	9.53	9.79	---	11.30	23.60	15.05	0.00	5.92
	Median (by Catena)		4.33	7.63	0.00	10.16	0.00	0.00	8.33

Table 3.5 continued.

Sulfate		Median (by Date)							
	181	0.00	0.00	---	0.00	---	0.00	0.00	7.54
	183	12.42	16.79	---	14.90	---	5.68	12.42	10.45
	186	11.47	---	11.44	---	10.48	---	13.17	12.71
	188	5.27	0.00	---	0.00	2.31	---	11.70	8.42
	191	15.12	10.59	---	16.76	15.12	13.29	13.47	23.85
	Median (by Catena)		4.14	11.44	0.00	7.04	3.48	12.24	9.55

	Statistical Analysis					
	Chloride		Nitrogen		Sulfate	
Variable	Date[1]	Catena[1]	Date[1]	Catena[2]	Date[2]	Catena[2]
Significance or Probability (α=0.2)	0.195	0.003	0.002	0.010	0.000	NS[3]

[1]analyzed by ANOVA (GLM)

[2]analyzed by Kruskall Wallis test

[3]not significant

3.3.3.6 Temperature, Eh and pH

Temperature and Eh in super-permafrost groundwater varied by date (p=0.007, Temperature; p=0.011, Eh) and reached a maximum across all catenas on day 189. The temperature on day 189 was 6.7 ± 0.36ºC and Eh was 400 ± 15.1 mV. On the same day (day 189) pH was 7.3 ± 0.11, its lowest (p=0.027) value over the summer thaw. The pH of Truelove Lowland groundwater followed a decreasing trend from its maximum value of 7.8 ± 0.16 on day 181 to its lowest value on day 189. It increased slightly on the final sampling day (day 191).

Temperature, Eh and pH were also spatially variable. However, unlike the trend in temporal differences, these parameters did not reach their maximum and minimum values at the same catenas. Temperature was lowest at catena 5 (4.6 ± 2.51˚C) and highest at catena 1 (6.4 ± 0.35˚C) (p<0.001). Eh was highest in catena 2 (470, only one observation) and lowest in catena 1 (320 ± 13.7 mV) (p<0.001). And, pH reached its maximum value at catena 7 (8.0 ± 0.09) and its minimum at catena 3 (6.9 ± 0.18) (p=<0.001).

3.4 Discussion

3.4.1 Mercury partitioning in snow, standing water and groundwater

Total Hg in snow at Truelove Lowland (5.9 pmol L^{-1}) is comparable to the range of concentrations documented in snow at Ellesmere Island (St. Louis et al., 2005) and Amituk Lake on Cornwallis Island (Semkin et al., 2005). Mercury concentrations in super-permafrost groundwater on Cornwallis Island, NU reported by Loseto (2004) were less than those observed on Truelove lowland. Nevertheless, Loseto (2004) found that THg in super-permafrost groundwater had a mean concentration of 14.0 pmol L^{-1} and was not spatially variable. Likewise, in our study, THg in Truelove Lowland super-permafrost groundwater was not spatially variable. The mean concentration of THg in Truelove Lowland super-permafrost groundwater in this study was 19 ± 1.1 pmol L^{-1}.

Inundation of lowlands, creating ephemeral standing water, is a common feature of Arctic lowlands during the annual spring rise of streams in cold climates as a result of snow melt (Woo and Young, 2006). Reported concentrations of THg in High Arctic lakes range from: 1.2 to 1.7 pmol L^{-1} (Semkin et al., 2005), and 2.8 to 7.2 pmol L^{-1} (8 High Arctic Lakes (Loseto et al., 2004)), to 8.5 pmol L^{-1} (Toolik Lake (Tseng et al., 2004)). Reported THg concentrations in temperate surface waters range from 5.8 to 32 pmol L^{-1} (15 Nova Scotia Lakes (Daughney et al.,

2002)), and 14 to 15 pmol L^{-1} (Northern Wisconsin lake (Watras et al., 2005)), to 10 pmol L^{-1} (Beverly Swamp, Ontario (Galloway and Branfireun, 2004)). In this study the mean THg concentration in ephemeral standing water at Truelove Lowland was 13 pmol L^{-1}, which is within the range documented for temperate surface waters. THg in ephemeral standing water was greater than concentrations documented in High Arctic lakes and ponds.

Significant differences in THg and DHg concentrations, and thus sorption and partitioning, were observed in snow, ephemeral standing water and super-permafrost groundwater at Truelove Lowland. In addition to the differences between matrices, a decrease in Hg sorption to particulate matter with increasing pH was also observed.

Changes in pH result in differences in Hg speciation (Freeze and Cherry, 1979; Silberberg, 1996). In the pH range observed in Truelove lowland snow (9.9 ± 0.22) the dominant Hg species would be $Hg(OH)_2^0$ (Freeze and Cherry, 1979). The $Hg(OH)_2^0$ species is uncharged and does not readily sorb to particulate matter. As pH decreases other charged Hg species become more prevalent (Freeze and Cherry, 1979; Ravichandran, 2004) and an increase in sorption would be expected. Indeed, in the inter-matrix study PHg was highest in super-permafrost groundwater which had the lowest pH of the three matrices (7.6 ± 0.07). A similar decline in Hg sorption with increasing pH was observed in a laboratory study (Kim et al., 2004a), albeit over a lower pH range (pH 4 to 8). Kim et al. (2004) postulate that the decline in Hg sorption is due to the pH dependence of Hg speciation.

Although there was not a correlation between anion and PHg concentrations (data not shown), the concentration of all anions analyzed in this study (Cl^-, NO_2^-+NO_3^-, SO_4^{2-} and S^{2-}) differed among matrices. Many chemical and physicochemical parameters differ between matrices; however, differences in partitioning can not be attributed to one parameter. It is thought that the difference in partitioning between matrices at Truelove Lowland is due to dissimilarity in the biogeochemistry.

3.4.2 Temporal variation in mercury partitioning in groundwater

PHg in super-permafrost groundwater at Truelove Lowland increased by nearly 20% between Julian day 181 and 188; on the final sampling day (Julian day 191), PHg decreased substantially. There is a dearth of knowledge concerning PHg dynamics in High Arctic super-permafrost groundwater and in uncontaminated temperate groundwater systems. However, a temperate surface water study (Lake Superior) revealed that PHg was temporally dynamic with

PHg averaging 18% of THg in April and 26% of THg in August (Rolfhus et al., 2003). Rolfhus et al. (2003) also found that the suspended particulate mass did not vary temporally indicating that partitioning differed temporally. The observations of Rolfhus et al. (2003) are in agreement with this study where THg was not temporally dynamic indicating that partitioning differed temporally.

Oiffer (2008) recorded DHg concentrations in Truelove Lowland super-permafrost groundwater between Julian Day 207 and 225. Their field study was conducted later in the summer than this study (Julian Day 181 to 191) and found that DHg concentrations did not change over time (mean DHg, 19 pmol L^{-1}) (Oiffer, 2008). Oiffer observed higher DHg concentrations than this study, where DHg was temporally dynamic and ranged from 1.69 pmol L^{-1} to 6.28 pmol L^{-1}. Also in contrast to this study, where Eh was temporally dynamic, Oiffer found that Eh did not differ over the duration of their study.

The difference between the two studies may be a result of seasonal differences. Oiffer's work was conducted during the summer, while this study was conducted during the spring thaw when many geochemical parameters are changing.

As in this study, Quinton and Pomeroy (2006) found that the chemistry of super-permafrost groundwater changed through the summer thaw. In the initial and mid-stages of the thaw they found that the geochemistry of the super-permafrost groundwater was primarily controlled by the chemistry of the snow pack (Quinton and Pomeroy, 2006). During the later part of the summer thaw, after snow drifts had ablated, geochemistry of the groundwater was influenced predominantly by the chemistry of the matrix (Quinton and Pomeroy, 2006).

Research has also shown that a phenomenon known as "preferential elution" occurs in melting snow which results in different ions being eluted from the snow pack at different times. In general, less soluble ions such as SO_4^{-2} will elute sooner than more soluble ions such as NO_3^- and Cl^- (Cragin et al., 1996). In this study a pulse of N ($NO_3^- + NO_2^-$) was observed on Julian day 188. Such a pulse is indicative of preferential elution from the snow pack (Kuhn, 2001).

The anion chemistry of Truelove Lowland super-permafrost groundwater was dynamic through the summer thaw. It is known that the speciation of dissolved Hg influences its interaction with particulate matter in aqueous systems (Kim et al., 2004c; Turner et al., 2001; Turner et al., 2004). Furthermore, anions are important to Hg speciation because they are potential ligands. Anions such as chloride and sulfide form stable, uncharged complexes with Hg

and are known to diminish Hg sorption to mineral phases (Harter and Ravendra, 2001; Kim et al., 2004b). Despite their importance, anion concentrations in this study were not correlated with PHg indicating that a single parameter does not ultimately control Hg partitioning in this system. This finding is in agreement with Daughney et al. (2002) who found that chloride concentration alone was a poor predictor of Hg sorption in temperate surface water.

The results of this study clearly show that there are differences in THg and PHg concentrations in snow, ephemeral standing water, and super-permafrost groundwater at Truelove Lowland. Further, the results indicate that THg in groundwater is not dynamic through the summer thaw, whereas PHg concentrations change through the thaw. It is thought that the dynamic PHg concentrations coupled with the static THg concentrations is indicative of changes in Hg partitioning.

This study provides the basis for further research into Hg speciation and partitioning in Truelove Lowland super-permafrost groundwater. Although it is thought that changes in Hg speciation drive the observed changes in Hg partitioning, the lack of empirical Hg speciation data precludes the author from making that conclusion. In Chapter 4 a laboratory microcosm experiment investigates whether changes in the biological component of the super-permafrost groundwater system influences Hg partitioning.

4. MERCURY PARTITIONING: THE IMPACT OF BACTERIA FUNCTIONAL GROUPS IN LOW TEMPERATURE MICROCOSMS

4.1 Introduction

Bacteria make up a large part of the biotic component in groundwater systems and are ubiquitious in the subsurface (Chapelle, 2001). These organisms have been identified in extreme aquatic environments such as ocean-floor geothermal vents (Geptner et al., 2002), hot springs (Hamid et al., 2003), alpine lakes (Felip et al., 2002; Peduzzi et al., 2003) and the sediments of polar oceans (Nichols et al., 2005a; Nichols et al., 2005b). As demonstrated in the wide variety of niches they inhabit, bacteria are extremely adaptable and are the domain with the greatest diversity (Pace, 1997). Of necessity, scientists have separated bacteria into functional groups based upon metabolic processes rather than phylogeny.

Despite diversity in phylogeny, because functional groups have common metabolic requirements, entire functional groups can be selectively inhibited. Inhibitors are bactericidal or bacteriostatic (suspending metabolism while present) (Sorensen, 1982). An ideal inhibitor prevents the metabolism of a targeted functional group while allowing all other functional groups to continue metabolizing, thus, revealing the effect of the inhibited group on its surroundings. Molybdate is widely accepted as an effective bacteriostatic inhibitor of sulfate reducing bacteria (SRB); however, it is also a bactericidal inhibitor of methanogens (Sorensen, 1982). Molybdate inhibits SRB by acting as an analogue of sulfate and irreversibly binding to AMP, which prevents SRB from generating energy (Oremland and Capone, 1988). Molydate does not affect the metabolism of dissimilatory iron reducing bacteria (Sorensen, 1982). Nitrite and nitrate are bacteriostatic inhibitors of dissimilatory iron reducing bacteria (DIRB) (Sorensen, 1982). Nitrate inhibits DIRB by modifying the redox status to be energetically unfavorable for DIRB metabolism (Oremland and Capone, 1988).

The results of Chapter 3 indicate that mercury (Hg) speciation is an important determinant of Hg partitioning in High Arctic super-permafrost groundwater. Bacteria influence the Hg speciation in a variety of ways. Bacteria are known to: reduce, methylate and demethylate

Hg (Compeau and Bartha, 1984; Gilmour et al., 1992; Hintelmann et al., 2000); produce and consume Hg ligands (Chapelle, 2001; Freeze and Cherry, 1979); sorb metals to their cell surface (Boyanov et al., 2003; Daughney et al., 2001; Daughney et al., 2002; Hard et al., 1999); and manipulate physicochemical parameters such as pH and Eh (Chapelle, 2001; Freeze and Cherry, 1979). However, it is not known if microbial populations are responsible for changes in Hg speciation observed in Truelove Lowland super-permafrost groundwater. Because of their potential to influence Hg geochemistry via their metabolism SRB and DIRB functional groups are the focus of this chapter.

The microcosm experiment described in this chapter employed aerobic and anaerobic incubation and SRB and DIRB selective inhibitors. These experiments are designed to test two hypotheses. First, that free sulfide and bacterial surface-associated sulfide are the predominant sorbents of Hg in High Arctic super-permafrost groundwater; and second, by altering the biogeochemistry of the system, functional groups of bacteria will alter the partitioning of Hg in High Arctic super-permafrost groundwater.

4.2 Materials and Methods

4.2.1 Experimental design

The microcosm experiment was conducted in two batches. Batch 1 selectively inhibited and stimulated SRB. Batch 2 selectively inhibited and stimulated SRB and DIRB populations. The microcosm experiment described in this chapter was designed for analysis by two-way analysis of variance (ANOVA). Soil from catenas (5, 6, 7, and 9) served as replicates, and treatments were applied to two different soil types, lower foreslope (LFS) soil or wet sedge meadow (WSM) soil. The microcosms were incubated at 10˚C, in the dark. Microcosms were arranged randomly and were re-randomized after each sampling event.

4.2.2 Soil sampling for microcosms

The microcosms were assembled with soil collected on Day 192 at Truelove Lowland, NU. A five-point composite sample of the mineral soil horizons was collected from the LFS and WSM of catenas 5, 6, 7, and 9. Samples were collected with a shovel and small trowel, placed in Ziploc™ bags, and frozen for transport to Saskatoon. Frozen soil was stored at -20ºC until the microcosms were assembled.

4.2.3 Microcosm construction and sampling

4.2.3.1 Microcosm construction

Microcosms were contained in 250 mL high density polyethylene (I-Chem certified, HDPE) (Nalge Nunc International, USA), wide mouth amber bottles. Seven and a half grams of mineral soil from the LFS and WSM of each catena were placed into sterile HDPE bottles, to which the treatments were added. A saturated aerobic control, saturated anaerobic control, SRB-inhibited, and SRB-stimulated treatments were applied in 250 mL nanopure water in batch 1 of the microcosm experiment. In batch 2, an aerobic control, anaerobic control, SRB-inhibited, SRB-stimulated, DIRB-inhibited and DIRB-stimulated treatments were applied. Three microcosms for each landscape position and soil type were assembled. Microcosm bottles and treatments were autoclaved prior to assembly.

Microcosms were incubated in a darkened phytotron chamber (Conviron™), at 10ºC on the lowest setting of an orbital shaker. Prior to sampling, microcosms were shaken and allowed to settle for 30 minutes. The pH, Eh, and temperature were determined (using a ThermoOrion Pentrode™) and samples for the analytes of interest were collected. Aerobic microcosms were sampled on the lab bench and anaerobic microcosms were sampled in an anaerobic system (Model 1025, Forma Scientific, Inc., USA) with an atmosphere of 10% H_2, 10% CO_2 and 80% N_2 (Praxair, Saskatoon, SK). After sampling, the microcosms were closed tightly and removed from the anaerobic chamber. Anaerobic microcosms were inverted during incubation. Aerobic microcosms were incubated with the lid on, but not tightly closed. Sampling of batch 1 of the microcosm experiment occurred on Day 1, Day 6, Day 11, Day 16 and Day 49. Sampling of batch 2 of the microcosm experiment occurred on Day 14, Day 30, Day 44, Day 60, and Day 74. Table 4.1 shows the treatments included in batches 1 and 2 of the microcosm experiment.

4.2.3.2 Microcosm treatments

The treatments were dissolved in distilled water, autoclaved and then applied to the microcosms. Treatments were: aerobic control (distilled water), anaerobic control (distilled water), anaerobic SRB-inhibited (3mM $Na_2MoO_4 \cdot 2H_2O$ (Merck and Co., Rahway, N.J.)), anaerobic SRB-stimulated (3mM Na_2SO_4 (BDH Chemicals, Toronto, ON), anaerobic DIRB-inhibited (3mM $NaNO_3$ (CAS# 7631-99-4, J.T. Baker, Phillipsburg, NJ) and anaerobic DIRB-stimulated (3mM Fe(III)citrate (Anachemica Chemicals Ltd, Montreal, PQ). Batch 1 included only an aerobic control, anaerobic control and SRB-inhibited treatment. Batch 2 included an

Table 4.1 Microcosm experimental design and treatments for batch 1 and batch 2.

Batch 1[1]	Batch 2[2]	Treatment
AC	AC	-
ANC	ANC	-
SRB-	SRB-	3 mM $Na_2MoO_42H_2O$
SRB+	SRB+	3 mM Na_2SO_4
-	DIRB-	3 mM $NaNO_3$
-	DIRB+	3 mM Fe(III)-citrate

[1] Experiment ran for 49 days

[2] Experiment ran for 74 days

anaerobic control, SRB-inhibited, SRB-stimulated, DIRB-inhibited and DIRB-stimulated treatments and was conducted to further examine the role of SRB in Hg partitioning, and to determine whether DIRB activity influences Hg partitioning.

After assembly and prior to incubation anaerobic microcosms were reduced with titanium(III)nitrilotriacetate (TiNTA) (4 mL L^{-1}). To prepare the TiNTA 9.6g of nitrilotriacetic free acid (ICN Biomedicals Inc, Aurora, OH) was added to 300 mL of anaerobic water (prepared by autoclaving and cooling under a N_2 atmosphere). Next, 12.8 mL of anaerobic 15% $TiCl_3$ stock was slowly added to the solution, keeping the pH above 2 with an anaerobic, saturated solution of $NaCO_3$ (J.T. Baker Chemical Co., Phillipsburg, NJ). The final pH was adjusted to 7.0 with saturated $NaCO_3$. The TiNTA was filter sterilized with a syringe mounted 0.45μm pore size PVDF membrane filter with a polypropylene housing (Whatman Inc, Clifton, NJ). Titanium(III)nitrilotriacetate was chosen as a reductant because it had the lowest binding affinity (K_{sp}) for Hg of the potential reductants available (cysteine, sulfide, TiNTA, thioglycollic acid) (Ravichandran, 2004).

4.2.4 Reagent water

Nanopure water referred to in this section was processed by a NANOpure Diamond Ultrapure water system, Model D11911 (Barnstead International, Dubuque, IA). The water generated by this system is pure up to 18.2 MΩ cm^{-1} with a final 0.2 μm filter.

4.2.5 Mercury

Total and dissolved Hg in microcosm samples was analyzed by cold vapor atomic fluorescence spectroscopy using EPA Method 1631 (USEPA, 1999). The analysis was performed on a Tekran 2600 (Tekran Inc., Toronto, ON) using ultra high purity (UHP) argon supplied by Praxair (Saskatoon, SK). The Tekran was operated in a Clean Ceil Fan Filter Module (Microzone Corporation, Model No. VLF-2-4, Ottawa, Canada).

Approximately 25 mL of filtered (dissolved Hg) and unfiltered (total Hg) samples were collected from the microcosms in 50 mL polypropylene falcon tubes (Becton Dickinson & Co, Franklin Lakes NJ). Samples were preserved with 250 μl bromine chloride solution (BrCl) (preparation described in section 3.2.4) as soon as possible after sampling. Prior to analysis 100 μl of hydroxylamine hydrochloride ($NH_2OH{\cdot}HCl$) (preparation described in section 3.2.4) was added to consume excess BrCl. Stannous chloride ($SnCl_2$) was used as the reductant according to EPA Method 1631.

4.2.6 Anions

Anion analysis was conducted according to the protocol described in section 3.2.5.

4.2.7 Sulfide

Sulfide in microcosm experiments was analyzed according to the protocol outlined in section 3.2.6.

4.2.8 Iron speciation

The protocol outlined in section 3.2.7 was used to determine iron speciation in microcosm experiments.

4.2.9 Organic carbon

Total organic carbon (TOC) and dissolved organic carbon (DOC) was determined using the non-purgeable organic carbon (NPOC) method outlined in the Shimadzu TOC-5050A manual (Shimadzu). Filtered (DOC) and unfiltered (TOC) samples were collected in 9 mL borosilicate glass Solvent Saver™ vials (Cat # 66022-300, VWR). Samples were stored at 4ºC in the lab until analysis.

The organic carbon standard was prepared according to the manual (Shimadzu) by dissolving 1.0625 g of reagent grade potassium hydrogen phthalate (Nacalai Tesque, Inc., Kyoto, Japan) in 500 mL of fresh Nanopure water using a volumetric flask. Non-purgeable total organic carbon and non-purgeable dissolved organic carbon samples were run with a 50µl injection volume, 3 injections (maximum 5 injections), maximum SD of 200, maximum coefficient of variation of 2, and 4 washes. Analyses were run in range 5 setting.

4.2.10 Statistical analysis

Data from microcosm experiments was assessed for normality and homogeneity of variance using the protocol outlined for groundwater data (see section 3.2.9). When data was normal or non-normal and variances were homogeneous, data was analyzed with ANOVA by GLM (Sokal and Rohlf, 1995). When variances were heterogeneous statistical analysis was conduced using the Kruskal Wallis test (Sokal and Rohlf, 1995). The Kruskal Wallis test is a non-parametric test for use with heteroscedastic data sets (Sokal and Rohlf, 1995). Table 4.2 summarizes the method of statistical analysis for each parameter.

Table 4.2 Summary of statistical analysis methods for microcosm experiments

	Microcosm Experiments							
Variable	Date		Landscape Position		Catena		Treatment	
	ANOVA (GLM)[1]	Kruskall-Wallis	ANOVA (GLM)	Kruskall-Wallis	ANOVA (GLM)	Kruskall-Wallis	ANOVA (GLM)	Kruskall-Wallis
THg[2]		X		X	X			X
DHg[3]		X	X		X		X	
PHg[4]	X		X			X	X	
Chloride	X		X			X	X	
Nitrogen	X		X			X		X
Sulfate		X	X			X		
Sulfide		X		X		X		X
pH		X		X		X		X
Eh		X		X		X		X
Fe(II)		X	X		X		X	
Fe(III)		X	X		X			X
TOC[5]		X	X		X		X	
DOC[6]		X	X		X		X	

[1] analysis of variance by general linear model

[2] Total mercury

[3] Dissolved mercury

[4] Particulate mercury

[5] Total organic carbon

[6] Dissolved organic carbon

4.3 Results

4.3.1 Mercury

Particulate Hg and THg (total suspended mercury) are significantly different between treatments (p = 0.000; PHg; p = 0.000, THg); however, DHg did not differ between treatments. In laboratory microcosm experiments PHg was lowest in the DIRB- treatment (61 (38.5, 79.2) % (median (Q1, Q3)) and was 18% higher in the AC, ANC and SRB- treatments (p = 0.000, GLM, treatment) which had approximately 79 % PHg (Figure 4.1).

Total Hg concentrations followed the same distribution as PHg with the highest concentration in the ANC treatment (60 ± 4.7 pmol L^{-1}) and the lowest concentration in the DIRB- treatment (23 ± 2.6 pmol L^{-1}) (Figure 4.2). Total Hg at the initial sampling event was not consistent across treatments (Figure 4.3). With the exception of the ANC and SRB+ treatment there were changes in THg for each treatment over the duration of the experiment.

Particulate Hg in microcosms ranked: ANC ≈ SRB- ≈ AC > SRB+ > DIRB+ > DIRB-. Unlike PHg and THg, DHg did not differ between treatments (10 (4.7, 17.4) pmol L^{-1}) (p = 0.232, GLM, treatment) indicating that there is a difference in Hg partitioning between treatments.

There was also a temporal change in PHg concentrations in microcosms (p = 0.000). In batch 1 PHg decreased by approximately 11% over 49 days and in batch 2 PHg decreased by approximately 19 % over 74 days. Moreover, in both batches PHg was highest on the initial sampling day (89 (85.8, 90.8) %, batch 1; 82 (77.3, 89.7) %, batch 2. In batch 1 PHg decreased over time with the lowest PHg (77 (75.1, 81.0) %) observed on the final sampling day (day 49) (Figure 4.4a). In batch 2, which ran longer, PHg exhibited a parabolic curve with the lowest PHg (59 (58.4, 71.5) %) observed on day 44 (Figure 4.4b). In both batches PHg reached a minimum on a similar day. THg (p = 0.000) and DHg (p = 0.000) also differed between dates.

The distribution of PHg concentrations also differed between landscape positions (p = 0.034, GLM, landscape). The WSM and LFS had a median PHg content of 75 %, however the distribution of PHg differed significantly (WSM, 65.1, 84.0 (Q1, Q3) %; LFS, 58.6, 82.4 %) (Figure 4.5).

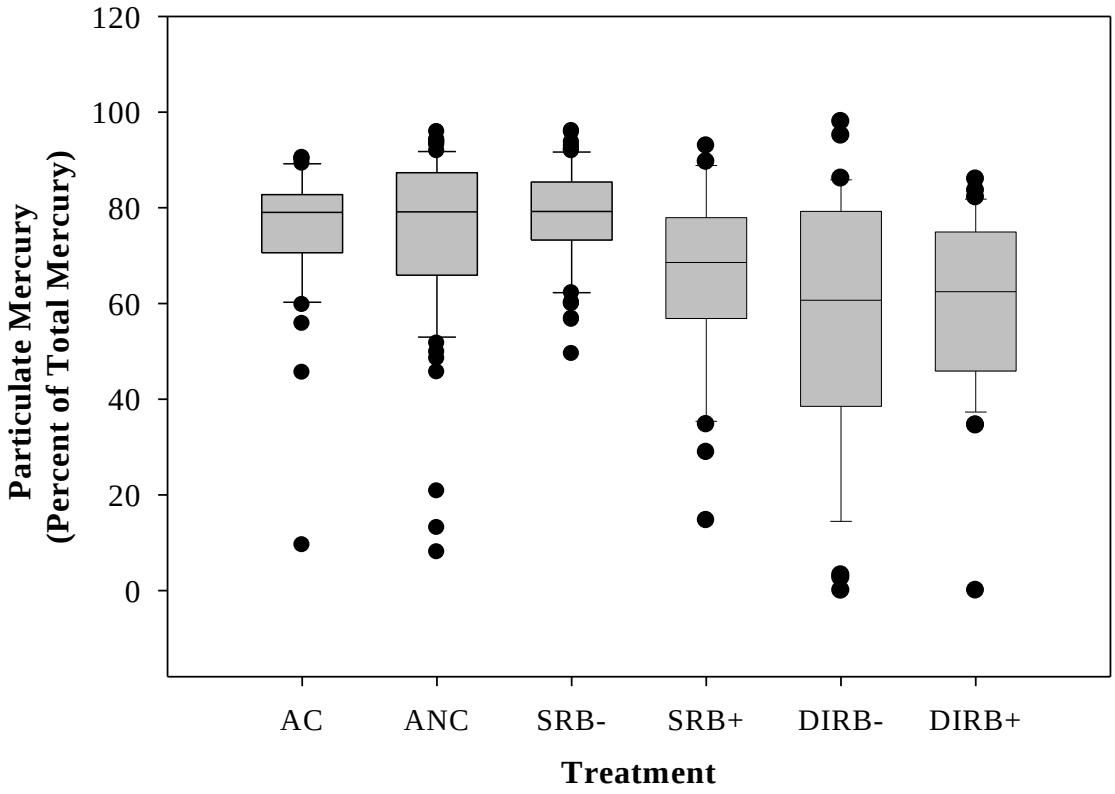

Figure 4.1 Boxplot of particulate mercury, as percent of total mercury, in microcosms by treatment. Aerobic control (AC), anaerobic control (ANC), sulfate reducing bacteria inhibited (SRB-), sulfate reducing bacteria stimulated (SRB+), dissimilatory iron reducing bacteria inhibited (DIRB-), and dissimilatory iron reducing bacteria stimulated (DIRB+). The line within the box represents the median, outer boundaries of the box represent the 25^{th} and 75^{th} percentiles, and the whiskers represent the 10^{th} and 90^{th} percentiles. The dots are data points outlying the 10^{th} and 90^{th} percentiles.

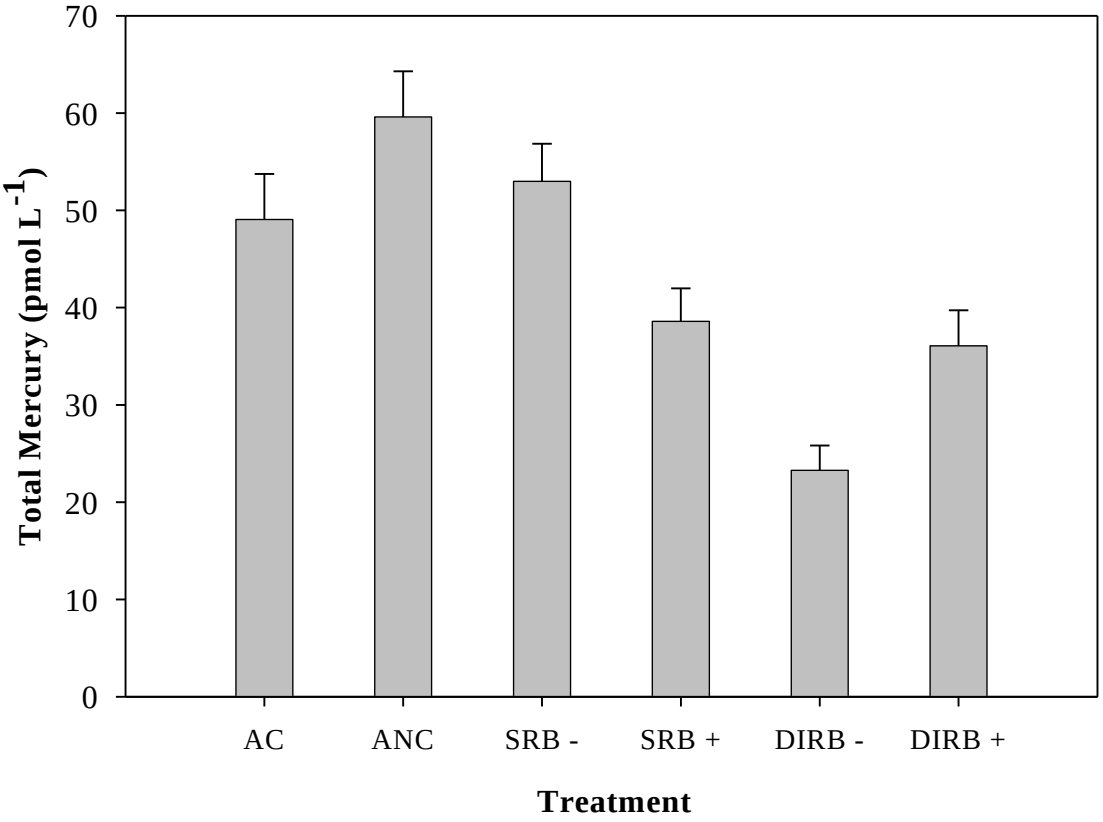

Figure 4.2 Mean total suspended mercury in microcosms by treatment over duration of microcosm experiment. Aerobic control (AC), anaerobic control (ANC), sulfate reducing bacteria inhibited (SRB-), sulfate reducing bacteria stimulated (SRB+), dissimilatory iron reducing bacteria inhibited (DIRB-), and dissimilatory iron reducing bacteria stimulated (DIRB+). Error bars represent standard error of the mean.

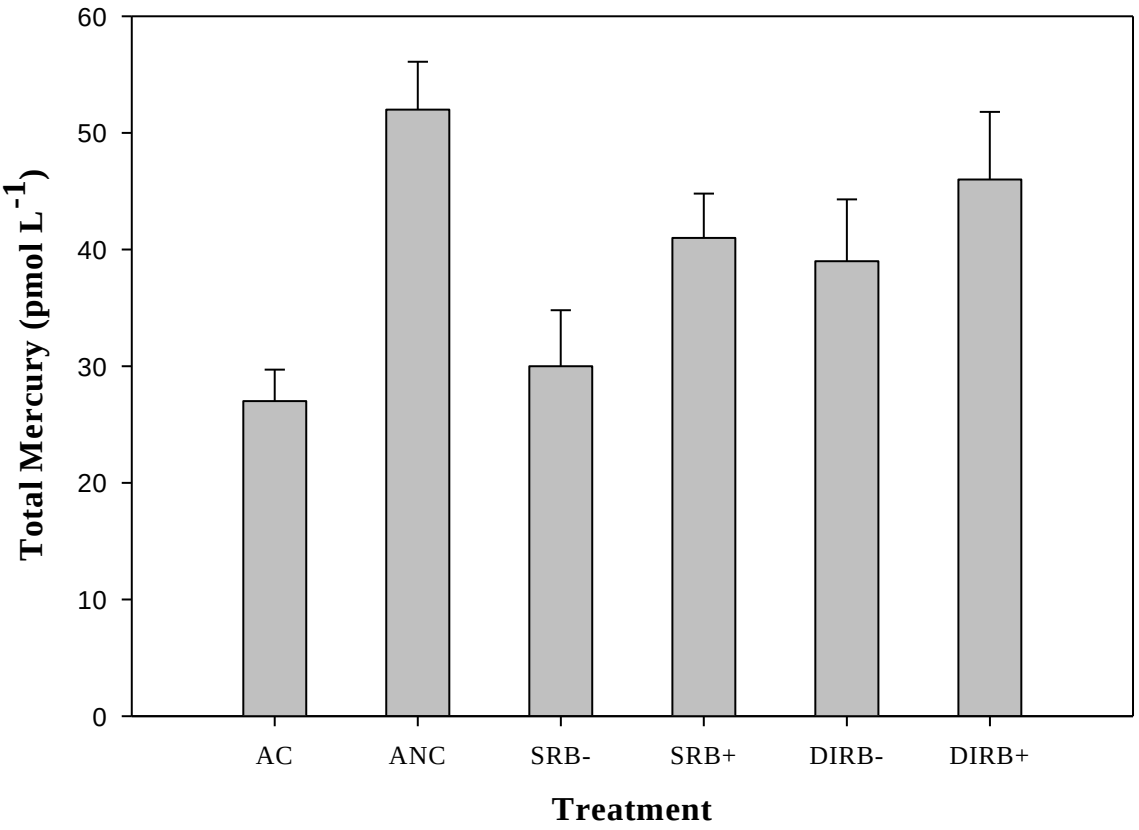

Figure 4.3 Mean total suspended mercury in microcosms by treatment at initial sampling of microcosm experiment. Aerobic control (AC), anaerobic control (ANC), sulfate reducing bacteria inhibited (SRB-), sulfate reducing bacteria stimulated (SRB+), dissimilatory iron reducing bacteria inhibited (DIRB-), and dissimilatory iron reducing bacteria stimulated (DIRB+). Error bars represent standard error of the mean.

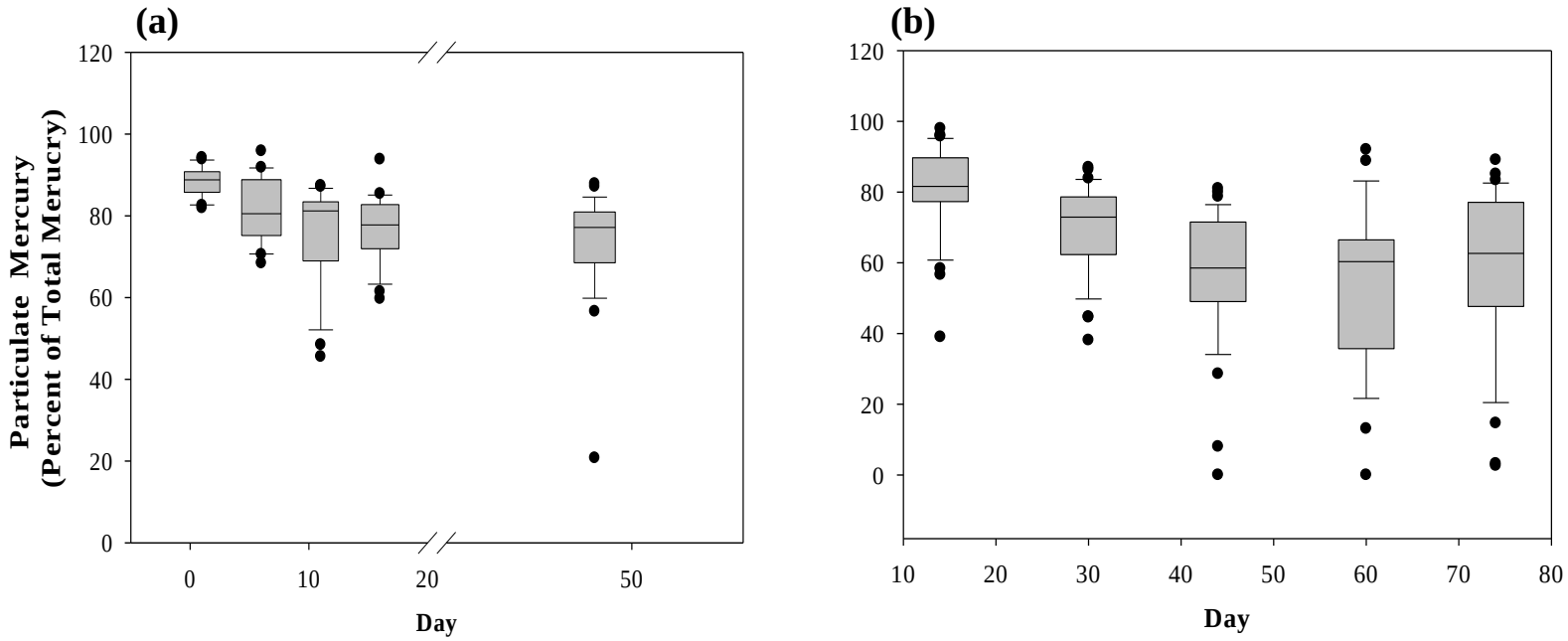

Figure 4.4 Microcosm Experiment - box plot showing temporal change in particulate mercury in (a) batch 1 and (b) batch 2. Minimum n = 24. The line within the box represents the median, outer boundaries of the box represent the 25th and 75th percentiles, and whiskers represent the 10th and 90th percentiles. The dots are data points outlying the 10th and 90th percentiles.

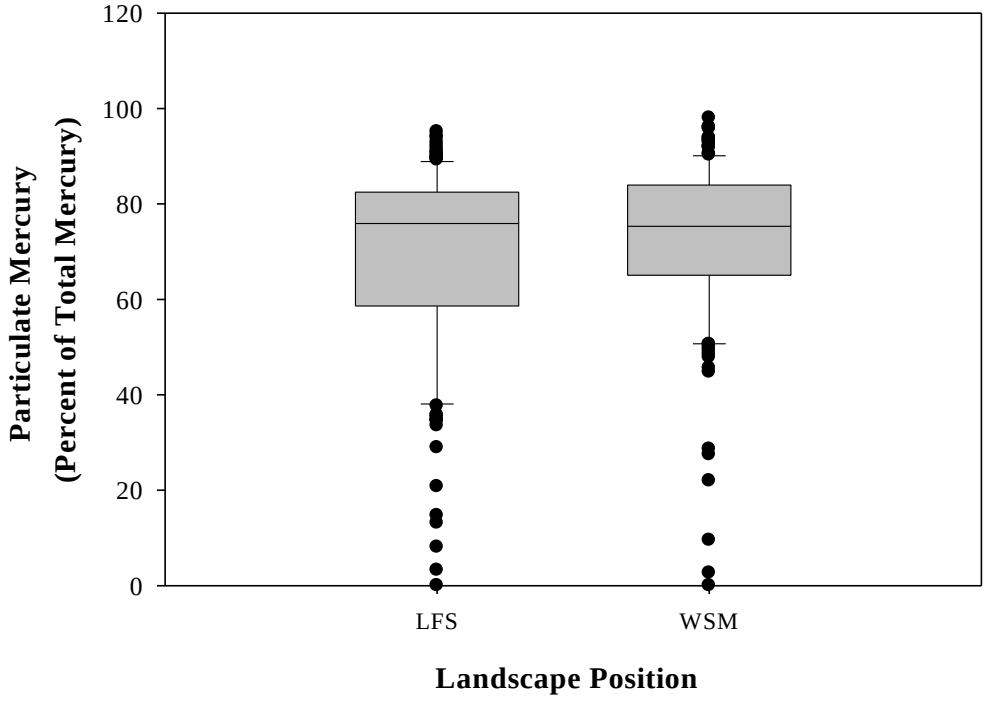

Figure 4.5. Particulate mercury in microcosms by landscape position. Lower foreslope (LFS) and wet sedge meadow (WSM). LFS n = 147; WSM n = 145. The line within the box represents the median, outer boundaries of the box represent the 25th and 75th percentiles, and the whiskers represent the 10th and 90th percentiles. The dots are data points outlying the 10th and 90th percentiles.

4.3.2 Anions

Chloride in the SRB- treatment (100 (0, 350) μmol L^{-1}) was approximately one-third of the concentration observed in all other treatments (p = 0.000, GLM, treatment) (Figure 4.6). Median Cl concentrations in other treatments ranged from 300 (210, 390) μmol L^{-1} to 380 (320, 470) μmol L^{-1}. Maximum Cl concentrations in both batches of the microcosm experiment occurred on the first day of sampling, day 1 (370 (0.0, 419) μmol L^{-1}) and day 14 (470 (302, 518) μmol L^{-1}), respectively. In general, chloride decreased over time (p = 0.000, GLM, date) (Figure 4.7). The median chloride concentrations in each treatment showed a strong negative correlation (Figure 4.8; r = -0.79) with PHg concentrations. Chloride concentrations were highest in the SRB-stimulated treatment ($NaSO_4$ amended) and the DIRB-inhibited treatment ($NaNO_3$ amended); however, chloride contamination via treatments can be ruled out as the chloride content in these treatments was below the detection limit.

Excluding the DIRB- treatment (3 mM $NaNO_3$ addition), nitrogen (as NO_2^- + NO_3^-) concentrations in all microcosm treatments was very low or undetectable (p = 0.132, Kruskal-Wallis, treatment) across all dates (0 (0.0, 0.0) μmol L^{-1}). However, a significant difference in nitrogen between sampling days (p = 0.044, GLM, date) was detected.

With the exception of the SRB+ treatment (3 mM $NaSO_4$ addition) the sulfate concentration was negligible in microcosms. Median sulfate concentration was 0.0 μmol L^{-1} in the AC, ANC, SRB-, DIRB- and DIRB+ treatments. When the SRB+ treatment (510 (437, 610) μmol L^{-1} SO_4^{2-}) was excluded there was no difference in sulfate between treatments (p = 0.999, GLM, treatment). Sulfate concentration did not exhibit a clear trend over time; however, there was a significant difference in SO_4^{2-} between dates in the microcosm experiment (p = 0.012, GLM, date).

4.3.3 Sulfide

Sulfide concentrations were an order of magnitude greater in the DIRB+ treatment than in all other treatments (p = 0.000, Kruskal-Wallis, treatment) (Figure 4.9). In the DIRB+ treatment the sulfide concentration was 1200 (636, 2010) μmol L^{-1}. Sulfide concentrations in other treatments ranged from 93 (57.3, 119) μmol L^{-1} to 250 (161, 324) μmol L^{-1}; sulfide concentrations in treatments ranked: DIRB+ >> DIRB- > SRB+ > SRB- > ANC > AC.

There was significant temporal variation in sulfide concentrations in the microcosm experiment (p = 0.000, Kruskal-Wallis, date). Sulfide concentrations in batch 1 steadily

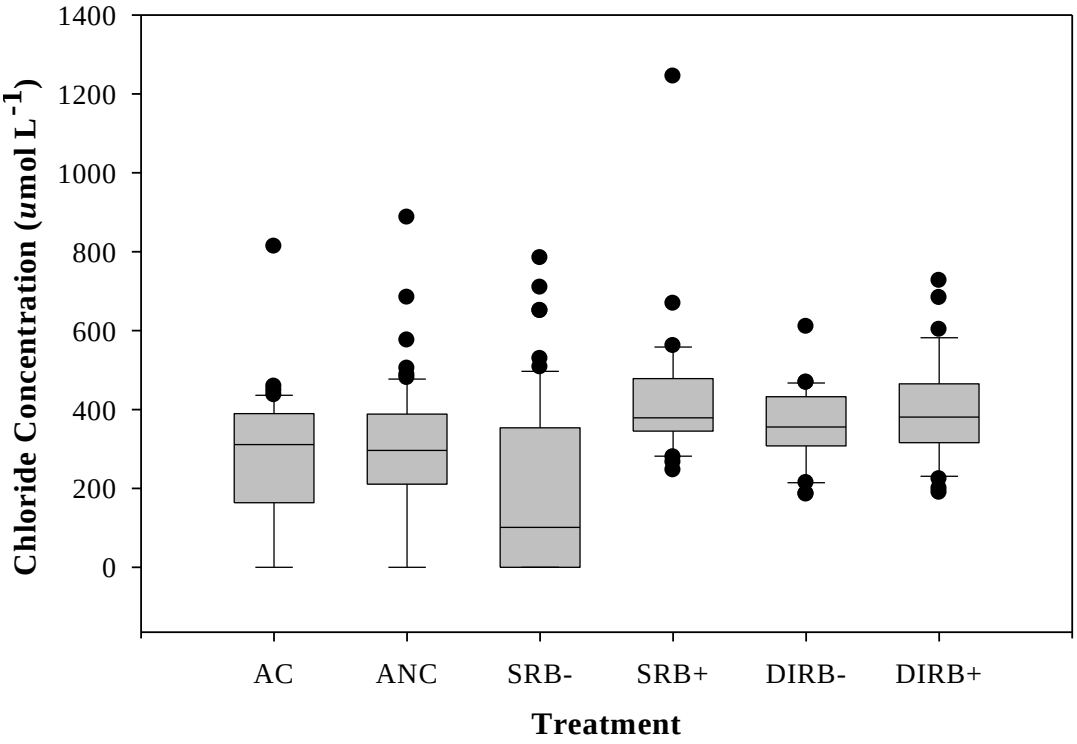

Figure 4.6 Boxplot of chloride concentration in microcosm experiment by treatment. Minimum n = 21. The line within the box represents the median, outer boundaries of the box represent the 25th and 75th percentiles, and the whiskers represent the 10th and 90th percentiles. The dots are data points outlying the 10th and 90th percentiles.

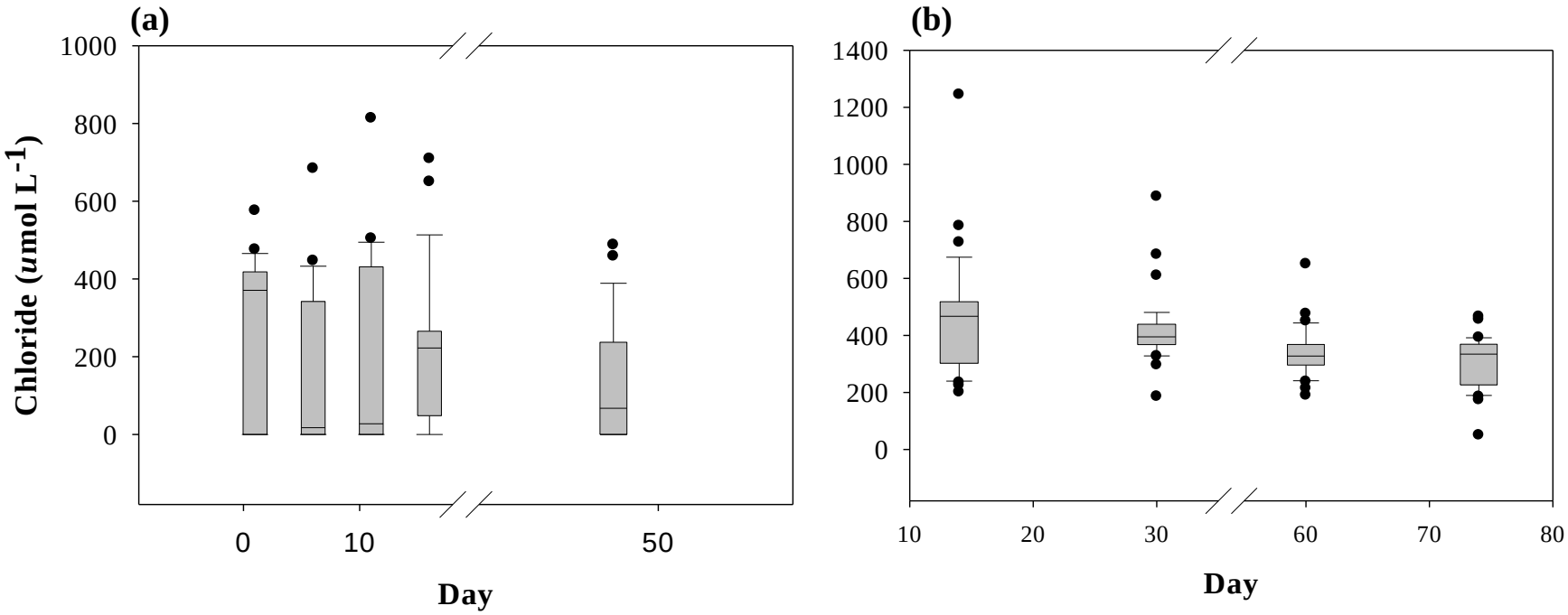

Figure 4.7 Boxplot of temporal change in chloride concentration in microcosm experiment (a) batch 1 and (b) batch 2. Minimum n = 21. The line within the box represents the median, outer boundaries of the box represent the 25th and 75th percentiles, and the whiskers represent the 10th and 90th percentiles. The dots are data points outlying the 10th and 90th percentiles.

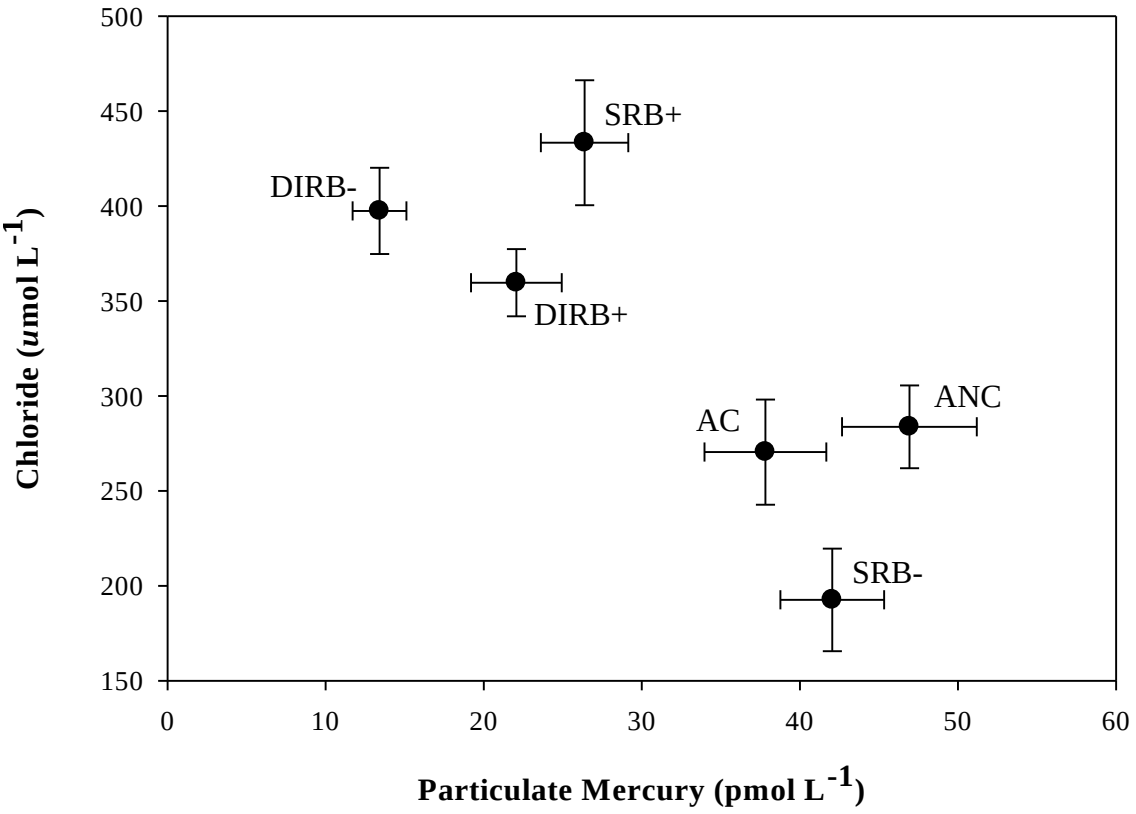

Figure 4.8 Average chloride and particulate mercury concentrations in each treatment. Error bars represent standard error of the mean. Minimum n = 21.

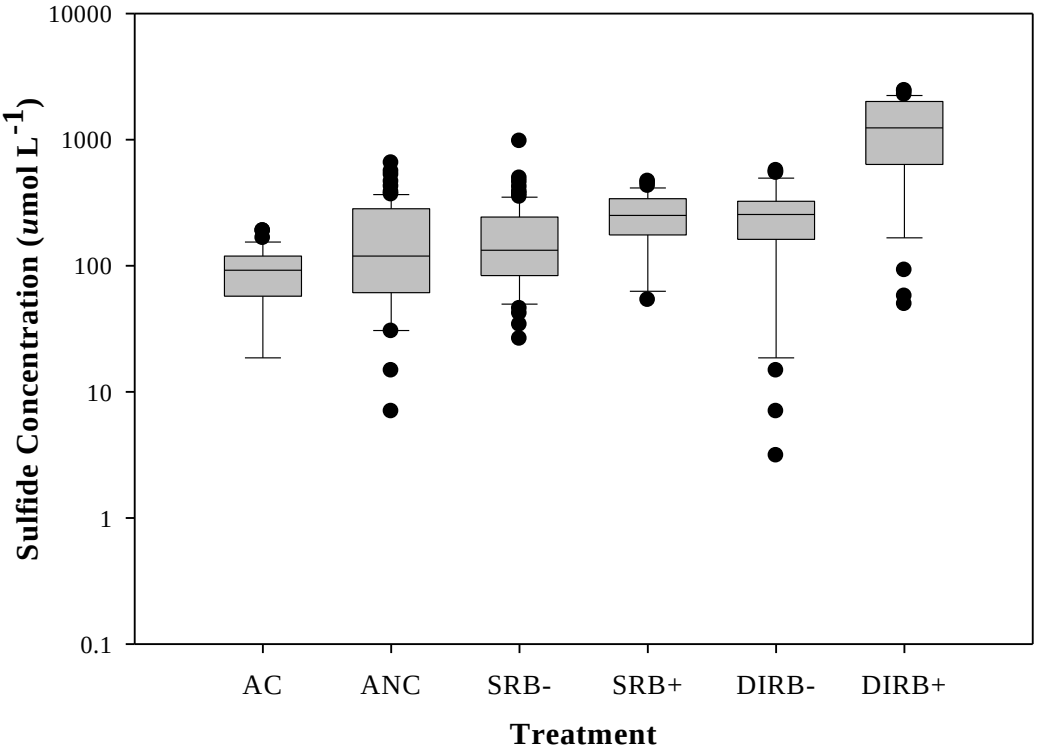

Figure 4.9 Boxplot of sulfide concentration in microcosm experiment by treatment. Aerobic control (AC), anaerobic control (ANC), sulfate reducing bacteria inhibited (SRB-), sulfate reducing bacteria stimulated (SRB+), dissimilatory iron reducing bacteria inhibited (DIRB-), and dissimilatory iron reducing bacteria stimulated (DIRB+). Minimum n = 30. The line within the box represents the median, outer boundaries of the box represent the 25^{th} and 75^{th} percentiles, and the whiskers represent the 10^{th} and 90^{th} percentiles. The dots represent data points outlying the 10^{th} and 90^{th} percentiles.

decreased over time (with the exception of day 16) from 110 (49.6, 158) µmol L^{-1} on the first sampling day to 69 (49.8, 108) µmol L^{-1} on the final sampling day. Conversely, sulfide concentrations in batch 2 exhibited an opposite trend, steadily increasing from 120 µmol L^{-1} on the first sampling day to 320 µmol L^{-1} on the final sampling day.

4.3.4 Iron speciation

As expected, iron(II) and iron(III) concentrations were significantly higher in the DIRB+ treatment (120 (99.5, 210) µmol L^{-1} and 550 (400, 731) µmol L^{-1}, respectively), which was amended with ferric citrate. Concentration of iron(II) was lowest in the anaerobic control (9.0 (0.00, 18.7) µmol L^{-1}); whereas, iron(III) concentrations were lowest in the DIRB- treatment (8.8 (5.1, 17.1) µmol L^{-1}). Figure 4.10a and 4.10b show Fe(II) and Fe(III) concentrations in treatments, respectively. Figure 4.11 shows the strong relationship (r=0.82) between iron(III) and PHg concentrations in microcosm treatments. Iron(II) and iron(III) concentrations also differed between sampling dates (p = 0.000, Kruskal-Wallis, date), however there was not a clear trend in iron(II) concentrations.

4.3.5 Organic carbon

Total organic carbon concentration was similar in all anaerobically incubated microcosms ranging from 17 (16.6, 19.6) ppm to 18 (15.6, 20.1) ppm. Total organic carbon in the aerobic control microcosm was nearly double the anaerobic microcosms (32 (19.3, 44.4) ppm) (p = 0.036, GLM, treatment). Total organic carbon does not vary between landscape, catena or sampling days. Organic carbon in the DIRB+ treatment was not analyzed due to the addition of ferric citrate.

Unlike TOC, DOC did not differ between treatments (p = 0.677, GLM, treatment), nor does it differ between landscapes or catenas. Dissolved organic carbon differs between sampling days, however there is not a clear trend in concentrations (p = 0.000, Kruskal-Wallis, date).

4.3.6 Eh and pH

pH was 6.3 (6.08, 6.68) in the DIRB+ treatment, more than 2 pH-units lower than in all other treatments (p = 0.000, Kruskal-Wallis, treatment). In other treatments pH ranged from 8.5 (6.73, 9.04) in the aerobic control to 9.3 (8.66, 10.3) in the SRB- treatment (Figure 4.12a). Likewise, Eh was lowest in the DIRB+ treatment (-140 (-294, 80.3) mV) (p = 0.000, Kruskal-

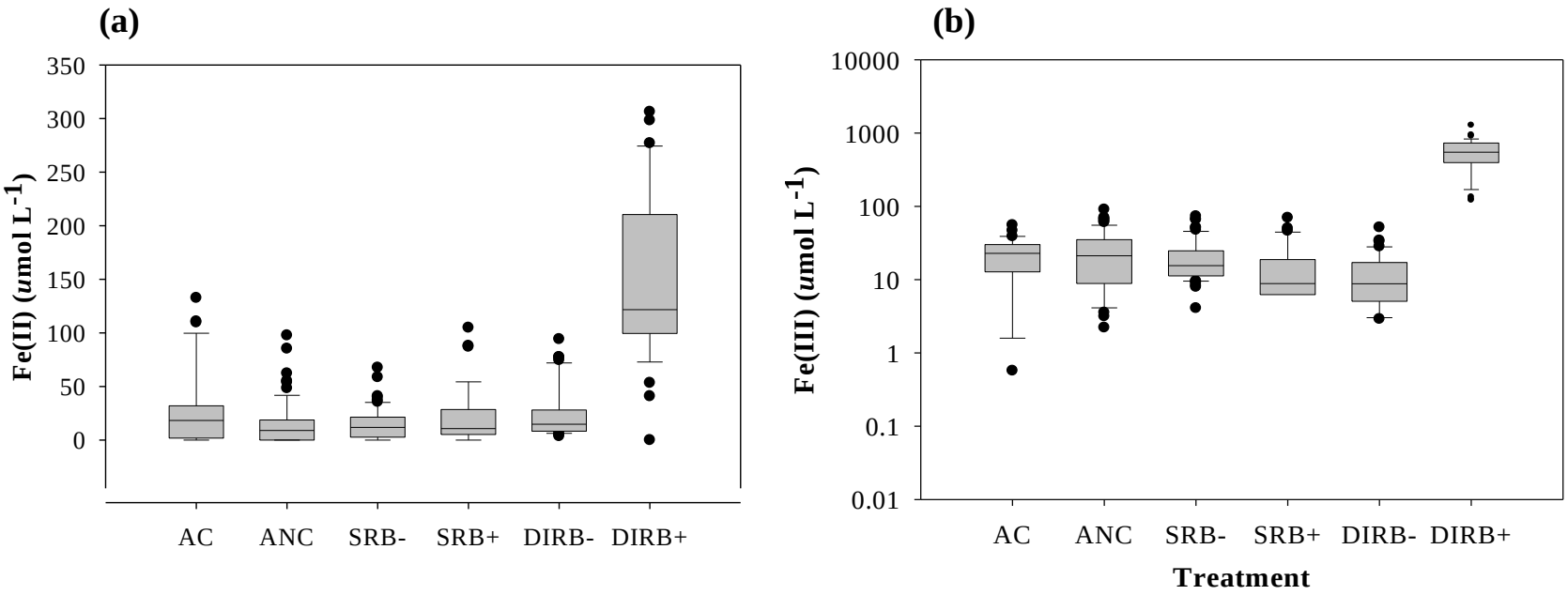

Figure 4.10 Boxplot of Fe(II) concentration in microcosm experiment (a) batch 1 and (b) batch 2. Minimum n = 32 for Fe(II) and Fe(III). The line within the box represents the median, outer boundaries of the box represent the 25th and 75th percentiles, and the whiskers represent the 10th and 90th percentiles. The dots represent data points outlying the 10th and 90th percentiles.

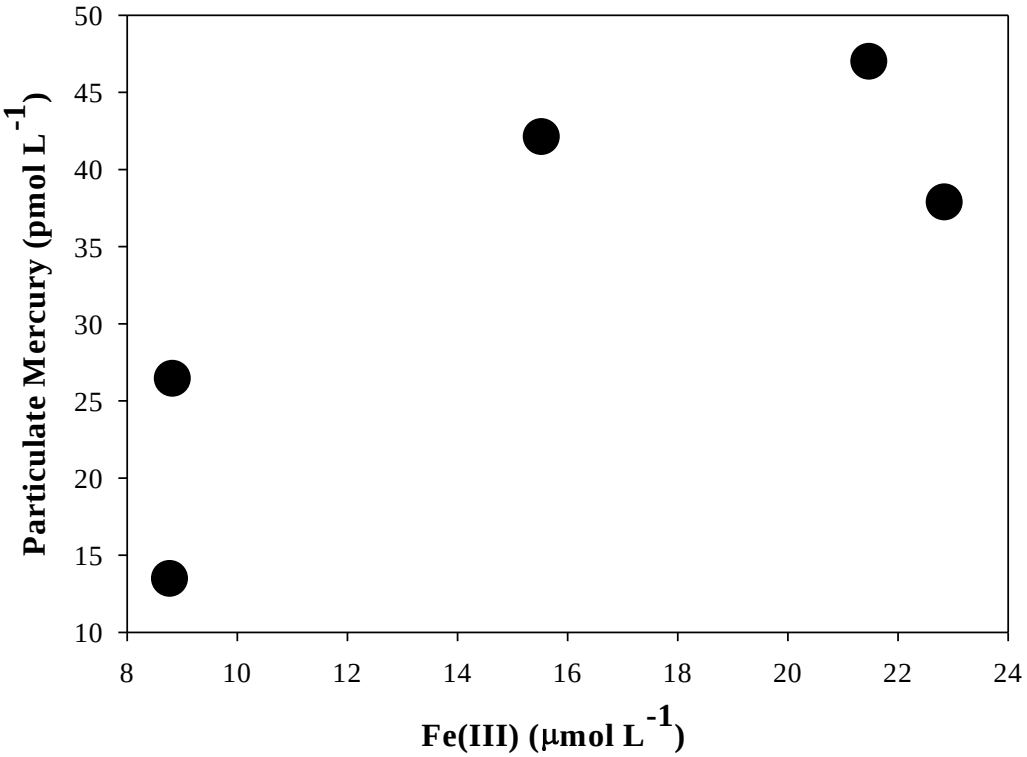

Figure 4.11 Correlation of median iron(III) concentration and mean particulate mercury concentration in microcosm experiment treatments (excluding DIRB+ treatment) (r = 0.82). Minimum n = 30.

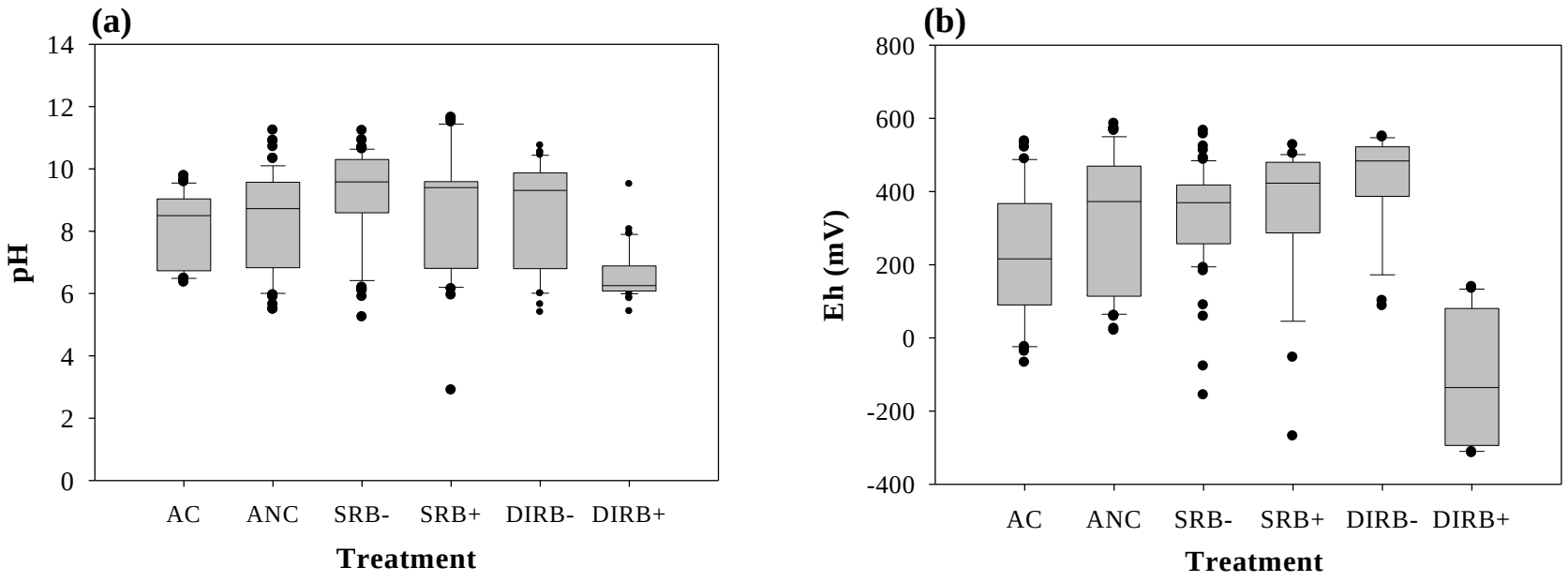

Figure 4.12 Boxplot of (a) pH and (b) Eh in microcosm experiment by treatment. Minimum n = 24 for both pH and Eh. The line within the box represents the median, outer boundaries of the box represent the 25th and 75th percentiles, and the whiskers represent the 10th and 90th percentiles. The dots represent data points outlying the 10th and 90th percentiles.

Wallis, treatment) (Figure 4.12b). pH and Eh also differed between sampling days (p = 0.000, Kruskal-Wallis, date); however, there was not a clear trend in these values.

4.4 Discussion

PHg in microcosms appears to be controlled by the redox cycling of Fe and the presence of HFO as a sorbent. Similar to results obtained for temperate freshwaters (Babiarz et al., 2001; Daughney et al., 2002) individual measurements of PHg in microcosms are not well correlated with the corresponding concentrations of ancillary parameters such as TOC, DOC, pH, Eh, Cl^-, NO_3^++NO_2^-, SO_4 or S^{2-}. However, median Cl^- and Fe(III) concentrations in each treatment are strongly correlated with PHg concentrations.

The inverse relationship between chloride concentration and PHg is in agreement with research showing that there is a decrease in sorption with a concomitant increase in chloride (Kim et al., 2004b). The reduced sorption is due to the formation of stable, neutral Hg-chloride complexes (Kim et al., 2004b). An effort was made to ensure the microcosms were not contaminated with chloride by avoiding the use of treatments containing chloride. However, a marked increase in the chloride concentration of microcosms compared to field conditions (presented in Chapter 3) was observed.

The high chloride concentration observed in the microcosm experiment is not likely due to contamination by treatments as the AC and ANC treatments (to which no treatment was added) have similar concentrations to SRB+, DIRB- and DIRB+ (Figure 4.5). SRB- to which Na_2MoO_4 was added has a much lower median concentration. Truelove Lowland soils are marine in origin. The high chloride concentration in the microcosm experiment may be due to the mechanical breakdown of the soil due to the action of the orbital shaker causing a release of chloride.

The positive correlation between Fe(III) and PHg is also in agreement with literature documenting Hg sorption to HFO. High Arctic soils are generally poor in organic matter (Bliss, 1997; Tedrow, 1977; Williams and Smith, 1979), and in the absence of organic matter HFO are known to be important sorbents of Hg (Miller, 2006; Regnell et al., 2001; Tiffreau et al., 1995). Although, the presence of HFO in microcosms was not analytically verified, an opaque light orange precipitate was observed in the bottom of some sample containers during this experiment suggesting that precipitation of HFO was indeed occurring.

Iron oxides have been identified as important sorbents of Hg in temperate freshwaters (Babiarz et al., 2001; Bilali et al., 2002; Pokrovsky et al., 2006).The results of this study indicate that Fe(III), likely in the form of HFO which have a high affinity for Hg, is the primary sorbent of Hg. It is postulated that this relationship is due to co-precipitation, surface complexation, and/or adsorption of Hg on HFO and subsequent settling from the soil/water suspension, which would decrease PHg and THg in microcosms. It is further hypothesized that when dissimilatory iron reduction occurs (in all treatments except DIRB-) the reductive dissolution of HFO, the release and readsorption of associated Hg, and the subsequent chemical oxidation of Fe(II) to Fe(III) under aerobic conditions will prevent sequestration of Hg in association with precipitated HFO. By preventing sequestration of Hg in association with HFO precipitates, THg and PHg concentrations in other treatments are not diminished to the same extent as in the DIRB- treatment.

Despite poising the microcosms with TiNTA, the average Eh of microcosms was only reducing in the DIRB+ treatment (-136 mV). All other treatments were within the overlapping zones of oxygen, nitrate, manganese, and iron reduction. The experimental design was intended to create and maintain reducing conditions in the ANC, SRB-, SRB+, DIRB- and DIRB+ treatments. However, reducing conditions only occurred in the DIRB+ treatment.

The Eh difference between the DIRB+ treatment and all other treatments is likely due to redox "poising" of the treatment by DIRB activity. This poising likely created preferential conditions for sulfate reduction which, in turn, lowered the Eh further. SRB activity in this treatment is apparent in the high sulfide concentration compared to other treatments. That is not to say that sulfate reduction did not occur at reducing microsites within other microcosms, however the overall aerobic nature of the other treatments would rapidly oxidize any sulfide produced.

A disparity in pH values between treatments was observed in this study. The pH in the DIRB+ treatment was at least 2 pH-units lower than all other treatments. The lower pH observed in this treatment is likely due to the addition of Fe(III)-citrate as a DIRB stimulant. Since many components of natural geologic systems have pH-dependent charge this difference in pH will influence sorptive processes. In particular, organic matter, microbial biomass and HFO, all of which are known to sorb Hg, have pH-dependent charge (Boyanov et al., 2003; Kim et al., 2004a; Ledin et al., 1999; Mishra and Vijaya, 2006; Ravichandran, 2004; Tiffreau et al., 1995).

If the pH of the DIRB+ treatment could have been maintained in the range of the other treatments (8.5-9.3) PHg concentrations would likely have been higher than observed. A higher PHg concentration in the DIRB+ treatment would reinforce the DIRB- treatment as being significantly lower than other treatments, thus confirming the results of this study.

This experiment attempted to simulate groundwater conditions using batch-type microcosms. The microcosms are a static system, as opposed to groundwater, which functions as a flow-through system. The primary difference between static and flow-through systems is that waste materials are not flushed through the system, and there are no inputs. This is also the primary difference between the microcosm experiment and field conditions. In the field flow conditions prevail, and thus waste materials are flushed away. Under field conditions there are also inputs which may differ over time.

This study is the first report of an *ex-situ* investigation of Hg partitioning in High Arctic polar oasis soils. These soils have very little organic matter compared to mineral soils in temperate latitudes. Organic carbon, which is important to Hg speciation and partitioning in temperate regions, appears to be less important in High Arctic soils. Controls on Hg partitioning in the High Arctic differ from those observed in temperate mineral soils.

The results of this study fail to support the hypothesis that free sulfide and microbial surface associated sulfide is the primary sorbent of Hg in this system. However, the observed difference in PHg between treatments supports the hypothesis that by altering the biogeochemistry of the system Hg partitioning can be altered. The results of this study indicate that HFO are the primary sorbent of Hg in High Arctic polar oasis mineral soils, and redox cycling of Fe influences the amount of PHg in these soils. Furthermore, since DIRB play an important role in the redox cycling of Fe, they too play an important role in the partitioning of Hg.

5. GENERAL DISCUSSION AND CONCLUSIONS

The principal findings of this study are that mercury (Hg) partitioning differs among snow, ephemeral standing water, and super-permafrost groundwater in the High Arctic, and that Hg partitioning in super-permafrost groundwater changes as the summer thaw progresses. Moreover, the activity of dissimilatory iron reducing bacteria (DIRB) and the redox cycling of iron appear to prevent Hg from being sequestered in flocculated HFO, thus maintaining Hg in the dissolved and particulate phases. Sulfides were expected to be important ligands of Hg in this system and were hypothesized to have an important impact on Hg partitioning. Unexpectedly, results indicate that sulfides do not have a strong influence on Hg partitioning in this system because the groundwaters never reached a condition where substantial sulfide was produced. Eh measurements of super-permafrost groundwater indicate that reducing conditions did not occur during the summer thaw. However, the observed Eh and pH values in the field and laboratory studies are firmly in the range where $Fe(OH)_3$ is the dominant iron species, confirming that HFO are likely to be the dominant form of iron present in this system.

Results of the field study (Chapter 3) indicate that biogeochemistry is an important determinant of partitioning in Truelove Lowland super-permafrost groundwater. However, the nature of the primary sorbent of Hg in the groundwater was not resolved. Unlike many temperate soils, the soils of Truelove Lowland are marine in origin, and are known to contain chloride (Walker and Peters, 1977). The results of the microcosm study (Chapter 4) indicate that there is a negative correlation between chloride concentration and PHg. This finding is in agreement with the findings of other researchers who note that chloride forms stable uncharged complexes with Hg, resulting in diminished Hg sorption to mineral phases (Harter and Ravendra, 2001; Kim et al., 2004b).

High Arctic polar oasis mineral soils also differ from temperate mineral soils in their lack of organic matter and low clay content. Organic matter and clay minerals have a large surface area and an abundance of functional groups which act as sorption sites for Hg. Despite lacking an abundance of organic matter and clay constituents, Truelove Lowland mineral soils, which are

partly derived from iron-bearing parent material (gneisses and metamorphic granulites) (Krupicka, 1977) were able to sorb significant amounts of Hg. Empirical evidence from the microcosm study suggests that HFO were present in the microcosms. Hydrous ferric oxides are known sorbents of Hg (Tiffreau et al., 1995). Although direct evidence of HFO as the primary sorbent of Hg in this system was not obtained, a host of indirect evidence supports this conclusion. This indirect evidence includes: a correlation between Fe(III) concentrations and PHg, low PHg concentrations in the DIRB- microcosm treatment and the presence of iron oxides in the microcosms.

The studies presented and discussed in this thesis were designed to test three hypotheses:

1. Partitioning of Hg in snow, standing water and super-permafrost groundwater differs, and Hg partitioning in super-permafrost groundwater will change through the summer thaw.
2. Free sulfide and bacterial surface-associated sulfide is the predominant ligand of Hg in High Arctic super-permafrost groundwater.
3. Functional groups of bacteria alter the partitioning of Hg in High Arctic super-permafrost groundwater via metabolic processes.

The Truelove Lowland field study validated hypothesis 1. As expected, the predicted Hg speciation indicates that sulfide should be an important Hg ligand in this system. However, results of the field and laboratory experiments did not confirm that sulfide and bacterial associated sulfides are dominant sorbents of Hg in the Truelove Lowland super-permafrost groundwater system (hypothesis 2). Results of the laboratory microcosm experiments indicate that hypothesis 3 can be accepted, and functional groups of bacteria are able to alter partitioning of Hg between the aqueous and particulate phase. Further study under more precisely controlled conditions, with confirmation of bacteria functional group activity would be necessary to conclusively determine the magnitude of the influence by bacteria.

Recent literature highlights the susceptibility of the Arctic environment to changes in ecosystem structure, biogeochemistry and contaminant transport as a result of global climate change (Keller et al., 2007; Macdonald et al., 2005; Schindler and Smol, 2006). In addition, polar scientists note the potential for unique, permafrost-related geochemical and hydrological changes due to global climate change (Keller et al., 2007; Macdonald et al., 2005; Schindler and Smol, 2006).

Keller et al. (2007) compared the geochemistry of soils and streams on surfaces of varying ages on the North Slope of Alaska. They conclude that an increase in the active layer thickness creates a measurable change in the geochemistry of the soils and streams, leading to increased weathering and nutrient release. In a separate study, an increase in lake water alkalinity was attributed to weathering of newly thawed glacial till (Hinzman et al., 2005). Such phenomenon will accompany increasing Arctic temperatures, and can be expected to influence the environment from a nanoscale (geochemistry) to a microscopic (microbial populations) and macroscopic scale (plant communities and animal populations).

Macdonald et al. (2005) note that historical waste disposal of hazardous substances has occurred in solid waste dumps, dump sites at DEW line installations, mine tailings and oil drilling sumps across the Arctic. Containment strategies for these sites rely at least in part on the integrity of the permafrost itself (Macdonald et al., 2005). Although the majority of anthropogenic Hg in the Arctic is a result of atmospheric transport, there are several known point sources (Terra #1 (Northrim Mine), Discovery Mine, Aishihik airstrip and the Border pump station/Rainy Hollow (Gregor et al., 2003) for which degradation of the permafrost may result a lack of containment and migration of Hg from these point sources into surface and groundwater systems.

Of utmost concern to regulators and researchers alike, is the knowledge that Hg in its methylated form poses a risk to human health (Morel et al., 1998; Van Oostdam et al., 2003). It is thought that particle associated Hg is not bioavailable, and thus can not be methylated (Benoit et al., 2001b). Consequently, the partitioning of Hg between the particulate and aqueous phases has implications for production of MHg. In turn, MMHg and DMHg have unique characteristics, resulting in bioaccumulation and biomagnification of Hg in ecosystems (Morel et al., 1998). Furthermore, in saturated coarse grained soils, which are typical of High Arctic mineral soils, facilitated transport of particulate-associated Hg is likely to cause an increase in the average velocity of particulate-bound Hg (Guine et al., 2003). This increase in velocity allows PHg to move through the landscape more quickly and reach wetlands, ponds and lakes where Hg-methylating SRB populations are most active. So, in summary, partitioning of Hg influences the fate and transport and bioavailability of Hg in the environment.

Scientific research supports the assertion that global climate change will alter the biogeochemistry of the High Arctic hydrologic system (Keller et al., 2007; Macdonald et al.,

2005; Schindler and Smol, 2006). The anticipated changes will alter the already poorly understood processes of partitioning, fate and transport of Hg in High Arctic super-permafrost groundwater. The research presented in this thesis is an initial attempt to elucidate the parameters that govern the partitioning of Hg and to determine the primary sorbent of Hg in the High Arctic super-permafrost groundwater system. Further investigation is necessary to verify the results of this research and to gain a better understanding of Hg transport at the landscape scale. Continuing research is necessary to build a foundation on which the impending risk to human and ecosystem health, resulting from a permafrost-related Hg release, can be understood and mitigated.

High Arctic research is a challenging milieu. The community is relatively small, and in many cases researchers are willing to share their wealth of knowledge on topics ranging from logistics and weather to experimental design. The research reported in this thesis was a first attempt by the Laboratory of Soil Environmental Toxicology (LaSET) at the University of Saskatchewan to characterize mercury partitioning in three matrices at Truelove Lowland. There were many lessons learned. A few are outlined below for the benefit of others planning High Arctic field research.

First and foremost the safety of the research team must be considered. Planning should include an assessment of possible hazards and the risk associated with them. Activities where the risk can not be mitigated by adequate planning should not be undertaken. A well equipped remote area safety kit should be taken to the field. Over-the-counter medications that may be of use in the field are: analgesics, anti-inflammatory, decongestant, anti-nausea and anti-diarrhea medication.

Regarding logistics, a stay of one day in Resolute, NU (or other jumping off point) is essential. This time can be used to ensure that all of the gear shipped from the south has arrived and is in good condition. If gear is missing, it allows the team an opportunity to borrow an item or to improvise with materials available in the area.

It is essential to plan experiments thoroughly so that all required supplies can be accounted for. Our team found it particularly useful to visualize each step of the process (from preparation, to implementing the experimental design, to data collection) and record the items necessary to conduct the work. The utility of duct tape can not be disputed. It has many

applications. During our field study it was used for repairing tears in field clothing, securing boxes, fixing broken objects, and repairing holes in shelters.

A rule of thumb regarding High Arctic fieldwork: expect the unexpected. The conditions at your field site, particularly if you have not visited it before, may not be what you expect. The adaptability of experimental design and/or objectives is essential. Also, a first attempt to implement an experimental design may not be successful. It is important to remain positive and open minded, as an alternate experimental design, or sampling method may realize results and new opportunities that were not initially recognized.

High Arctic field work is usually an intense period of setting up experiments and collecting data. The team may be away from the base camp area for the better part of a day at times. Upon returning to camp the preparation of a hearty warm meal is a good way to keep fatigue at bay. Our group often organized our daily tasks so that one member was at or near camp and could begin preparation of the evening meal. This allowed the team to remain energized throughout the field campaign. Our team also had great success shipping an assortment of long-lasting vegetables (carrot, turnip, onion, potato, cabbage) packed in newspaper in a ventilated container. The vegetables added a nice variety to our meals. When conducting research in the High Arctic you are in an incredibly beautiful location that many people will never have an opportunity to visit. Remember to take the time to absorb the experience, take in the sights and enjoy the High Arctic.

LIST OF REFERENCES

Ababneh, F.A., S.L. Scott, H.A. Al-Reasi, and D.R.S. Lean. 2006. Photochemical reduction and reoxidation of aqueous mercuric chloride in the presence of ferrioxalate and air. Sci. Total Environ. 367:831-839.

Amyot, M., D.R.S. Lean, and G. Mierle. 1997. Photochemical formation of volatile mercury in high artic lakes. Environmental Toxicology and Chemistry 16:2054-2063.

Amyot, M., G. Mierle, D.R.S. Lean, and D.J. McQueen. 1994. Sunlight-induced formation of dissolved gaseous mercury in lake waters. Environmental Science and Technology 28:2366-2371.

Ariya, P.A., A. Khalizov, and A. Gidas. 2002. Reactions of gaseous mercury with atomic and molecular halogens: Kinetics, product studies, and atmospheric implications. J. Phys. Chem. 106:7310-7320.

Babiarz, C.L., J.P. Hurley, S.R. Hoffman, A.W. Andren, M.M. Shafer, and D.E. Armstrong. 2001. Partitioning of total mercury and methylmercury to the colloidal phase in freshwaters. Environ. Sci. Technol.:4773-4782.

Becker, M.W., S.A. Collins, D.W. Metge, R.W. Harvey, and A.M. Shapiro. 2004. Effect of cell physicochemical characteristics and motility on bacterial transport in groundwater. J. Contam. Hydrol. 69:195-213.

Benoit, J.M., C.C. Gilmour, and R.P. Mason. 2001a. Aspects of bioavailability of mercury for methylation in pure cultures of *Desulfobulbus propionicus* (1pr3). Appl. Environ. Microbiol. 67:51-58.

Benoit, J.M., C.C. Gilmour, and R.P. Mason. 2001b. The influence of sulfide on solid phase mercury bioavailability for methylation by pure cultures of Desulfobulbus propionicus (1pr3). Environ. Sci. Technol. 35:127-132.

Benoit, J.M., R.P. Mason, C.C. Gilmour, and G.R. Aiken. 2001c. Constants for mercury binding by dissolved organic matter isolates from the Florida Everglades. Geochim. Cosmochim. Acta 65:4445-4451.

Bilali, L.E., P.E. Rasmussen, G.E.M. Hall, and D. Fortin. 2002. Role of sediment composition in trace metal distribution in lake sediments. Appl. Geochem. 17:1171-1181.

Bliss, L.C. 1997. Arctic tundra and polar desert, p. 708 Polar and alpine tundra. Cambridge University Press, Cambridge, UK.

Boyanov, M.I., S.D. Kelly, K.M. Kemner, B.A. Bunker, J.B. Fein, and D.A. Fowle. 2003. Adsorption of cadmium to *Bacillus subtilis* bacterial cell walls: A pH-dependent X-ray absorption fine structure spectroscopy study. Geochim. Cosmochim. Acta 67:3299-3311.

Carey, S., and M.-K. Woo. 2000. The role of soil pipes as a slope runoff mechanism, Subarctic Yukon, Canada. J. Hydrol. (Amsterdam) 233:206-222.

Casarett, and Doull. 2001. Casarett and Doull's toxicology: The basic science of poisons. 6th ed. McGraw Hill, New York.

Chapelle, F. 2001. Ground-water microbiology and geochemistry Wiley, New York.

Choi, S.C., T. Chase, and R. Bartha. 1994. Metabolic pathways leading to mercury methylation in *desulfovibrio desulfuricans* LS. Appl. Environ. Micro. 60:4072-4077.

Cline, J.D. 1969. Determination of sulfide in natural waters. Limnol. Oceanogr. 14:454-458.

Compeau, G., and R. Bartha. 1984. Methylation and demethylation of mercury under controlled redox, pH and salinity conditions. Appl. Environ. Micro. 48:1203-1207.

Costa, M., and P.S. Liss. 1999. Photoreduction of mercury in sea water and its possible implications for Hg^o air-sea fluxes. Marine Chemistry 68:87-95.

Courtin, G.M., and C.L. Labine. 1977. Microclimatological studies on Truelove Lowland, p. 73-106, *In* L. C. Bliss, ed. Truelove Lowland, Devon Island, Canada: A High Arctic Ecosystem. The University of Alberta Press, Edmonton.

Cragin, J.H., A.D. Hewitt, and S.C. Colbeck. 1996. Grain-scale mechanisms influencing the elution of ions from snow. Atmos. Environ. 30:119-127.

Daughney, C.D., J.B. Fein, and N. Yee. 1998. A comparison of the thermodynamics of metal adsorption onto two common bacteria. Chem. Geol. 144:161-176.

Daughney, C.D., D.A. Fowle, and D. Fortin. 2001. The effect of growth phase on proton and metal adsorption by *Bacillus subtilis*. Geochim. Cosmochim. Acta 67:1025-1035.

Daughney, C.D., S.D. Siciliano, A.N. Rencz, D. Lean, and D. Fortin. 2002. Hg(II) adsorption by bacteria: A surface complexation model and its application to shallow acidic lakes and wetlands in Kejimkujik National Park, Nova Scotia, Canada. Environ. Sci. Technol. 36:1546-1553.

Davranche, M., and J.-C. Bollinger. 2000. Release of metals from iron oxyhydroxides under reductive conditions: effect of metal/solid interactions. J. Colloid Interface Sci. 232:165-173.

Domenico, P.A., and F.W. Schwartz. 1990. Physical and chemical hydrogeology John Wiley & Sons.

Doyle, R.J. 1989. How cell walls of gram-positive bacteria interact with metal ions, *In* T. J. Beveridge and R. J. Doyle, eds. Metal ions and bacteria. John Wiley and Sons.

Drexel, R.T., M. Haitzer, J.N. Ryan, G.R. Aiken, and K.L. Nagy. 2002. Mercury(II) sorption to two Florida Everglades peats: evidence for strong and weak binding and competition by dissolved organic matter released from the peat. Environ. Sci. Technol. 36:4058-4064.

Eberhardt, L.L., and J.M. Thomas. 1991. Designing environmental field studies. Ecol. Monogr. 61:53-73.

Ekstrom, E.B., F.M.M. Morel, and J.M. Benoit. 2003. Mercury methylation independent of the acetyl-coenzyme A pathway in sulfate-reducing bacteria. Appl. Environ. Micro. 69:5414-5422.

Faust, S.D., and O.M. Aly. 1981. Chemistry of natural waters Ann Arbor Science, Ann Arbor.

Felip, M., A. Wille, B. Sattler, and R. Psenner. 2002. Microbial communities in the winter cover and the water column of an alpine lake: system connectivity and uncoupling. Aquatic Microb. Ecol. 29:123-134.

Ferris, F.G. 1989. Metallic ion interactions with the outer membrane of gram-negative bacteria, p. 295-324, *In* T. J. Beveridge and R. J. Doyle, eds. Metal ions and bacteria. John Wiley & Sons, New York.

Fishback, L.A. 2002. Establishing the provenance of catchment-derived pond sediments: Truelove Lowland, Devon Island. PhD, University of Western Ontario, London.

Fitzgerald, W.F., D.R. Engstrom, R.P. Mason, and E.A. Nater. 1998. The case for atmospheric mercury contamination in remote areas. Environ. Sci. Technol. 32:1-7.

Fleming, E.J., E.E. Mack, P.G. Green, and D.C. Nelson. 2006. Mercury methylation from unexpected sources: Molybdate-inhibited freshwater sediments and an iron-reducing bacterium. Appl. Environ. Micro. 72:457-464.

Freeze, and Cherry. 1979. Groundwater Prentice-Hall, Inc., Englewood Cliffs, NJ.

Galloway, M.E., and B.A. Branfireun. 2004. Mercury dynamics of a temperate forested wetland. Sci. Total Environ.:239-254.

(ed.) 1995a. Canadian Mercury Network Workshop.

(ed.) 1995b. Canadian Mercury Network Workshop.

Garrett, R.G. 1995c. Regional and large scale patterns of mercury distribution: Influentual factors [Online]. Available by Environment Canada (posted September 7, 2000; verified August 25, 2005).

Geesey, G.G., and L. Jang. 1989. Interactions between metal ions and capsular polymers, p. 325-358, *In* T. J. Beveridge and R. J. Doyle, eds. Metal ions and bacteria. John Wiley & Sons, New York.

Geptner, A., H. Kristmannsdottir, J. Kristjansson, and V. Marteinsson. 2002. Biogenic saponite from an active submarine hot spring, Iceland. Clays Clay Miner. 50:174-185.

Gilmour, C.C., E.A. Henry, and R. Mitchell. 1992. Sulfate stimulation of mercury methylation in freshwater sediments. Environ. Sci. Technol. 26:2287-2294.

Gregor, D., J. Stow, D. Kennedy, K. Reimer, and C. Ollson. 2003. Local sources of contamination in the Canadian Arctic. Indian and Northern Affairs Canada, Ottawa.

Guine, V., J. Martins, and J.P. Faudet. 2003. Facilitated transport of heavy metals by bacterial colloids in sand columns. J. Phys. IV 107:593-596.

Haitzer, M., G.R. Aiken, and J.N. Ryan. 2003. Binding of mercury(II) to aquatic humic substances: influence of pH and source of humic substances. Environ. Sci. Technol. 37:2436-2441.

Hall, J.A., B.J. Mailloux, T.C. Onstott, T.D. Scheibe, M.E. Fuler, H. Dong, and M.F. DeFlaun. 2005. Physical versus chemical effects on bacterial and bromide transport as determined from onsite sediment column pulse experiments. J. Contam. Hydrol. 76:295-314.

Hamid, N.S.A., H.B. Zen, O.B. Tein, Y.M. Halifah, N. Saari, and F. Abu Bakar. 2003. Screening and identification of extracellular lipase-producing thermophilic bacteria from a Malaysian hot spring. World J. Microbiol. Biotechnol. 19:961-968.

Hard, B.C., C. Walther, and W. Babel. 1999. Sorption of aluminum by sulfate-reducing bacteria isolated from uranium mine tailings. Geomicro. J. 16:267-275.

Harkins, M., A.J.R. Porter, and G.I. Paton. 2004. The role of host organism, transcriptional switches and reporter mechanisms in the performance of Hg-induced biosensors. J. Appl. Geochem. 97:1192-1200.

Harter, R.D., and N. Ravendra. 2001. An assessment of environmental and solution parameter impacts on trace-metal sorption by soils. Soil Sci. Soc. Am. J. 65:597-612.

Hinkel, K.M., F. Paetzold, F.E. Nelson, and J.G. Bockheim. 2001. Patterns of soil temperature and moisture in the active layer and upper permafrost at Barrow, Alaska: 1993-1999. Global Planet. Change 29:293-309.

Hintelmann, H., K. Keppel-Jones, and D. Evans. 2000. Constants of mercury methylation and demethylation rates in sediments and comparison of tracer and ambient mercury availability. Environ. Tox. Chem. 19:2204-2211.

Hinzman, L.D., N.D. Bettez, W.R. Bolton, F.S. Chapin, M.B. Dyurgerov, C.L. Fastie, B. Griffith, and R.D. Hollister. 2005. Evidence and implications of recent climate change in northern Alaska and other Arctic regions. Clim. Change 72:251-298.

Hodgson, R., and K.L. Young. 2001. Preferential groundwater flow through a sorted net landscape, Arctic Canada. Earth Surf. Processes Landforms 26:319-328.

Jaffe, D., E. Prestbo, P. Swartzendruber, P. Weiss-Penzias, S. Kato, A. Takami, S. Hatakeyama, and Y. Kajii. 2005. Export of atmospheric mercury from Asia. Atmos. Environ.:3029-3038.

Jay, J.A., F.M.M. Morel, and H.F. Hemond. 2000. Mercury speciation in the presence of polysulfides. Environ. Sci. Technol. 34:2196-2200.

Johnson, R.A., and G.K. Bhattacharyya. 1992. Statistics: principles and methods. 2 ed. John Wiley & Sons, New York, NY.

Jordan, F.L., S.K. Sandrin, R.J. Frye, M.L. Brusseau, and R.M. Maier. 2004. The influence of system complexity on bacterial transport in saturated porous media. J. Contam. Hydrol. 74:18-38.

Keller, K., J.D. Blum, and G.W. Kling. 2007. Geochemistry of soils and streams on surfaces of varying ages in Arctic Alaska. Arct. Alp. Res. 39:84-98.

Kerin, E.J., C.C. Gilmour, E. Roden, M.T. Suzuki, J.D. Coates, and R.P. Mason. 2006. Mercury methylation by dissimilatory iron-reducing bacteria. Appl. Environ. Micro. 72:7919-7921.

Kim, C.S., J.J. Rytuba, and G.E. Brown Jr. 2004a. EXAFS study of mercury(II) sorption to Fe- and Al-(hydro)oxides I. Effects of pH. J. Colloid Interface Sci. 271.

Kim, C.S., J.J. Rytuba, and G.E. Brown Jr. 2004b. EXAFS study of mercury(II) sorption to Fe- and Al-(hydr)oxides II. Effects of chloride and sulfate. J. Colloid Interface Sci. 270.

Kim, D., Q.R. Wang, G.A. Sorial, D.D. Dionysiou, and D. Timberlake. 2004c. A model approach for evaluating effects of remedial actions on mercury speciation and transport in a lake system. Sci. Total Environ. 327:1-15.

Kirk, G. 2004. Biogeochemistry of submerged soils John Wiley & Sons, West Sussex, UK.

Krupicka, J. 1977. Bedrock geology of the Truelove River area, p. 73-106, *In* L. C. Bliss, ed. Truelove Lowland, Devon Island, Canada: A high Arctic ecosystem. The University of Alberta Press, Edmonton.

Kuhn, M. 2001. The nutrient cycle through snow and ice, a review. Aquat. Sci. 63:150-167.

Lalonde, J.D., M. Amyot, A.M.L. Kraepiel, and F.M.M. Morel. 2001. Photooxidation of Hg(0) in artificial and natural waters. Environmental Science and Technology 35:1367-1372.

Lamborg, C.H., C.M. Tseng, W.F. Fitzgerald, and C.R. Hammerschmidt. 2003. Determination of the mercury complexation characteristics of dissolved organic matter in natural waters with "reducible Hg" titrations. Environ. Sci. Technol. 37:3316-3322.

Ledin, M., C. Krantz-Rulker, and B. Allard. 1999. Microorganisms as metal sorbents: comparison with other soil constituents in multi-compartment systems. Soil Biol. Biochem. 31:1639-1648.

Lev, A., and R.J. King. 2002. Spatial development of soil in a high Arctic soil landscape, Truelove Lowland, Devon Island, Nunavut. Permafrost Periglac. Process. 10:289-307.

Levy, S.J. 2006. Arsenic in a High Arctic soil ecoysystem, Devon Island, Nunavut. Masters of Science, University of Saskatchewan, Saskatoon.

Lin, C.J., M.D. Cheng, and W. Schroeder. 2001. Transport patterns and potential sources of gaseous mercury measured in High Arctic atmosphere in 1995. Atmos. Environ. 35:1141-1154.

Lindberg, S.E., S. Brooks, C.J. Lin, K.J. Scott, M.S. Landis, R.K. Stevens, M. Goodsite, and A. Richter. 2002. Dynamic oxidation of gaseous mercury in the Arctic troposphere at polar sunrise. Environ. Sci. Technol. 36:1245-1256.

Loseto, L.L., D.R.S. Lean, and S.D. Siciliano. 2004. Snowmelt sources of methylmercury to High Arctic ecosystems. Environ. Sci. Technol.:3004-3010.

Lowry, G.V., S. Shaw, C.S. Kim, J.J. Rytuba, and G.E. Brown Jr. 2004. Macroscopic and microscopic observations of particle-facilitated mercury transport from New Idria and Sulfur Bank mercury mine tailings. Environ. Sci. Technol. 38:5101-5111.

Macdonald, R.W., T. Harner, and J. Fyfe. 2005. Recent climate change in the Arctic and its impact on contaminant pathways and interpretation of temporal trend data. Sci. Total Environ. 342:5-86.

Macdonald, R.W., L.A. Barrie, T.F. Bidleman, M.L. Diamond, D.J. Gregor, R.G. Semkin, W.M.J. Strachan, Y.F. Li, F. Wania, C. Gobeil, C.J. Halsall, T. Harner, J.T. Hoff, L.M.M. Jantunen, W.L. Lockhart, D. Mackay, D.C.G. Muir, J. Pudykiewicz, K.J. Reimer, J.N. Smith, G.A. Stern, W.H. Schroeder, R. Wagemann, and M.B. Yunker. 2000. Contaminants in the Arctic: 5 years progress in understanding sources, occurrence and pathways. Sci. Total Environ. 254:94-234.

Markai, S., Y. Andres, G. Montavon, and B. Grambow. 2003. Study of the interaction between europium(III) and *Bacillus subtilis* fixation sites, biosorption modeling and reversibility. J. Colloid Interface Sci. 262:351-361.

Marvin-Dipasquale, M., J. Agee, C. McGowan, R.S. Oremland, M. Thomas, D. Krabbenhoft, and C.C. Gilmour. 2000. Methyl-mercury degradation pathways: a comparison among three mercury-impacted ecosystems. Environ. Sci. Technol. 34:4908-4916.

Marvin-Dipasquale, M.C., and R.S. Oremland. 1998. Bacterial methylmercury degradation in Florida Everglades peat sediment. Environ. Sci. Technol. 32:2556-2563.

Miller, C.L. 2006. The role of organic matter in the dissolved phase speciation and solid phase partitioning of mercury. Ph.D. Dissertation, University of Maryland, College Park.

Mishra, S.P., and M. Vijaya. 2006. Inorganic particulates in removal of heavy metal toxic ions - Part X: Rapid and efficient removal of Hg(II) ions from aqueous solutions by hydrous ferric and hydrous tungsten oxides. J. Colloid Interface Sci.:383-388.

Morel, F.M.M., A.M.L. Kraepiel, and M. Amyot. 1998. The chemical cycle and bioaccumulation of mercury. Annu. Rev. Ecol. Syst. 29:543-566.

Muc, M., and L.C. Bliss. 1977. Plant communities of the Truelove Lowland, p. 143-154, *In* L. C. Bliss, ed. Truelove Lowland, Devon Island, Canada: A high Arctic Ecosystem. The University of Alberta Press, Edmonton.

Murphy, E.M., and T.R. Ginn. 2000. Modeling microbial processes in porous media. Hydrogeol. J. 8:142-158.

Nichols, C.A.M., J. Guezennec, and J.P. Bowman. 2005a. Bacterial exopolysaccharides from extreme marine environments with special consideration of the southern ocean, sea ice, and deep-sea hydrothermal vents: A review. Marine Biotechnol. 7:253-271.

Nichols, C.M., S.G. Lardiere, J.P. Bowman, P.D. Nichols, J.A.E. Gibson, and J. Guezennec. 2005b. Chemical characterization of exopolysaccharides from Antarctic marine bacteria. Microb. Ecol. 49:578-589.

Oates, P.M., C. Castenson, C.F. Harvey, M. Polz, and P. Culligan. 2005. Illuminating reactive microbial transport in saturated porous media: demonstration of a visualization method and conceptual transport model. J. Contam. Hydrol. 77:233-245.

Oiffer, L. 2008. Biogeochemical factors affecting mercury methylation in High Arctic soils on Devon Island, Canada. M.Sc., University of Saskatchewan, Saskatoon.

Oremland, R.S., and D.G. Capone. 1988. Use of "specific" microbial inhibitors in biogeochemistry and microbial ecology. Adv. Microb. Ecol. 10:285-383.

Pacyna, J.M., E.G. Pacyna, F. Steenhuisen, and S. Wilson. 2003. Mapping 1995 global anthropogenic emissions of mercury. Atmos. Environ. 37:S109-S117.

Peduzzi, S., M. Tonolla, and D. Hahn. 2003. Isolation and characterization of aggregate-forming sulfate-reducing and purple sulfur bacteria from the chemocline of meromictic Lake Cadagno, Switzerland. FEMS Microbiol. Ecol. 45:29-37.

Pennock, D.J. 2004. Designing field studies in soil science. Can. J. Soil Sci. 84:1-10.

Pirrone, N., I. Allegrini, G.J. Keeler, J.O. Nriagu, R. Rossman, and J.A. Robbins. 1998. Historical atmospheric mercury emissions and depositions in North America compared to mercury accumulations in sedimentary records. Atmos. Environ. 32:929-940.

Pokrovsky, O.S., J. Schott, and B. Dupre. 2006. Trace element fractionation and transport in boreal rivers and soil porewaters of permafrost-dominated basaltic terrain in Central Siberia. Geochim. Cosmochim. Acta 70:3239-3260.

Pomeroy, J.W., and E. Brun. 2001. Physical properties of snow, p. 378, *In* H. G. Jones, et al., eds. Snow Ecology an interdisciplinary examination of snow-covered ecosystems. Cambridge University Press, Cambridge, UK.

Quantin, C., T. Becquer, J.H. Rouiller, and J. Berthelin. 2002. Redistribution of metals in a New Caledonia Ferralsol after microbial weathering. Soil Sci. Soc. Am. J. 66:1797-1804.

Quinton, W.L., and P. Marsh. 1998. The influence of mineral earth hummocks on subsurface drainage in the continuous permafrost zone. Permafrost Periglac. Process. 9:213-228.

Quinton, W.L., and P. Marsh. 1999. A conceptual framework for runoff generation in a permafrost environment. Hydrol. Process. 13:2563-2581.

Quinton, W.L., and J.W. Pomeroy. 2006. Transformations of runoff chemistry in the Arctic tundra, Northwest Territories, Canada. Hydrol. Process. 20:2901-2919.

Quinton, W.L., D.M. Gray, and P. Marsh. 2000. Subsurface drainage from hummock-covered hillslopes in the Arctic Tundra. J. Hydrol. (Amsterdam) 237:113-125.

Rancourt, D.G., P.-J. Thibault, D. Mavrocordatos, and G. Lamarche. 2005. Hydrous ferric oxide precipitation in the presence of nonmetabolizing bacteria: Constraints on the mechanism of a biotic effect. Geochim. Cosmochim. Acta 69:553-577.

Ravichandran, M. 2004. Interactions between mercury and dissolved organic matter - a review. Chemosphere 55:319-331.

Ravichandran, M., G.R. Aiken, M.M. Reddy, and J.N. Ryan. 1998. Enhanced dissolution of cinnabar (mercuric sulfide) by dissolved organic matter isolated from the Florida Everglades. Environ. Sci. Technol. 32:3305-3311.

Regnell, O., T. Hammar, A. Helgee, and B. Troedsson. 2001. Effects of anoxia and sulfide on concentrations of total and methyl mercury in sediment and waterin two Hg-polluted lakes. Can. J. Fish. Aquat. Sci. 58:506-517.

Rolfhus, K.R., H.E. Sakamoto, L.B. Cleckner, R.W. Stoor, C.L. Babiarz, R.C. Back, H. Manolopoulos, and J.P. Hurley. 2003. Distribution and Fluxes of Total and Methylmercury in Lake Superior. Environ. Sci. Technol. 37:865-872.

Ryden, B.E. 1977. Hydrology of Truelove Lowland, p. 107-136, *In* L. C. Bliss, ed. Truelove Lowland, Devon Island, Canada: A high Arctic Ecosystem. The University of Alberta Press, Edmonton.

Schaeffer, J.K., J. Letowski, and T. Barkay. 2002. *mer*-mediated resistance and volatilization of Hg(II) under anaerobic conditions. Geomicro. J. 19:87-102.

Schindler, D.W., and J.P. Smol. 2006. Cumulative effects of climate warming and other human activities on freshwaters of Arctic and Subarctic North America. Ambio 35:160-168.

Schroeder, W., and J. Munthe. 1998. Atmospheric mercury - An overview. Atmos. Environ. 32:809-822.

Schroeder, W., K.G. Anlauf, and L.A. Barrie. 1998. Arctic springtime depletion of mercury. Nature 394:331-332.

Sellers, P., C.S. Kelly, J.W.M. Rudd, and A. MacHutchon. 1996. Photodegradation of methylmercury in lakes. Nature 380:694-697.

Semkin, R.G., G. Mierle, and R.J. Neureuther. 2005. Hydrochemistry and mercury cycling in a High Arctic watershed. Sci. Total Environ. 342:199-221.

Shimadzu. Instruction manual total organic carbon analyzer model TOC-5050A, pp. 139. Shimadzu Corporation, Tokyo, Japan.

Siciliano, S.D., and D.R.S. Lean. 2002. Methyltransferase: an enzyme assay for microbial methylmercury formation in acidic soils and sediments. Environ. Tox. Chem. 21:1184-1190.

Siciliano, S.D., N.J. O'Driscoll, R. Tordon, J. Hill, S. Beauchamp, and D.R.S. Lean. 2005. Abiotic production of methylmercury by solar radiation. Environ. Sci. Technol. 39:1071-1077.

Silberberg. 1996. Chemistry: the molecular nature of matter and change Mosby-Year Book, Inc., St. Louis, MI.

Skov, H., J.H. Christensen, M.E. Goodsite, N.Z. Heidam, B. Jensen, P. Wahlin, and G. Geernaert. 2004. Fate of elemental mercury in the Arctic during atmospheric mercury depletion episodes and the load of atmospheric mercury to the Arctic. Environ. Sci. Technol. 38:2373-2382.

Slowey, A.J., J.J. Rytuba, and G.E. Brown Jr. 2005. Speciation of mercury and mode of transport from placer gold mine tailings. Environ. Sci. Technol. 39:1547-1554.

Smith, R.M., A.E. Martell, and R.J. Moitekaitis. 2004. NIST standard reference database National Institute of Standards and Technology (NIST), Gaithersburg, MD.

Sokal, R.R., and F.J. Rohlf. 1995. Biometry: the principles and practice of statistics in biological research. 3 ed. W.H. Freeman and Company.

Sorensen, J. 1982. Reduction of ferric iron in anaerobic, marine sediment and interaction with reduction of nitrate and sulphate. Appl. Environ. Micro. 43:445-451.

Sparks, D.L. 2003. Environmental soil chemistry. 2 ed. Academic Press, New York.

St. Louis, V.L., M.J. Sharp, A. Steffen, A. May, J. Barker, J.L. Kirk, D.J.A. Kelly, S.E. Arnott, B. Keatley, and J.P. Smol. 2005. Some sources and sinks of monomethyl and inorganic mercury on Ellesmere Island in the Canadian High Arctic. Environ. Sci. Technol. 39:2686-2701.

Starr, M., A.-J. Londroos, L. Ukonmaanaho, T. Tarvainen, and H. Tanskanen. 2003. Weathering release of heavy metals from soil in comparison to deposition, litterfall and leaching fluxes in a remote, boreal coniferous forest. Appl. Geochem. 18:607-613.

Steffen, A., W. Schroeder, L. Poissant, and R. Macdonald. 2003. Mercury in the Arctic atmosphere. Indian and Northern Affairs Canada, Ottawa.

Stumm, and Morgan. 1995.

Taylor, S.R. 1964. Abundance of chemical elements in the continental crust: a new table. Geochim. Cosmochim. Acta 28:1273-1285.

Tedrow, J.C.F. 1977. Soils of the polar landscapes Rutgers University Press, New Brunswick, New Jersey.

Thibodeaux, L.J. 1996. Environmental chemodynamics: Movement of chemicals in air, water and soil. 2 ed. John Wiley & Sons, New York.

Tiffreau, C., J. Lutzenkirchen, and P. Behra. 1995. Modeling the adsorption of mercury(II) on (hydr)oxides. J. Colloid Interface Sci. 172:82-93.

Tranter, M., and H.G. Jones. 2001. The chemistry of snow: process and nutrient cycling, p. 127-167, *In* H. G. Jones, et al., eds. Snow ecology an interdisciplinary examination of snow-covered ecosystems. John Wiley & Sons, Cambridge, UK.

Tseng, C.M., C. Lamborg, W.F. Fitzgerald, and D.R. Engstrom. 2004. Cycling of dissolved elemental mercury in Arctic Alaskan lakes. Geochim. Cosmochim. Acta 68:1173-1184.

Turner, A., G.E. Millward, and S.M. Le Roux. 2001. Sediment-water partitioning of inorganic mercury in estuaries. Environ. Sci. Technol. 35:4648-4654.

Turner, A., G.E. Millward, and S.M. Le Roux. 2004. Significance of oxides and particulate organic matter in controlling trace metal partitioning in a contaminated estuary. Marine Chem.:179-192.

USEPA. 1999. Method 1631, Revision B: Mercury in water by oxidation, purge and trap, and cold vapor atomic fluorescence spectrometry EPA-821-R-99-005. United States Environmental Protection Agency, Washington, DC.

Van Oostdam, J., S. Donaldson, M. Feeley, N. Tremblay, D. Arnold, P. Ayotte, G. Bondy, L. Chan, E. Dewailly, C. Furgal, U. Gill, S. Kalhok, H. Kuhnlein, E. Loring, G. Muckle, E. Myles, O. Receveur, Y. Stokker, and B. Tracy. 2003. Exposure assessment. Indian and Northern Affairs Canada, Ottawa.

Walker, B.D., and T.W. Peters. 1977. Soils of Truelove Lowland and plateau, p. 31-62, *In* L. C. Bliss, ed. Truelove Lowland, Devon Island, Canada: A high Arctic ecosystem. The University of Alberta Press, Edmonton.

Watras, C.J., K.A. Morrison, A. Kent, N. Price, O. Regnell, C. Eckley, H. Hintelmann, and T. Hubacher. 2005. Sources of methylmercury to a wetland-dominated lake in Northern Wisconsin. Environ. Sci. Technol.:4747-4758.

WHO. 1990. Environmental health criteria 101: Methylmercury. World Health Organization, Geneva.

Williams, P.J., and M.W. Smith. 1979. The frozen earth: fundamentals of geocryology Cambridge University Press, Cambridge, UK.

Woo, M.-k., and K.L. Young. 2006. High Arctic wetlands: Their occurrence, hydrological characteristics and sustainability. J. Hydrol. (Amsterdam) 320:432-450.

Wood, J.M. 1985. Effects of acidification on the mobility of metals and metaloids: An overview. Environmental Health Perspectives 63:115-119.

Table A-1. All data from superpermafrost groundwater from Truelove Lowland, NU.

Catena	Well #	Date	Julian Day	Water Column (cm)	pH	Eh (mV)	Temp (°C)	DHg (pM)	THg (pM)	PHg (pM)	DHg (ppt)	THg (ppt)
1	1	29-Jun	181	6	7.8	320	6.5	7.4	23	16	1.5	4.7
1	2	29-Jun	181	7	8.3	330	6.0	7.5	23	16	1.5	4.7
3	1	29-Jun	181	7	6.9	330	4.8	4.5	14	9.3	0.91	2.8
3	2	29-Jun	181	6	7.0	370	5.0	6.3	21	14	1.3	4.2
6	1	29-Jun	181	9	7.5	390	5.8	7.4	39	32	1.5	7.9
6	2	29-Jun	181	12	8.2	440	4.6	5.9	12	6.3	1.2	2.4
6	3	29-Jun	181	8	8.1	430	6.4	6.7	25	18	1.4	5.0
7	1	29-Jun	181	10	8.4	460	4.6	5.5	16	10	1.1	3.1
7	2	29-Jun	181	10	8.5	460	5.1	5.2	31	26	1.1	6.3
7	3	29-Jun	181	14	8.2	470	6.5	6.5	13	6.2	1.3	2.5
9	1	29-Jun	181	10	8.1	330	6.5	5.7	22	5.8	1.2	2.3
9	3	29-Jun	181	12	7.1	380	4.9	6.7	32	25	1.3	6.4
1	1	1-Jul	183	4	7.7	270	6.3	2.4	5.1	2.7	0.48	1.0
1	2	1-Jul	183	5	8.0	280	5.3	8.7	43	34	1.8	8.6
3	1	1-Jul	183	5	7.4	300	4.3	2.8	10	7.5	0.56	2.1

Table A-1. Continued

Catena	Well #	Date	Julian Day	Water Column (cm)	pH	Eh (mV)	Temp (°C)	DHg (pM)	THg (pM)	PHg (pM)	DHg (ppt)	THg (ppt)
6	2	1-Jul	183	6	7.7	-	4.3	4.9	39	34	1.0	7.8
6	3	1-Jul	183	4	7.7	-	4.3	3.9	13	9.4	0.78	2.7
7	1	1-Jul	183	10	8.1	460	4.4	3.2	56	53	0.65	11
7	2	1-Jul	183	10	7.8	460	5.2	3.5	22	18	0.71	4.3
7	3	1-Jul	183	15	7.8	460	5.4	2.9	19	16	0.57	3.9
9	1	1-Jul	183	4	7.8	350	5.1	3.3	17	14	0.67	3.5
2	3	4-Jul	186	6	7.3	470	4.8	4.1	17	13	0.83	3.4
5	1	4-Jul	186	14	7.2	300	3.6	4.1	11	8.0	0.83	2.3
5	2	4-Jul	186	12	7.1	370	3.8	4.5	72	68	0.89	15
5	3	4-Jul	186	11	7.1	390	5.6	4.6	12	7.0	0.91	2.3
7	1	4-Jul	186	12	8.3	420	6.1	1.2	6.4	5.3	0.23	1.3
7	2	4-Jul	186	12	8.5	420	7.0	4.4	21	17	0.88	4.3
7	3	4-Jul	186	12	8.4	430	6.4	5.0	57	52	1.0	11
9	1	4-Jul	186	10	8.0	360	6.8	4.2	5.6	1.4	0.84	1.1

Table A-1. Continued

Catena	Well #	Date	Julian Day	Water Column (cm)	pH	Eh (mV)	Temp (°C)	DHg (pM)	THg (pM)	PHg (pM)	DHg (ppt)	THg (ppt)
9	2	4-Jul	186	13	8.2	360	6.8	4.1	12	8.1	0.81	2.4
9	3	4-Jul	186	13	7.2	370	5.3	5.3	78	72	1.1	16
1	1	6-Jul	188	8	6.8	390	8.4	1.9	19	17	0.38	3.8
1	3	6-Jul	188	8	7.0	350	5.5	2.0	16	14	0.40	3.2
3	2	6-Jul	188	6	6.7	450	7.2	0.1	10	10	0.01	2.0
5	2	6-Jul	188	14	7.3	340	4.3	2.7	11	8.1	0.53	2.2
5	3	6-Jul	188	7	7.3	400	5.7	0.4	36	36	0.07	7.3
7	1	6-Jul	188	12	7.4	470	6.6	1.2	12	11	0.25	2.5
7	2	6-Jul	188	10	7.6	460	7.2	2.8	7.8	5.1	0.55	1.6
7	3	6-Jul	188	15	7.5	470	8.4	2.1	9.3	7.2	0.42	1.9
9	1	6-Jul	188	10	7.9	370	6.8	1.8	9.5	7.7	0.36	1.9
9	2	6-Jul	188	10	7.4	360	6.6	1.0	12	22	0.2	4.6
9	3	6-Jul	188	10	7.4	370	6.6	2.7	60	58	0.54	12
1	1	9-Jul	191	-	7.1	320	7.0	4.5	6.4	1.9	0.89	1.3
1	2	9-Jul	191	-	7.1	300	5.8	7.0	19	12	1.4	3.8

Table A-1. Continued

Catena	Well #	Date	Julian Day	Water Column (cm)	pH	Eh (mV)	Temp (°C)	DHg (pM)	THg (pM)	PHg (pM)	DHg (ppt)	THg (ppt)
3	1	9-Jul	191	-	6.3	400	4.1	2.7	11	7.9	0.53	2.1
5	1	9-Jul	191	-	7.7	360	3.7	3.9	7.6	3.7	0.78	1.5
5	3	9-Jul	191	-	7.6	380	5.4	3.7	12	8.0	0.74	2.3
6	1	9-Jul	191	-	8.1	410	3.7	3.5	30	26	0.7	5.9
6	3	9-Jul	191	-	8.4	400	4.2	5.2	10	5.0	1.0	2.0
7	1	9-Jul	191	-	7.9	360	5.9	3.4	15	12	0.69	3.1
7	2	9-Jul	191	-	7.9	340	5.4	5.3	12	7.0	1.1	2.5
7	3	9-Jul	191	-	7.9	360	6.4	5.2	9.2	4.0	1.0	1.8
9	2	9-Jul	191	-	-	-	-	3.6	7.0	3.3	0.73	1.4
9	3	9-Jul	191	-	-	-	-	4.4	34	30	0.88	6.9

Table A-1. Continued

Catena	Well #	Date	Julian Day	PHg (ppt)	%PHg	Cl- (ppm)	NO2- (ppm)	NO3- (ppm)	S2- (ppm)	Fe III (uM)	FeII (uM)
1	1	29-Jun	181	3.2	68	1.1	0.00	0.00	0.1	33	6.4
1	2	29-Jun	181	3.2	68	-	-	-	0.1	21	5.4
3	1	29-Jun	181	1.9	67	-	-	-	0.1	4.8	130
3	2	29-Jun	181	2.9	70	-	-	-	0.1	34	63
6	1	29-Jun	181	6.4	81	-	-	-	0.15	9.9	7.7
6	2	29-Jun	181	1.3	52	-	-	-	0.15	6.2	4.9
6	3	29-Jun	181	3.6	73	0.20	0.00	0.00	0.26	13	20
7	1	29-Jun	181	2.0	64	-	-	-	0.05	12	38
7	2	29-Jun	181	5.3	83	-	-	-	0.26	8.9	11
7	3	29-Jun	181	1.2	49	-	-	-	0.21	7.5	18
9	1	29-Jun	181	1.2	50	0.010	0.00	0.00	0.05	21	37
9	3	29-Jun	181	5.0	79	0.12	0.00	1.7	0.1	19	36
1	1	1-Jul	183	0.53	53	0.89	0.00	0.72	0.26	21	7.8
1	2	1-Jul	183	6.8	80	0.42	0.00	0.54	0.1	9.9	54
3	1	1-Jul	183	1.5	73	0.38	0.00	0.00	0.21	28	12

Table A-1. Continued

Catena	Well #	Date	Julian Day	PHg (ppt)	%PHg	Cl- (ppm)	NO2- (ppm)	NO3- (ppm)	S2- (ppm)	Fe III (uM)	FeII (uM)
6	2	1-Jul	183	6.8	87	0.040	0.00	0.00	0.31	7.4	12
6	3	1-Jul	183	1.9	71	0.48	0.00	0.00	0.1	13	10
7	1	1-Jul	183	11	94	0.00	0.00	0.00	0.1	30	20
7	2	1-Jul	183	3.6	84	0.060	0.00	0.00	0.1	9.8	18
7	3	1-Jul	183	3.3	85	0.14	0.00	0.00	0.1	15	17
9	1	1-Jul	183	2.8	81	0.00	0.00	0.00	0.26	34	27
2	3	4-Jul	186	2.6	76	0.23	0.00	0.47	0.05	39	55
5	1	4-Jul	186	1.4	63	0.00	0.00	0.63	0.26	48	8.1
5	2	4-Jul	186	14	94	0.00	0.00	0.00	0.26	24	87
5	3	4-Jul	186	1.4	60	0.00	0.00	0.00	0.21	19	78
7	1	4-Jul	186	1.1	82	0.16	0.00	0.00	0.58	7.2	20
7	2	4-Jul	186	3.4	80	0.00	0.00	0.00	0	7.5	19
7	3	4-Jul	186	10	91	0.08	0.00	0.00	0.15	16	20
9	1	4-Jul	186	0.28	25	0.020	0.59	0.52	0.1	15	44
9	2	4-Jul	186	1.6	67	0.00	0.00	0.52	0.31	10	34

Table A-1. Continued

Catena	Well #	Date	Julian Day	PHg (ppt)	%PHg	Cl- (ppm)	NO2- (ppm)	NO3- (ppm)	S2- (ppm)	Fe III (uM)	FeII (uM)
9	3	4-Jul	186	15	93	0.00	0.00	0.00	0.15	24	120
1	1	6-Jul	188	3.4	90	0.94	0.00	0.58	0	14	210
1	3	6-Jul	188	2.8	87	0.56	0.00	0.00	0.05	10	13
3	2	6-Jul	188	2.0	99	0.24	0.00	0.00	0.21	10	200
5	2	6-Jul	188	1.6	75	0.00	2.30	0.59	0.47	18	21
5	3	6-Jul	188	7.2	99	0.00	1.3	0.00	0.21	23	66
7	1	6-Jul	188	2.2	90	0.00	2.9	0.00	0.26	20	22
7	2	6-Jul	188	1.0	65	0.00	1.1	1.9	0.0	9.8	19
7	3	6-Jul	188	1.5	77	0.20	3.0	0.00	0.26	29	10
9	1	6-Jul	188	1.6	81	0.00	0.00	1.5	0.1	10	26
9	2	6-Jul	188	4.4	96	1.6	1.7	0.00	0.05	6.4	9.4
9	3	6-Jul	188	12	96	0.00	0.00	0.00	0.05	29	120
1	1	9-Jul	191	0.39	30	0.37	0.00	0.00	-	30	56
1	2	9-Jul	191	2.4	63	0.49	0.00	1.2	-	37	64
3	1	9-Jul	191	1.6	75	0.16	0.00	0.70	-	21	99

Table A-1. Continued

Catena	Well #	Date	Julian Day	PHg (ppt)	%PHg	Cl- (ppm)	NO2- (ppm)	NO3- (ppm)	S2- (ppm)	Fe III (uM)	FeII (uM)
5	1	9-Jul	191	0.73	49	0.00	0.00	0.59	-	16	53
5	3	9-Jul	191	1.6	68	0.00	1.2	0.71	-	230	98
6	1	9-Jul	191	5.2	88	-	-	-	-	45	190
6	3	9-Jul	191	1.0	49	0.14	0.69	0.00	-	59	69
7	1	9-Jul	191	2.4	77	0.00	0.00	0.00	-	64	78
7	2	9-Jul	191	1.4	57	0.020	0.00	0.00	-	64	81
7	3	9-Jul	191	0.8	43	0.060	0.00	0.55	-	61	70
9	2	9-Jul	191	0.67	48	0.00	0.00	0.73	-	86	77
9	3	9-Jul	191	6.0	87	0.43	0.00	0.00	-	49	79